



Dipl.-Ing. David Fast

Novel organic electrode materials for secondary batteries

DISSERTATION

zur Erlangung des akademischen Grades

Doktor der technischen Wissenschaften

eingereicht an der

Technischen Universität Graz

Betreuer

Ao.Univ.-Prof. Dipl.-Ing. Dr.techn. Robert Saf

Institut für Chemische Technologie von Materialien

EIDESSTATTLICHE ERKLÄRUNG

AFFIDAVIT

Ich erkläre an Eides statt, dass ich die vorliegende Arbeit selbstständig verfasst, andere als die angegebenen Quellen/Hilfsmittel nicht benutzt, und die den benutzten Quellen wörtlich und inhaltlich entnommenen Stellen als solche kenntlich gemacht habe. Das in TUGRAZonline hochgeladene Textdokument ist mit der vorliegenden Dissertation identisch.

I declare that I have authored this thesis independently, that I have not used other than the declared sources/resources, and that I have explicitly indicated all material which has been quoted either literally or by content from the sources used. The text document uploaded to TUGRAZonline is identical to the present doctoral dissertation.

Datum / Date

Unterschrift / Signature

Abstract

In the course of this work novel redox-active polymers with tetrasubstituted p-phenylenediamine (TSPD) units were synthesized, characterized and tested as electrode materials in secondary batteries.

The underlying mechanism for energy storage is the reversible oxidation/reduction of the TSPD-unit in two one-electron redox steps, which occur at potentials of approximately 3.4 and 3.8 V vs. Li/Li⁺. Polymers containing these units can therefore be utilized as cathode-active materials in e.g. lithium-ion batteries.

A polymer with tetraphenyl-p-phenylenediamine units and a theoretical capacity of 94 mAh/g was synthesized and successfully applied as cathode-active material. The polymer showed very good high-rate capability, thus making fast charging/discharging possible. Capacity retentions of about 70 % at 100 C (dis-/charging of the cell in 36 seconds) compared to the capacity at 1 C (1 hour) were observed. A high specific power density of 32.7 kW/kg (with a specific energy density of 212 Wh/kg), in reference to the active material content, was reached. Constant current dis-/charging experiments revealed great electrochemical stability, with a capacity retention of approximately 89 % after 11,000 cycles. Furthermore the influence of the cathode composition (active material, conductive additive, binder) on the morphological and electrochemical properties was investigated.

Polymers with tetraalkyl-p-phenylenediamine units in the main- and side-chain were also synthesized. Very high theoretical capacities of up to 334 mAh/g can be reached due to the low molecular weight of the repeating units. Electrochemical characterizations revealed inapplicability as electrode materials because of electrochemical instability.

Furthermore, a polymer containing TEMPO- and TSPD-units with a theoretical capacity of 152 mAh/g was synthesized, but electrochemical characterizations also revealed inapplicability as electrode material because of electrochemical instability.

Kurzfassung

Im Zuge dieser Arbeit wurden neuartige redoxaktive Polymere mit tetrasubstituierten p-Phenylendiamin (TSPD)-Einheiten synthetisiert, charakterisiert und als Elektrodenmaterialien in Sekundärbatterien eingesetzt und getestet.

Der Mechanismus zur Energiespeicherung ist die reversible Oxidation/Reduktion der TSPD-Einheiten in zwei Ein-Elektronen-Redoxschritten, welche bei Potentialen von 3,4 und 3,8 V gg. Li/Li⁺ auftreten. Polymere mit diesen Einheiten können deshalb als Kathodenmaterialien in z.B. Lithium-Ionen Batterien eingesetzt werden.

Ein Polymer mit Tetraphenyl-p-phenylendiamin-Einheiten und einer theoretischen Kapazität von 94 mAh/g wurde synthetisiert und erfolgreich als Kathodenmaterial eingesetzt. Das Polymer weist sehr gute Ratenfähigkeit auf, was schnelles Laden/Entladen ermöglicht. Kapazitätserhaltung von circa 70 % bei 100 C (Laden/Entladen der Zelle in 36 Sekunden) im Vergleich zu den Kapazitäten bei 1 C (1 Stunde) konnten beobachtet werden. Daraus resultiert eine hohe spezifische Leistungsdichte von 32,7 kW/kg (mit einer spezifischen Energiedichte von 212 Wh/kg), in Bezug auf den Aktivmaterialanteil. Konstantstromzyklisierungen ergaben sehr gute elektrochemische Stabilität, mit einem Kapazitätserhalt von circa 89 % nach 11000 Zyklen. Weiters wurde der Einfluss der Kathodenzusammensetzung (Aktivmaterial, Leitfähigkeitsadditiv, Binder) auf die morphologischen und elektrochemischen Eigenschaften untersucht.

Polymere mit Tetraalkyl-p-phenylendiamin-Einheiten in der Haupt- und Seitenkette wurden ebenfalls synthetisiert. Sehr hohe theoretische Kapazitäten von bis zu 334 mAh/g können aufgrund der niedrigen molaren Masse der Wiederholeinheiten erreicht werden. Elektrochemische Charakterisierungen ergaben, dass diese als Elektrodenmaterialien, aufgrund elektrochemischer Instabilität ungeeignet sind.

Weiters wurde ein Polymer mit TEMPO- und TSPD-Einheiten und einer theoretischen Kapazität von 152 mAh/g synthetisiert. Aber auch hier ergaben elektrochemische Charakterisierungen, dass dieses als Elektrodenmaterial aufgrund elektrochemischer Instabilität ungeeignet ist.

Acknowledgement

Many people contributed to this work and I want to thank...

...Ao. Univ.-Prof. DI Dr. Robert Saf, my supervisor, for the opportunity to work on this project, his guidance, patience and for all the helpful discussions we had

...Univ.-Prof. DI Dr. Franz Stelzer, the head of our institute and my project supervisor, for the opportunity to work on this project and at the ICTM

...my colleagues who worked with me on this project, for all the discussions, support and the nice working atmosphere: Barbara Rupp, Astrid Knall and especially Katharina Gallas

...DI Dr. Martin Schmuck from VMI for the countless helpful discussions regarding electrochemistry

...our project partners Varta Micro Innovation GmbH, Isovoltaic AG and the Polymer Competence Center Leoben GmbH for funding and support, especially the project supervisors Harald Kren and Stefan Koller from VMI and Christina Schinagl and Albert Plessing from Isovoltaic

...everybody at VMI, who have all been very kind and helpful, especially Katharina Gruber, Stephania Toulis, Christoph Stangl, Andrea Droisner, Patricia Handel and Sandra Pötz

...Univ.-Prof. Mag.rer.nat. Dr.phil. Georg Gescheidt for his help with the EPR-measurements

...Karin Bartl and DI Dr. Petra Kaschnitz for their help with MS- and NMR-measurements

...everybody here at ICTM, especially everyone I worked with on a daily basis

...my family for all the support they provided throughout the years, this would not have been possible without you

Index

1	Preface	1
2	Introduction	3
2.1	History of organic batteries.....	3
2.2	Organic radical batteries	9
2.3	Tetrasubstituted p-phenylenediamines.....	12
3	Experimental.....	16
3.1	Materials and Methods	16
3.1.1	General cyclic voltammetry procedure for polymers.....	17
3.1.2	General half-cell procedure	18
3.2	Synthesis.....	20
4	Results and Discussion.....	34
4.1	Polymers with TAPD-units.....	34
4.1.1	TAPD-units in the main-chain	34
4.1.2	TAPD-units in the side-chain.....	37
4.2	Polymer with TPPD-units.....	40
4.2.1	Synthesis of polymer 7	40
4.2.2	Electrochemical behavior of polymer 7	41
4.2.3	Composite cathodes of polymer 7 - morphology	42
4.2.4	Composite cathodes of polymer 7 – basic electrochemistry	44
4.2.5	Composite cathodes of polymer 7 – battery testing	46

4.2.6	Influence of the cathode composition on the morphological and electrochemical properties	55
4.3	Polymer with TSPD- and TEMPO-units.....	63
4.3.1	Model compound.....	63
4.3.2	Polymer	67
5	Summary and outlook	71
6	References	75
7	Appendix.....	81
7.1	Abbreviations	81
7.2	Characterization	82
7.3	List of chemicals	105
7.4	List of Figures.....	108
7.5	List of Schemes.....	111
7.6	List of Tables.....	113

1 Preface

Energy storage is becoming increasingly important, not only for portable electronic devices, but also regarding electromobility and decentralized power generation from renewable resources like e.g. photovoltaics.

Lithium-ion batteries are the most frequently used secondary batteries for these purposes due to good energy densities and cycle stabilities. The mechanism for charge storage is based on the intercalation / deintercalation of Li-ions, typically in transition metal oxides like e.g. LiCoO_2 or LiFePO_4 (positive electrode or cathode) and carbon (negative electrode or anode). The rates of the electrode reactions are rather low due to the structural changes accompanied with intercalation, resulting in low capacity retentions at higher current densities and thus low power densities.

On the other hand the charge storage mechanism for (most) organic electrode materials is based on reversible redox reactions of an electroactive functional group, e.g. stable radicals like nitroxides. The electron transfer is usually much faster compared to inorganic intercalation materials, thus resulting in higher power densities. Higher specific energy densities (Wh/kg) can be reached due to the low densities of polymers (typically about 1 g/mL), but the resulting lower volumetric energy densities (Wh/l) have to be kept in mind.

The aims of this work were the synthesis of novel redox-active polymers and utilization as cathode-active materials in secondary batteries.

The anticipated properties of the new polymers were defined as:

- High capacity

- High electrochemical and cycle stability
- Fast electrode kinetics (resulting in high power capabilities)
- Low solubility in solvents typically used for electrolyte solutions (without additional crosslinking steps)

Novel redox-active polymers based on tetrasubstituted p-phenylenediamine (TSPD) units, which can exchange 2 electrons in two one-electron redox steps, were synthesized, characterized and tested as cathode-active materials in half-cells with lithium as counter electrode.

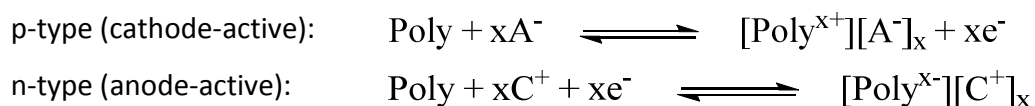
2 Introduction

Polymers have become an integral part of our everyday life, not only for standard applications like packaging, as components and assemblies, but also in modern fields like electronics, where tailored functional polymers are applied as active components, e.g. in organic light-emitting diodes (OLEDs)¹ or organic photovoltaics.²

In the last decades a lot of effort has been put into the design and application of small organic molecules and polymers as electrode materials in secondary batteries³⁻⁵, as a more environmentally benign alternative to conventional inorganic materials. Other advantages include higher safety, better processability, recyclability and potential low cost.⁴⁻⁶

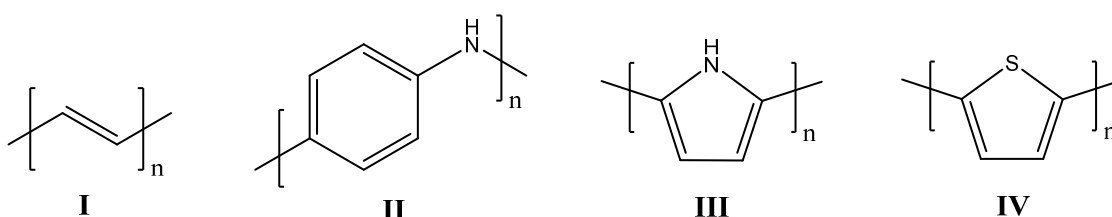
2.1 History of organic batteries

The first reports of organic electrode materials date back to 1969⁷, but research did not increase significantly until the discovery of conducting polymers in the late 1970s.^{8,9} These kind of polymers can be doped electrochemically. The process exhibits good reversibility, thus the polymers are promising for charge storage. Depending on the dopant or the doping ions (anions A^- or cations C^+ , respectively), they can either act as cathode-active (p-type) or anode-active (n-type) electrode materials.



x is the doping level (ratio of doped to all repeating units of the polymer, $0 \leq x \leq 1$).

The first example of a utilization as electrode material was shown for polyacetylene **I**^{10,11}, other examples include polyaniline **II**^{12,13}, polypyrrole **III**¹⁴ and polythiophene **IV**¹⁵ (Scheme 1).



Scheme 1: Examples of conducting polymers in their undoped state: polyacetylene^{10,11} (**I**), polyaniline^{12,13} (**II**), polypyrrole¹⁴ (**III**) and polythiophene¹⁵ (**IV**)

The doping level x is directly connected to the capacity, and thus energy density, but is limited due to structural/chemical reasons. Overoxidation can lead to a gradual decomposition of the polymer. For example polyacetylene, polypyrrole and polythiophene can be doped to about $x \leq 0.3$, resulting in theoretical capacities of less than 150 mAh/g.^{3,5} Experimental capacities were much lower. Polyaniline can be fully doped ($x = 1$) with a theoretical capacity of 295 mAh/g, but practical capacities seldom exceed 150 mAh/g.^{3,5}

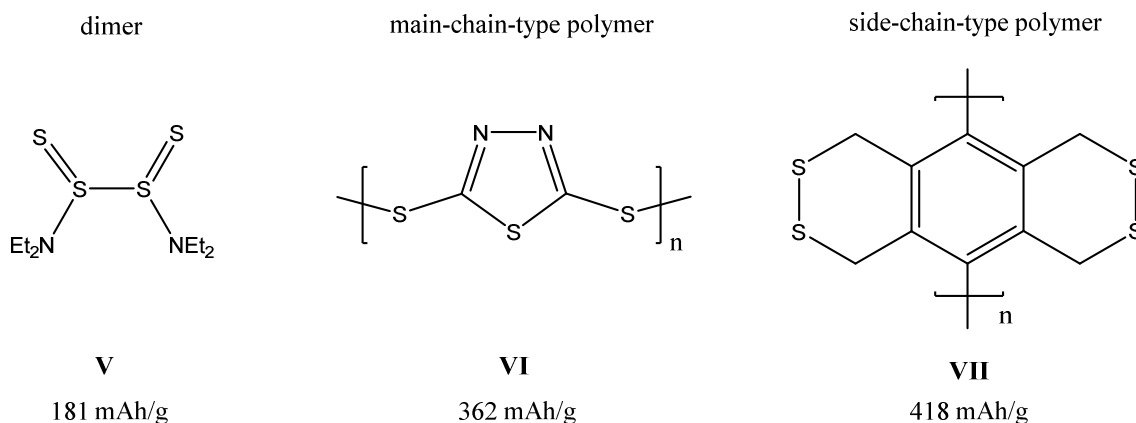
Critical drawbacks of conducting polymers are low coulombic efficiencies and high self-discharge. Thus the performance in batteries is poor compared to inorganic electrode materials. Up until now these aspects are a hindrance for a practical application of conducting polymers in secondary batteries, but due to their excellent electronic conductivity they are utilized as cathode materials for supercapacitors.¹⁶

Another class of organic electrode materials, based on disulfides, was introduced in the late 1980s.¹⁷ Scheme 2 shows the redox reaction of an organodisulfide, which is based on bond scission (resulting in the formation of thiolate) and bond reconstruction (electrodimerization). Because of the two-electron process, high theoretical capacities can be achieved.



Scheme 2: Redox couple organic disulfide/thiolate

One of the first examples within this class was tetraethylthiuram disulfide **V** (Scheme 3). It was used as cathode-active material in high-temperature sodium batteries.¹⁷ A model lithium battery was also reported.¹⁸ In this case compound **V** dissolved in DMSO was utilized as cathode. Both examples provided a proof of principle for the utilization of organic disulfide compounds as electrode materials. Studies on the electrochemical properties of the organic disulfide/thiolate redox couple at ambient temperature showed very poor kinetics (large peak potential separation in cyclic voltammetry experiments).¹⁹



Scheme 3: Examples of organic disulfides and their theoretical capacities: tetraethylthiuram disulfide¹⁷ (**V**), poly(2,5-dimercapto-1,3,4-thiadiazole)²⁰ (**VI**) and poly(5,8-dihydro-1H,4H-2,3,6,7-tetrathiaanthracene)²¹ (**VII**)

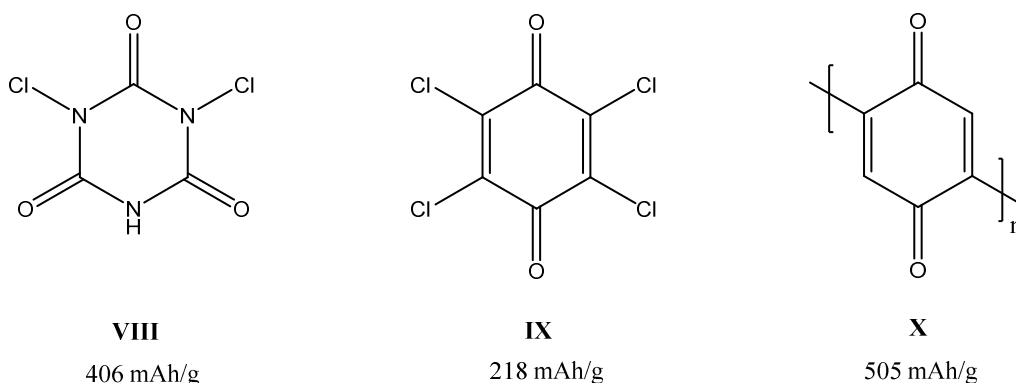
Polymers containing disulfide bonds in the main chain, for example poly(2,5-dimercapto-1,3,4-thiadiazole **VI**^{20,22} (Scheme 3) were introduced in the early 1990s and extensively studied due

to high theoretical specific capacities (362 mAh/g for polymer **VI**). The slow kinetics can be improved by the addition of conducting polymers such as polyaniline²² or poly(3,4-ethylenedioxythiophene) (PEDOT).²³

One intrinsic problem of main-chain-type polymers is the reduction to thiolate ions (monomer²⁻) upon discharging. The formed ions easily dissolve in solvents used for common electrolyte solutions, which would result in capacity fading. Therefore most systems have to utilize solid-state or gel electrolytes with lower ionic conductivity compared to liquid electrolytes.

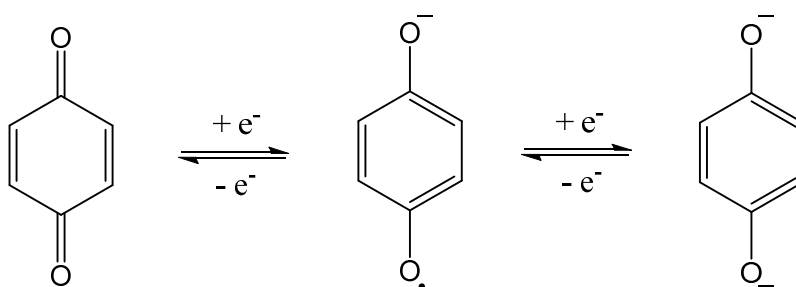
Polymers containing disulfide bonds in side chains^{21,24}, e.g. polymer **VII** (Scheme 3), have been synthesized to circumvent this problem. Side-chain-type polymers show improved but still unsatisfactory cycle stability and practical application is still unlikely due to the rather slow kinetics of the disulfide bond scission/reconstruction reaction.

The earliest attempts of utilizing organic compounds as electrode materials in batteries were made with quinones/carbonyl compounds, e.g. dichlorocyanuric acid **VIII**⁷ (Scheme 4).



Scheme 4: Examples of carbonyl compounds and their theoretical capacities: dichloroisocyanuric acid⁷ (**VIII**), chloranil²⁶ (**IX**) and polyquinone²⁹ (**X**)

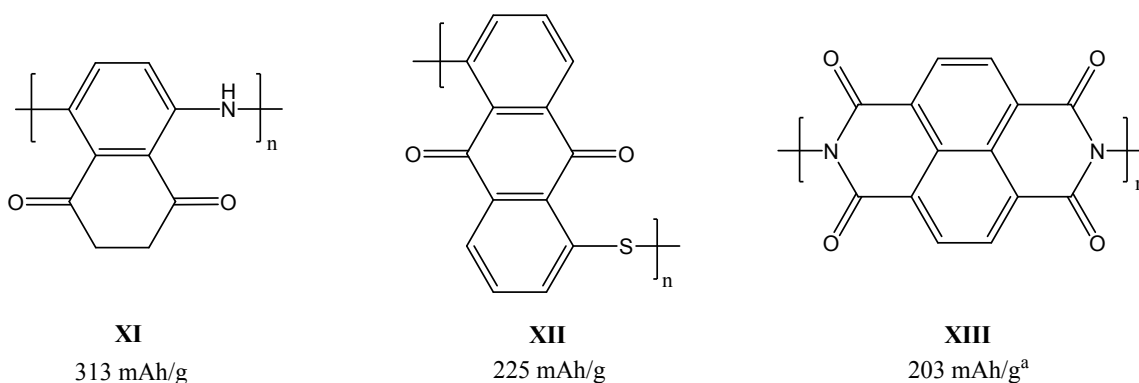
Scheme 5 shows the two-step redox reaction of benzoquinone²⁵, which is representative for similar carbonyl compounds.



Scheme 5: Redox reaction of benzoquinone

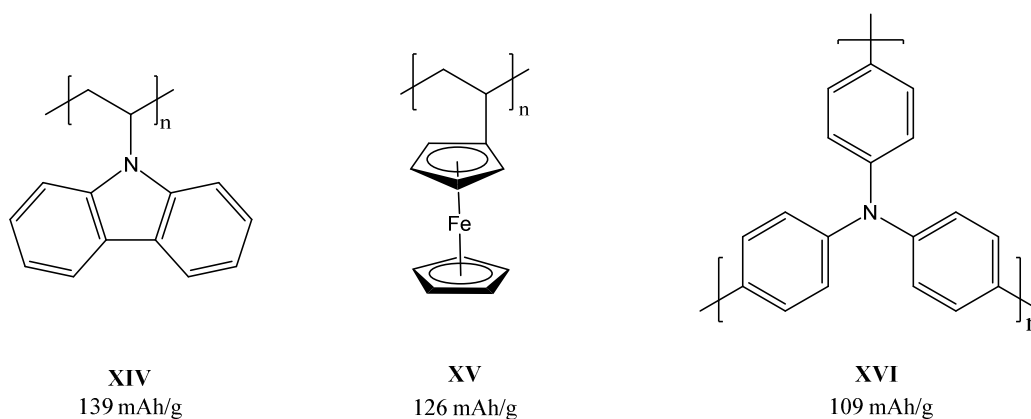
The first reports on secondary batteries focused on small molecules like benzoquinone and chloranil **IX**²⁶ (Scheme 4). Other examples include phenanthrenequinone²⁷ or anthraquinone²⁸, but they showed poor cycle stability due to dissolution into the electrolyte. Thus research shifted towards polymers containing corresponding groups, e.g. polyquinone **X**²⁹ (Scheme 4). It showed poor electrode utilization (only about 30 % of its theoretical capacity could be reached) and thus the research interest diminished until the late 1990s.

Polymer **XI**³⁰, which combines structural features of quinones and polyaniline (Scheme 6), showed improved electrode utilization (200 mAh/g after 10 cycles). Research towards polymers based on carbonyl groups once again attracted increased attention since this polymer. Recently developed polymers^{31,32}, including polymers **XII**³³ and **XIII**³⁴ (Scheme 6), with discharge potentials of approximately 2.5 V vs. Li/Li⁺ show good capacity, cycle stability, high-rate capability and appear to be promising candidates for organic electrode materials.



Scheme 6: Examples of polymers based on carbonyl groups and their theoretical capacities: poly(5-amino-p-naphthoquinone)³⁰ (**XI**), poly(anthraquinonyl sulfide)³³ (**XII**) and polyimide³⁴ (**XIII**)^a

Other concepts for organic electrode materials include poly(N-vinylcarbazole) **XIV**³⁵, poly(vinylferrocene) **XV**³⁶ and poly(para-triphenylamine) **XVI**³⁷ (Scheme 7), which are often categorized as redox polymers.



Scheme 7: Other organic electrode materials and their theoretical capacities

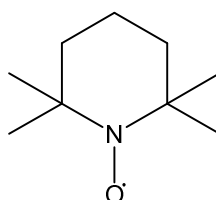
^a Only two of the four carbonyl-groups are electroactive, thus the theoretical capacity in Scheme 6 is calculated for 2 electrons per repeating unit

Poly(para-triphenylamine) **XVI** shows very good electrode utilization (discharge capacity of 103 mAh/g or 94 % of the theoretical value at 0.5 C), a high discharge potential of approximately 3.8 vs. Li/Li⁺ and great cycle stability. Furthermore it can be discharged with a rate of 20 C for 1000 cycles with a capacity retention of 95 %.

More extensive and detailed reviews on organic electrode materials can be found in the literature.³⁻⁵

2.2 Organic radical batteries

Stable organic radicals, especially nitroxyl radicals like 2,2,6,6-tetramethylpiperidine-1-oxyl (TEMPO)³⁸ (Scheme 8), have been found to be very useful in a wide variety of applications throughout chemistry and biochemistry.³⁹ They are used for example as catalysts in the oxidation of alcohols^{40,41}, as spin labels for electron paramagnetic resonance spectroscopy⁴² or in controlled free-radical polymerizations.^{43,44}

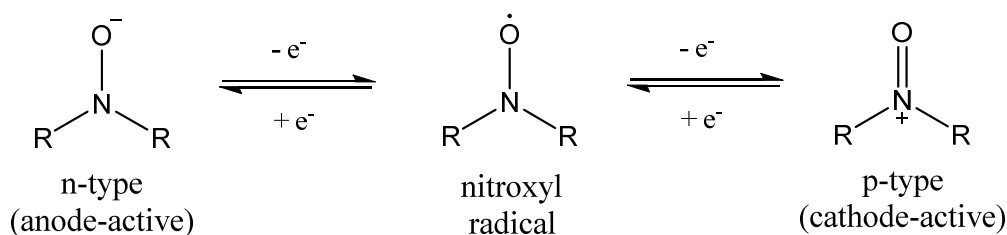


TEMPO

Scheme 8: Structure of 2,2,6,6-tetramethylpiperidine-1-oxyl (TEMPO)

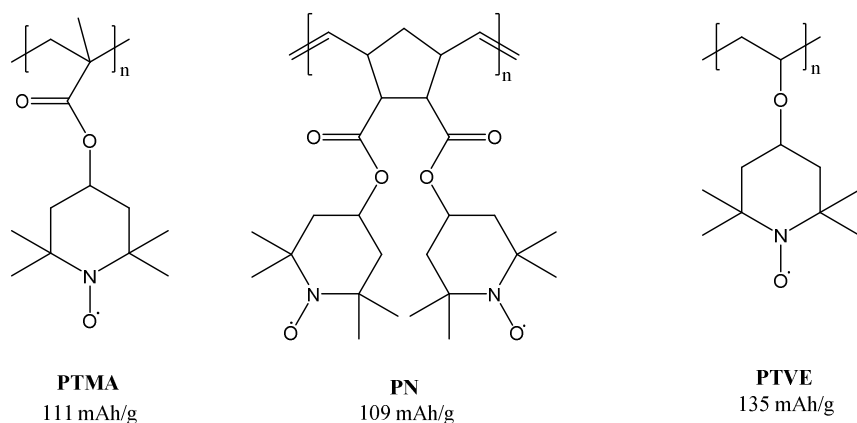
Polymers containing stable radical groups in the repeating unit, so-called polyradicals, were extensively studied as potential high-spin organic materials ('organic magnets').⁴⁵⁻⁴⁷

Furthermore, it is well known that these radical groups can be reversibly oxidized and reduced electrochemically.^{48,49} Scheme 9 shows the redox couples of a nitroxide radical, which can either be reversibly oxidized to form an oxoammonium cation (p-type or cathode-active) or, depending on the R-groups, also be reversibly reduced to form an aminoxyl anion (n-type or anode-active).



Scheme 9: Redox couples of nitroxyl radicals

In the early 2000s, the use of poly(2,2,6,6-tetramethylpiperidine-1-oxyl methacrylate) (PTMA) (Scheme 10) as cathode-active material in so-called organic radical batteries (ORBs) was introduced.^{50,51} In combination with lithium as anode it became a well-studied standard model for ORBs.^{52–61}



Scheme 10: Examples of polyradicals used for ORBs and their theoretical capacities

Figure 1 shows the working principle of an all-organic radical battery^{62,63} with two different polyradicals as cathode- and anode-active material.

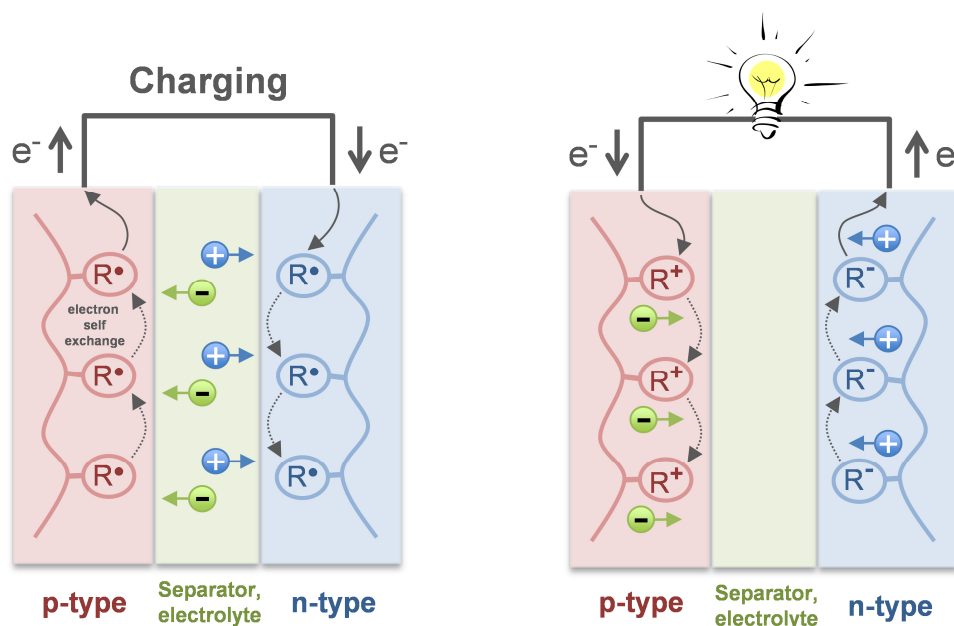


Figure 1: Working principle of an all-organic radical battery

In case of nitroxyl-based polyradicals, the p-type polymer is oxidized to form oxoammonium cations and the n-type polymer is reduced to form aminoxyl anions upon charging. Ions of the conducting salt (e.g. LiPF_6) in the electrolyte neutralize the formed charges of the polymers. Upon discharging the opposite reactions take place and the radicals are recovered. The charge transport within the polymer, as in other non-conductive redox-active polymers, occurs via an electron-hopping/electron self-exchange mechanism^{64–67} and bridges the distance to a conductive additive or, for thin films, to the current collector.⁶⁷

Only minor structural changes of the redox-active species occur during these processes⁶⁸, resulting in high cycle stability (≥ 1000)^{51,58,69}, fast redox reactions and thus very good high-rate capabilities.^{58,70,71}

Scheme 10 shows some examples of commonly used p-type polyradicals used as cathode-active materials in ORBs – **PTMA**, TEMPO-substituted polynorbornene (**PN**)^{72–74} and polyvinylether (**PTVE**)^{70,75} which have discharge potentials of about 3.6 vs. Li/Li⁺.

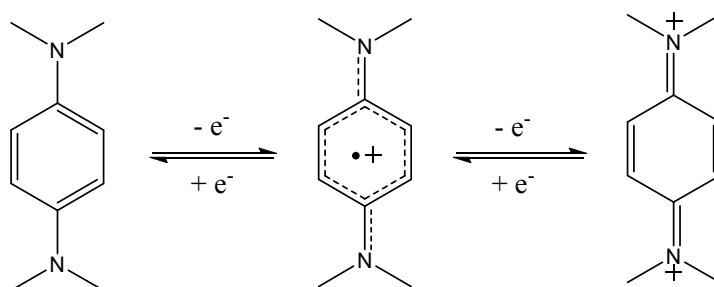
One of the biggest drawbacks of polyradicals, and also of other non-conjugated redox polymers like e.g. poly(vinylferrocene) **XV** or polyimide **XIII**, is their electronic insulating nature, which makes the addition of large amounts of conductive additive necessary (up to 80 wt-%). Therefore practical capacities of cathode composites are significantly reduced. ‘Polymer-rich’ electrodes containing only 15 wt-% conductive additive showed poorer electrode utilization and also poorer performance at higher current densities.⁶⁰

A recent study revealed that the ions of the conducting salt in the electrolyte-swollen or gel-like polymer layers play a significant role in charge transportation processes.⁷⁶ It was found that the charge transport is dominated by the mobility of the anion rather than the concentration of redox centers, thus being a limiting factor for the rate of electron transfer.

More detailed reviews on organic radical batteries can be found in literature.^{77,78}

2.3 Tetrasubstituted p-phenylenediamines

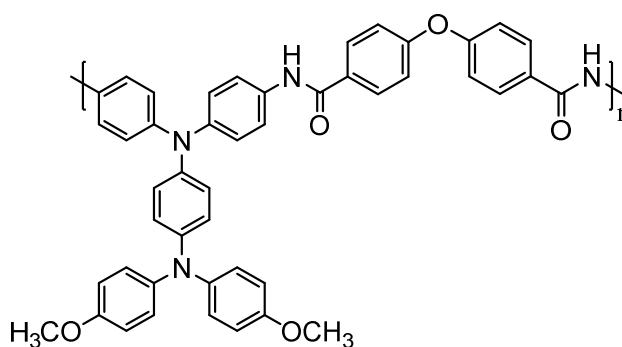
N,N,N',N'-tetramethyl-p-phenylenediamine (TMPD) is a very-well studied redox-active molecule.^{79–84} Scheme 11 shows the redox couples of TMPD: it can be reversibly oxidized to form a radical-cationic species (the so-called ‘Wurster’s blue’⁷⁹) and a dicationic species (quinone diimine), in two one-electron oxidation-steps.



Scheme 11: Redox couples of N,N,N',N'-tetramethyl-p-phenylenediamine (TMPD)

Due to its redox properties and the color change to blue upon oxidation (radical-cationic species) it can be used for example as redox indicator in the detection of cytochrome c oxidase.⁸⁵ Other applications include the utilization as redox shuttles for overcharge protection in low voltage lithium ion or lithium polymer batteries.^{86–88}

Polymers containing tetrasubstituted p-phenylenediamine (TSPD) units have been extensively studied as electrochromic materials.^{89–92} Especially polyamides containing tetraphenyl-p-phenylenediamine (TPPD) units (Scheme 12) show great stability of electrochromic characteristics.⁸⁹

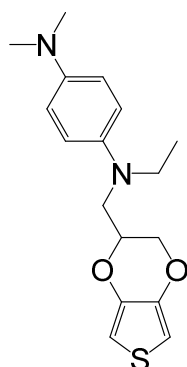


Scheme 12: Example of an electrochromic polymer based on TPPD-units⁸⁹

Cyclic voltammograms of ITO-coated glass substrates coated with these polymers show the same redox behavior as TMPD, namely two one-electron redox steps. Upon cyclic scans between 0 and 0.98 V (vs. Ag/AgCl) color changes from colorless to green and then blue with good coloration efficiencies over 1000 cycles were observed.⁸⁹

An electrochemical quartz crystal microbalance (EQCM) - study on a poly(amine-imide) containing TPPD-units revealed that both electrolyte salt anions and cations play an important role in the redox processes.⁹³ Upon oxidation of the polymer film, positive charges are formed (radical cationic and dicationic state) and anions insert into the polymer matrix to neutralize the charges. It was found that also cations play an important role in these processes, especially for the first redox step.⁹³

A utilization of a polymer containing TSPD-units as charge storage material has been shown recently.⁹⁴ Scheme 13 depicts a monomer example consisting of a 3,4-ethylenedioxythiophen (EDOT) and a tetraalkyl-p-phenylenediamine (TAPD) group, which was subsequently electropolymerized on glassy carbon electrodes.



Scheme 13: Monomer of PEDOT with TAPD-units

The resulting polymer film was capable of storing charge faradaically via the TAPD-units and as pseudocapacitor via the conducting polymer backbone (PEDOT), exchanging 2.6 electrons per repeating unit (theoretical capacity: 210 mAh/g).

Cyclic voltammograms at 500 mV/s revealed a peak current retention of 90 % over 25 cycles, although the performance as an electrode material in a battery was not reported.

3 Experimental

3.1 *Materials and Methods*

All chemicals and solvents were obtained from Sigma-Aldrich, Fluka, VWR, Alfa Aesar or Fisher Chemical and used as received unless stated otherwise (for a detailed list compare section 7.2). Ethanol and methanol were rotary evaporated prior to use. Toluene and THF were dried and deoxygenated with a solvent drying system (Innovative Technology, Inc.).

Electron impact (EI, 70 eV) mass spectra were recorded on a Waters GCT Premier equipped with an orthogonal acceleration time-of-flight (oa-TOF) mass analyzer. Direct insertion (DI) and gas chromatography (GC) were used as inlet systems (gas chromatograph: Agilent 7890A).

Matrix-assisted laser desorption/ionization time-of-flight (MALDI-TOF) mass spectrometry was performed on a Micromass ToFSpec 2E Time-of-Flight Mass Spectrometer equipped with a nitrogen laser (337 nm wavelength) and a time lag focusing unit. Spectra were acquired in reflectron mode at an accelerating voltage of 20 kV. α -Cyano-4-hydroxycinnamic acid (CHCA), trans-2-[3-(4-tert-Butylphenyl)-2-methyl-2-propenylidene]malononitrile (DCTB) and 1,8,9-Anthracenetriol (dithranol) were used as matrices. Sample solutions have been prepared by mixing solutions of CHCA or DCTB (10 mg/mL in THF) and the analyte (1 mg/mL in THF, CHCl_3 or methanol) in a ratio of 7/2 (v/v). Reference solutions have been prepared by mixing solutions of dithranol (10 mg/mL in THF), sodium trifluoroacetate (NaTFA; 1 mg/mL in THF) and polyethylene glycol (PEG; 5 mg/mL in THF) in a ratio of 7/2/2 (v/v/v). Data analysis was done with Waters MassLynx V4.1 software.

NMR spectroscopy (^1H , ^{13}C) was performed on a Bruker Avance 300 MHz spectrometer (75 MHz for ^{13}C). Attached proton test (APT) experiments were used to assign ^{13}C chemical shifts.

Chemical shifts (δ) are reported in ppm relative to tetramethylsilane (TMS) using the residual deuterated solvent signals as an internal reference (CDCl_3 : $\delta_{\text{H}} = 7.26$ ppm, $\delta_{\text{C}} = 77.16$ ppm; $\text{DMSO-}d_6$: $\delta_{\text{H}} = 2.50$ ppm, $\delta_{\text{C}} = 39.52$ ppm, $\text{Methanol-}d_4$: $\delta_{\text{H}} = 3.31$ ppm).⁹⁵ Deuterated solvents were obtained from VWR.

IR spectra were recorded on a Bruker ALPHA FT-IR Spectrometer in attenuated total reflection (ATR) mode.

Size Exclusion Chromatography (SEC) was performed on a WGE SEC-3010 equipped with a WGE G-2010 pump and a WGE Dn-2010 refractive index (RI) detector. THF was used as eluent. For calibration polystyrene standards from Polymer Standards Service were used.

Scanning electron microscopy (SEM) was performed on a JEOL JSM-5410 Scanning Microscope equipped with a secondary electron (SE) detector. An acceleration voltage of 5.0 kV was used. The composite cathodes were analyzed directly (without a prior gold sputtering step). Images were recorded using SemAfore.

Electron paramagnetic resonance (EPR) measurements were performed on a MiniScope MS300 (Magnettech, Germany) X-band spectrometer at room temperature. Analytes were dissolved in chloroform. For the measurement of polymer **14** a soluble fraction of an only partially crosslinked polymer was used.

3.1.1 General cyclic voltammetry procedure for polymers

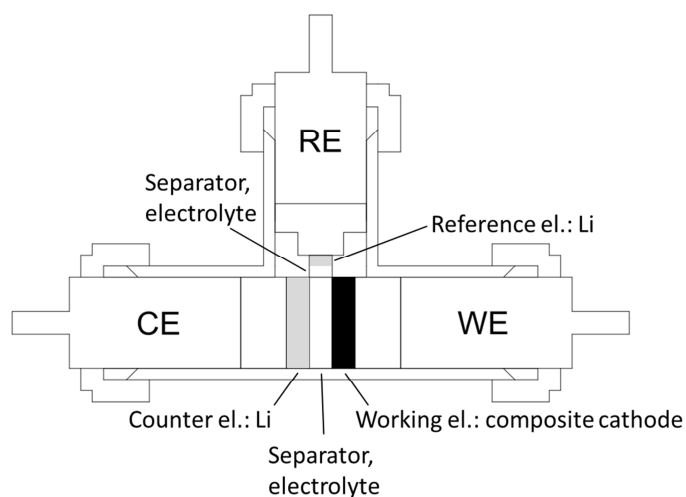
Cyclic voltammetry experiments were performed on a Bio-Logic VMP3:

- *In solution*: 1 mM in chloroform containing 0.1 M tetrabutylammonium perchlorate (TBAP), reference electrode: Ag/AgNO_3 , working electrode: Platinum disc, counter electrode: Platinum wire, scanrate: 20 - 50 mV/s
- *On ITO*: ITO-coated glass substrates were coated with the polymer by spincoating 20 μL of a solution of the polymer in chloroform (1 mg/mL) or dropcoating (on a hot plate)

with 20 μL of a solution of the polymer in DMF (1 mg/mL), electrolyte: acetonitrile containing 0.1 M TBAP, reference electrode: Ag/AgNO₃, counter electrode: Platinum wire, scanrate: 50 mV/s

3.1.2 General half-cell procedure

Composite cathodes were fabricated by doctor blading a slurry containing active material, PVdF as binder and Super P[®] as conductive additive in NMP on a carbon-coated aluminum or aluminum current collector. Electrodes with a diameter of 12 mm were die-cutted, dried at 80 °C under vacuum and weighed. Half-cells (Swagelok[®]) with a three-electrode set-up containing the composite cathode, lithium as counter and reference electrode, a separator (Freudenberg 2190) impregnated with the electrolyte (1 M LiPF₆ in ethylene carbonate/diethyl carbonate (EC/DEC) = 3:7 (v/v), provided by VARTA Micro Innovation GmbH) were assembled (Scheme 14).



Scheme 14: Schematic of the 3-electrode Swagelok[®]-setup

Before electrochemical characterization, the half-cells were allowed to rest for at least 24 hours to assure sufficient swelling of the polymer in the electrolyte. This is necessary to provide a sufficient conductivity for the ions of the electrolyte salt (LiPF₆), which is essential for charge transport processes.⁷⁶

Cyclic voltammetry experiments were performed on a Bio-Logic VMP3 with scan rates of 0.1 – 22 mV/s.

Cycling tests were performed on a Maccor Series 4000 battery tester.

Formal potentials $E^{0'}$ were calculated using equation [1].

$$E^{0'} = \frac{E_{p,a} - E_{p,c}}{2} \quad [1]$$

Peak-potential separation ΔE_p was calculated using equation [2].

$$\Delta E_p = E_{p,a} - E_{p,c} \quad [2]$$

$E_{p,a}$ anodic peak potential

$E_{p,c}$ cathodic peak potential

Theoretical specific capacities c (mAh/g) were calculated using equation [3].

$$c = \frac{F}{3.6 \frac{M}{z}} \quad [3]$$

F...Faraday constant (96485 C/mol)

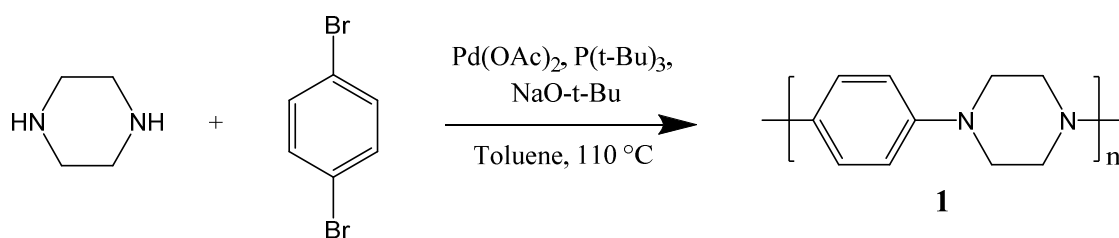
M...molecular mass of the repeating unit (in g/mol)

z...electrons transferred per repeating unit

3.2 Synthesis

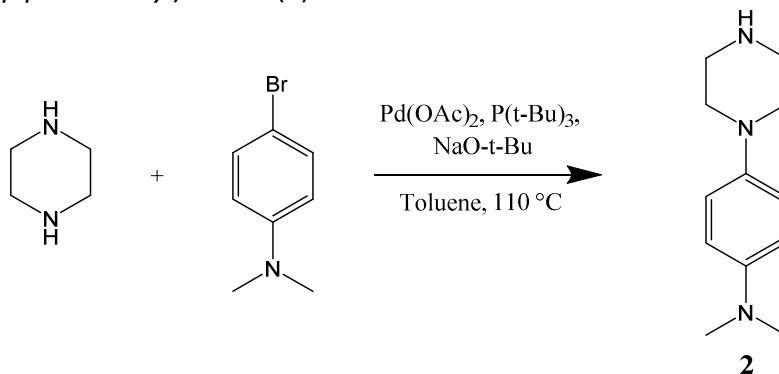
All syntheses were performed utilizing basic schlenk technique under nitrogen.

Poly(1,4-piperazinediyl-1,4-phenylene) (1)



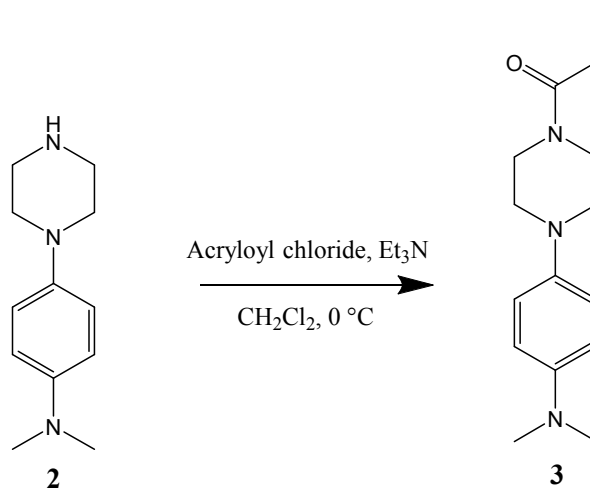
To piperazine (212.7 mg, 2.47 mmol), 1,4-dibromobenzene (583.5 mg, 1 eq.) and sodium *tert*-butoxide (710 mg, 3 eq.) in 10 mL of anhydrous toluene were added Pd(OAc)₂ (5.63 mg, 0.01 eq.) and tri-*tert*-butylphosphine (75 μL, 0.03 eq.). The reaction mixture was stirred at 110 °C and after half an hour a beige solid started to precipitate. Stirring was continued for 1 h. After cooling the precipitate was filtered and washed thoroughly with approximately 20 mL of toluene, water and methanol, respectively. The resulting solid was dispersed in 50 mL of boiling methanol for 2 hours and filtered. After drying under reduced pressure compound **1** was obtained as off-white insoluble solid (355.3 mg, 90 %).

IR: 3418, 2949, 2820, 1511, 1444, 1380, 1318, 1293, 1254, 1225, 1152, 1047, 1000, 942, 834, 717, 553 cm⁻¹

N,N-dimethyl-4-(piperazin-1-yl)aniline (**2**)

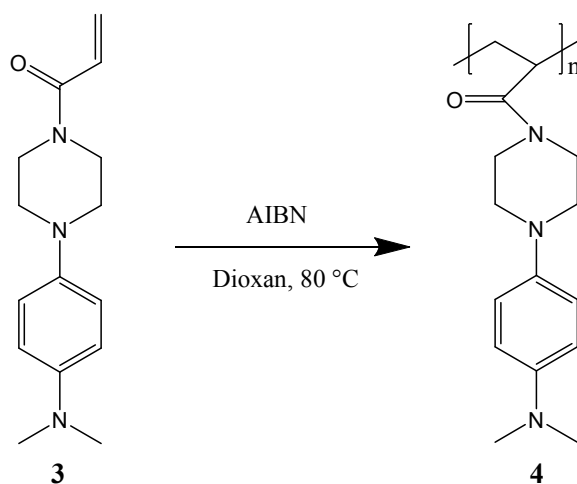
Piperazine (0.32 g, 3.72 mmol), 4-bromo-*N,N*-dimethylaniline (0.74 g, 1 eq.) and sodium *tert*-butoxide (0.54 g, 1.5 eq.) were dissolved in 15 mL of anhydrous toluene and heated to 110 °C. Pd(OAc)₂ (8.42 mg, 0.01 eq.) and tri-*tert*-butylphosphine (110 μL, 0.03 eq.) were added and the reaction mixture was stirred for 3.5 h. After cooling 15 mL of ethyl acetate were added, the mixture was washed 3 times with 30 mL of brine, dried over sodium sulphate and evaporated to dryness. After column chromatography on aluminum oxide (stepwise elution with ethyl acetate, ethyl acetate/methanol = 4/1, 1/1, pure methanol) compound **2** was obtained as off-white solid (0.48 g, 63 %).

¹H NMR (300.36 MHz, CDCl₃, δ in ppm): 6.95-6.86 (m, 2H), 6.79-6.71 (m, 2H), 3.08-2.98 (m, 8H), 2.87 (s, 6H); ¹³C NMR (APT, 75.53 MHz, CDCl₃, δ in ppm): 146.32, 143.14, 119.07, 114.48, 50.88, 44.99, 41.55; GC/EI-MS: M⁺, *m/z* found: 205.1599 Da, calculated for C₁₂H₁₉N₃: 205.1579 Da; IR: 3287, 2942, 2905, 2820, 1674, 1616, 1515, 1439, 1311, 1260, 1219, 1126, 1058, 1019, 943, 881, 806, 698, 593, 533 cm⁻¹

1-(4-(4-(dimethylamino)phenyl)piperazin-1-yl)prop-2-en-1-one (3)

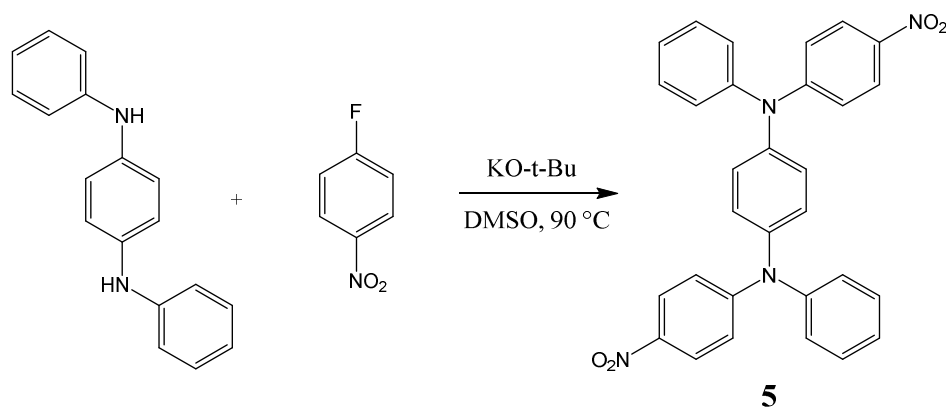
Compound **2** (157 mg, 0.77 mmol) was dissolved in 3.8 mL of dichloromethane and triethylamine (130 μ L, 1.2 eq) was added. The solution was cooled to 0 °C and acryloyl chloride (75 μ L, 1.2 eq., filtered through basic aluminum oxide prior to use) was added dropwise under stirring. After 2 h the reaction mixture was washed with approximately 5 mL of saturated aqueous NaHCO₃ and 5 mL of brine. After separation of the two phases, the aqueous phase was extracted with 10 mL of dichloromethane. The organic phases were combined, dried over Na₂SO₄ and concentrated. After column chromatography on aluminum oxide (eluent: ethyl acetate) compound **3** was obtained as white-yellowish solid (153 mg, 77 %).

¹H NMR (300.36 MHz, CDCl₃, δ in ppm): 7.00-6.53 (m, 5H), 6.38-6.25 (m, 1H), 5.76-5.66 (m, 1H), 3.90-3.66 (m, 4H), 3.15-2.78 (m, 10H); ¹³C NMR (APT, 75.53 MHz, CDCl₃, δ in ppm): 165.50, 146.42, 142.73, 128.03, 127.62, 119.25, 114.35, 51.83, 51.21, 46.16, 42.28, 41.46; EI-MS: M⁺, m/z found: 259.1678 Da, calculated for C₁₅H₂₁N₃O: 259.1685 Da; IR: 2823, 1636, 1612, 1515, 1446, 1320, 1274, 1221, 1156, 1101, 1055, 1031, 1006, 964, 946, 897, 810, 786, 716 686, 641, 533, 499, 410 cm⁻¹

Poly[1-(4-(4-(dimethylamino)phenyl)piperazin-1-yl)acrylamide] (4)

Monomer **3** (134 mg, 0.52 mmol) and 2,2'-azobis(2-methylpropionitril) (6.5 mg, 0.08 eq.) were dissolved in 650 μL of anhydrous dioxan and stirred for 18 h at 80 °C. After cooling, the reaction mixture was added dropwise to 20 mL of stirred diethyl ether. The precipitate was filtered, washed with 5 mL of diethyl ether and dried under vacuum to obtain polymer **4** as beige solid (107 mg, 80 %).

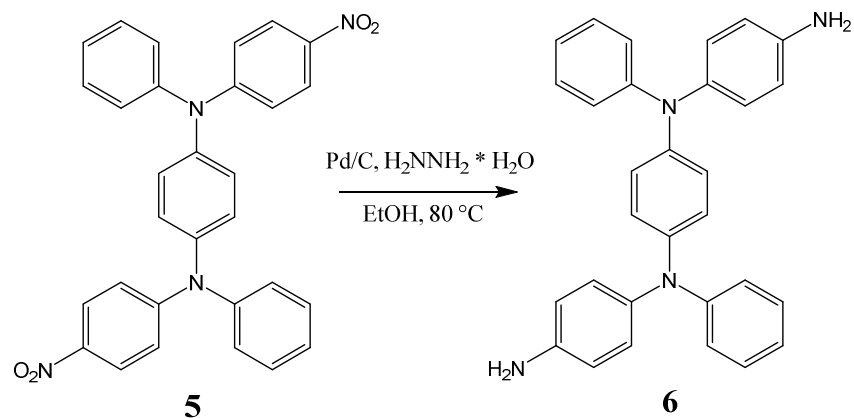
^1H NMR (300.36 MHz, CDCl_3 , δ in ppm): 7.00-6.49 (m, 4H), 4.14-3.27 (m, 4H), 3.18-2.60 (m, 10H), 2.10-1.05 (m, 3H); ^{13}C NMR (APT, 75.53 MHz, CDCl_3 , δ in ppm): 172.98, 146.06, 142.86, 119.12, 114.42, 51.57, 51.17, 45.72, 42.21, 41.51; SEC: $M_w = 36,000$ g/mol, $M_n = 20,000$ g/mol, PDI = 1.8; IR: 2800, 1636, 1515, 1441, 1320, 1274, 1226, 1152, 1027, 948, 814, 692, 544 cm^{-1}

N,N'-bis(4-nitrophenyl)-*N,N'*-diphenyl-*p*-phenylenediamine (**5**)⁹⁶

Commercially available *N,N'*-diphenyl-*p*-phenylenediamine was purified as described⁹⁶ prior to use.

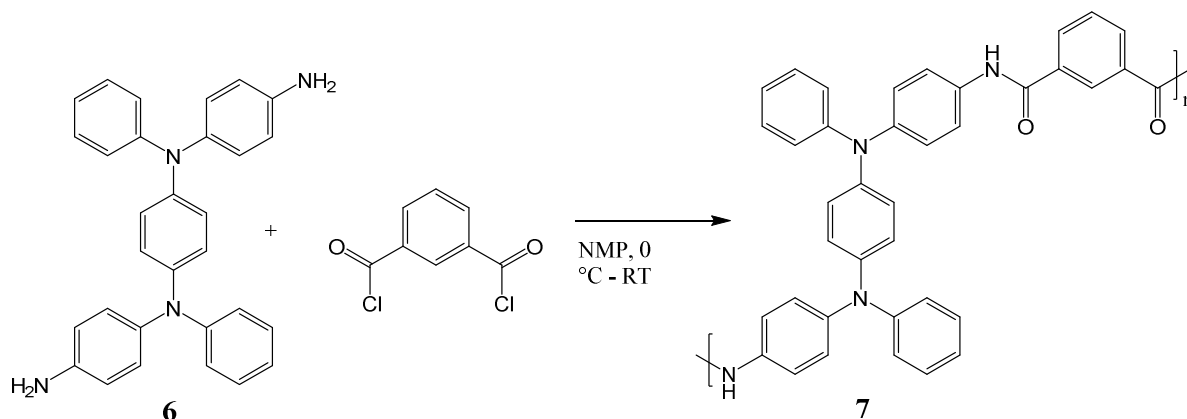
N,N'-diphenyl-*p*-phenylenediamine (2.03 g, 7.8 mmol) was dissolved in anhydrous DMSO (13.4 mL), potassium *tert*-butoxide (2.20 g, 2.5 eq.) and 1-fluoro-4-nitrobenzene (2.15 mL, 2.6 eq) were added and the reaction mixture was stirred for 17 h at 90 °C. The mixture was cooled to room temperature and added dropwise to 200 mL of a stirred solution of saturated aqueous NaCl. The resulting orange-brown precipitate was filtered, washed with 100 mL of water and dissolved in 100 mL of dichloromethane. The organic phase was washed 2 times with approximately 50 mL of water, dried over Na₂SO₄ and concentrated under reduced pressure. The crude product was dispersed in 100 mL of refluxing acetonitrile for 1 h, cooled, filtered and dried under vacuum to obtain compound **5** as orange-red solid (3.57 g, 91 %).

¹H NMR (300.36 MHz, DMSO-*d*₆, δ in ppm): 8.14-8.04 (m, 4H), 7.54-7.43 (m, 4H), 7.35-7.25 (m, 10H), 6.92-6.83 (m, 4H); ¹³C NMR (APT, 75.53 MHz, DMSO-*d*₆, δ in ppm): 153.18, 144.82, 142.38, 139.28, 130.37, 127.93, 127.00, 126.44, 125.65, 117.34; EI-MS: M⁺, *m/z* found: 502.1635 Da, calculated for C₃₀H₂₂N₄O₄: 502.1641 Da; IR: 1581, 1486, 1310, 1298, 1279, 1255, 1185, 1107, 997, 832, 749, 710, 691, 649, 553, 519, 502, 414 cm⁻¹

N,N'-bis(4-aminophenyl)-*N,N'*-diphenyl-*p*-phenylenediamine (**6**)⁹⁷

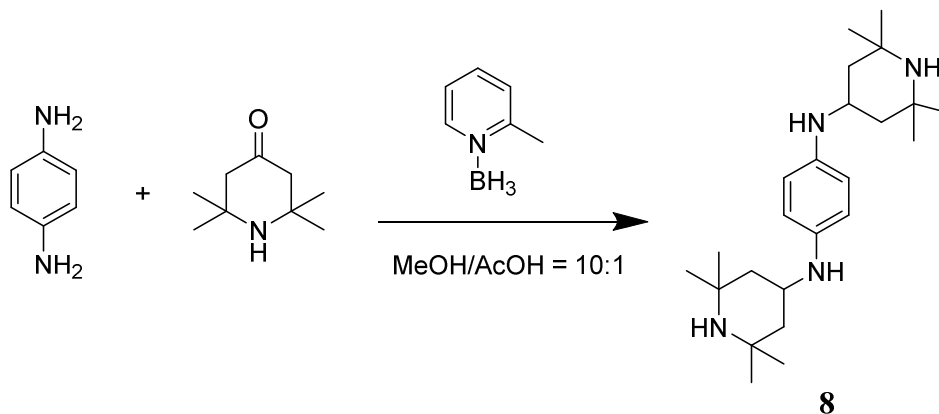
Compound **5** (1.52 g, 3 mmol) and Pd/C (80 mg, 5.3 wt-%) were dispersed in ethanol (10 mL), hydrazine hydrate (1.5 mL, 10.2 eq.) was added dropwise and the reaction mixture was stirred at 80°C for 17 h. After cooling, 20 mL of DMF were added, the mixture was filtered to remove the catalyst and washed thoroughly with approximately 30 mL of DMF. The filtrate was concentrated under reduced pressure, added dropwise to 100 mL of a stirred solution of saturated aqueous NaCl and the resulting precipitate was filtered. The crude product was slurried in 50 mL of boiling toluene for 3 h, cooled and filtered. This purifying procedure was repeated and the resulting solid was dried under vacuum to obtain compound **6** as beige solid (0.62 g, 46 %).

^1H NMR (300.36 MHz, $\text{DMSO-}d_6$, δ in ppm): 7.20-7.10 (m, 4H), 6.90-7.73 (m, 14H), 6.60-6.52 (m, 4H), 5.05 (s, 4H, $-\text{NH}_2$); ^{13}C NMR (APT, 75.53 MHz, $\text{DMSO-}d_6$, δ in ppm): 148.45, 146.11, 142.06, 135.27, 128.95, 127.91, 123.80, 119.95, 119.78, 115.0; EI-MS: M^+ , m/z found: 442.2146 Da, calculated for $\text{C}_{30}\text{H}_{26}\text{N}_4$: 442.2158 Da; IR: 3469, 3377, 3032, 1620, 1590, 1501, 1482, 1306, 1263, 1175, 1121, 1079, 1026, 834, 754, 723, 697, 665, 586, 534, 518, 507, 442, 409 cm^{-1}

Polyamide with TPPD-units (**7**)⁹⁷

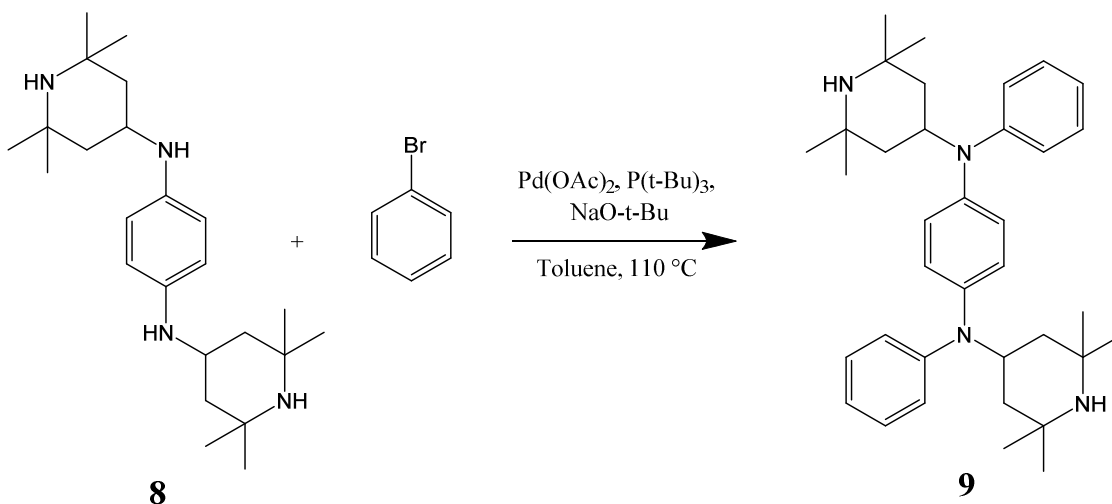
Monomer **6** (306 mg, 0.69 mmol) was dissolved in anhydrous NMP (1.85 mL), cooled to 0 °C and isophthaloyl dichloride (140 mg, 1 eq., recrystallized from n-hexane prior to use) was added in portions. The reaction mixture was gradually warmed up to room temperature with stirring. After 3 h the now highly viscous solution was added dropwise to 20 mL of stirred methanol. The precipitate was stirred in 20 mL of boiling methanol for 3 hours, filtered and dried under vacuum to obtain polymer **7** as green solid (389 mg, 98 %).

¹H NMR (300.36 MHz, DMSO-*d*₆, δ in ppm): 10.35 (s, 2H, -NH-CO-), 8.44 (s, 1H), 8.12-7.98 (m, 2H), 7.75-7.55 (m, 5H), 7.20 (br, 4H), 7.05-6.81 (m, 14H); ¹³C NMR (APT, 75.53 MHz, DMSO-*d*₆, δ in ppm): 164.78, 147.47, 142.97, 142.24, 135.19, 134.47, 129.40, 124.84, 124.49, 122.52, 121.72; IR: 3273, 3035, 1665, 1593, 1498, 1308, 1263, 1111, 827, 753, 718, 695, 522, 470, 411cm⁻¹

N,N'-bis(2,2,6,6-tetramethylpiperidin-4-yl)-*p*-phenylenediamine (**8**)

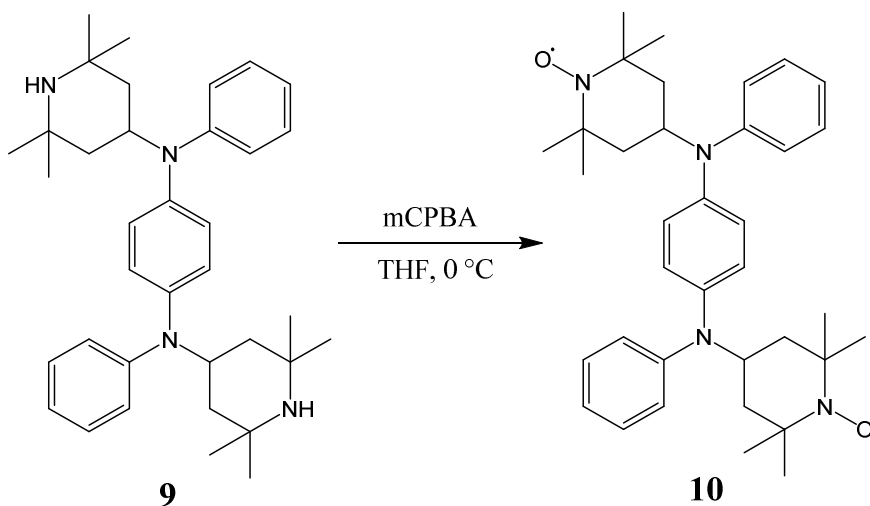
To 1,4-diaminobenzene (0.57 g, 5.3 mmol) and 2,2,6,6-tetramethylpiperidin-4-one (1.72 g, 2.1 eq.) in 31 mL of methanol/acetic acid (v/v = 10:1) was added 2-picolone-borane (1.19 g, 2.1 eq.) and the reaction mixture was stirred at room temperature. After 18 h the solvent was evaporated under reduced pressure and 1 M HCl (25 mL) was added under ice-cooling. The aqueous solution was stirred for 1 h and 1 M NaOH (approximately 26 mL) was added dropwise under ice-cooling to make the solution alkaline. The aqueous layer was extracted with ethyl acetate (3x50 mL) and the combined organic phases were dried over Na₂SO₄ and concentrated. The crude product was recrystallized from ethyl acetate (starting with 15 mL), filtered and dried under vacuum to obtain compound **8** as white crystals (1.52 g, 75 %).

¹H NMR (300.36 MHz, CDCl₃, δ in ppm): 6.55 (s, 4H), 3.70-3.51 (m, 2H), 2.93 (s, 2H, -Ph-NH-), 2.10-1.95 (m, 4H), 1.26 (s, 12H), 1.12 (s, 12H), 0.91-0.79 (m, 4H); ¹³C NMR (APT, 75.53 MHz, CDCl₃, δ in ppm): 139.532, 115.75, 51.42, 46.83, 46.52, 35.18, 28.81; EI-MS: M⁺, m/z found: 386.3404 Da, calculated for C₂₄H₄₂N₄: 386.3409 Da; IR: 3408, 2956, 2925, 1512, 1448, 1401, 1373, 1361, 1299, 1282, 1226, 1201, 1179, 1134, 1081, 1013, 957, 906, 811, 766, 686, 492, 466 cm⁻¹

N,N'-diphenyl-*N,N'*-bis(2,2,6,6-tetramethylpiperidin-4-yl)*p*-phenylenediamine (**9**)

To a solution of compound **8** (188 mg, 0.49 mmol), bromobenzene (123 μ L, 2.4 eq.) and sodium *tert*-butoxide (140 mg, 3 eq.) in 1 mL of anhydrous toluene was added a solution of Pd(OAc)₂ (1.25 mg, 0.01 eq.) and tri-*tert*-butylphosphine (14.6 μ L, 0.03 eq.) in 0.95 mL of anhydrous toluene, which has been stirred for 20 minutes at room temperature. The resulting reaction mixture was stirred at 110 °C for 18 h. After cooling 10 mL of toluene was added, the mixture was washed 3 times with 10 mL of brine, dried over sodium sulphate and evaporated to dryness. After column chromatography on silica (eluent: ethyl acetate + 2 vol-% triethylamine) compound **9** was obtained as off-white solid (195 mg, 74 %).

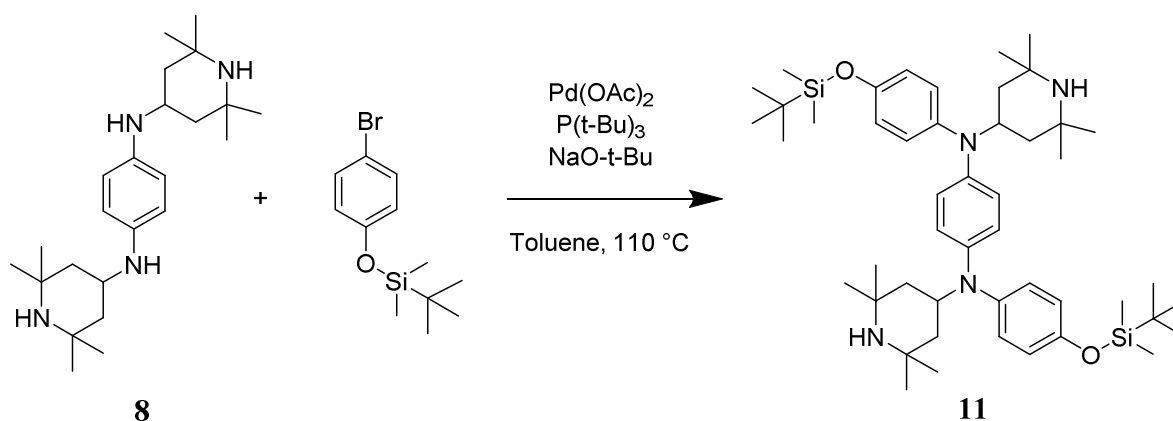
¹H NMR (300.36 MHz, Methanol-*d*₄, δ in ppm): 7.29-7.18 (m, 4H), 6.97-6.88 (m, 2H), 6.85-6.73 (m, 8H), 4.50-4.32 (m, 2H), 1.99-1.88 (m, 4H), 1.39 (s, 12H), 1.17-1.03 (m, 16H); ¹³C NMR (APT, 75.53 MHz, CDCl₃, δ in ppm): 146.94, 140.22, 129.33, 124.74, 121.47, 121.03, 51.72, 49.55, 43.70, 35.22, 28.75; EI-MS: M⁺, m/z found: 538.4038 Da, calculated for C₃₆H₅₀N₄: 538.4036 Da; IR: 2953, 1592, 1507, 1492, 1454, 1375, 1363, 1340, 1281, 1226, 1070, 1016, 988, 874, 800, 743, 702, 690, 646, 622, 566, 502 cm⁻¹

N,N'-diphenyl-*N,N'*-bis(2,2,6,6-tetramethylpiperidinyloxy-4-yl)-*p*-phenylenediamine (**10**)

Compound **9** (109 mg, 0.2 mmol) was dissolved in 1.6 mL of anhydrous THF and cooled to 0 °C. 3-Chloroperbenzoic acid (97 mg, 2.8 eq.) was added under stirring. After 3 h 10 mL of ethyl acetate was added and the mixture was washed with 10 mL of 1 M NaOH and 10 mL of brine. The organic phase was dried over sodium sulphate and evaporated to dryness. After column chromatography on silica (eluent: cyclohexane/ethyl acetate = 7/1) compound **10** was obtained as yellow solid (48 mg, 42 %).

EI-MS: M^+ , m/z found: 568.3798 Da, calculated for $C_{36}H_{48}N_4O_2$: 568.3777 Da; IR: 2964, 1594, 1508, 1491, 1379, 1365, 1259, 1188, 1167, 1083, 1014, 863, 795, 744, 699, 604, 541, 499 cm^{-1}

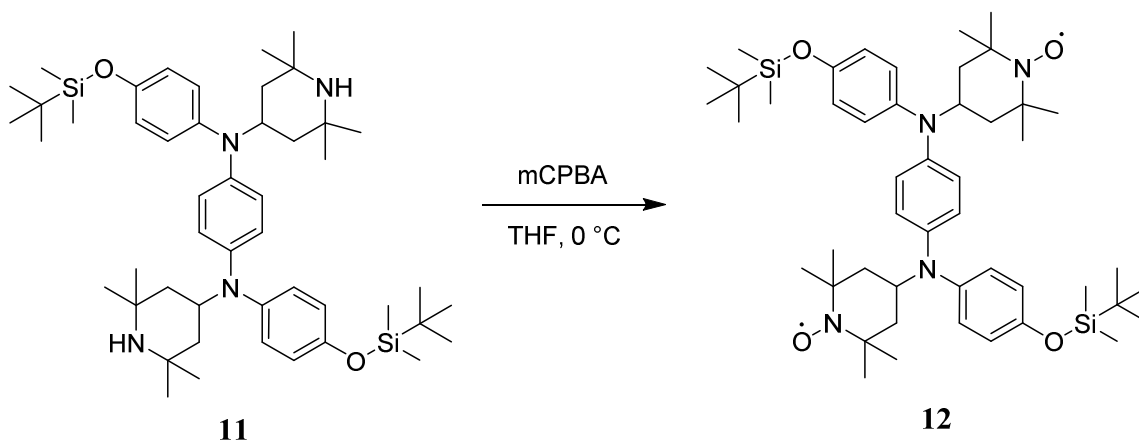
N,N'-bis(4-((*tert*-butyldimethylsilyl)oxy)phenyl)-*N,N'*-bis(2,2,6,6-tetramethylpiperidin-4-yl)-*p*-phenylenediamine (**11**)



To a solution of compound **8** (1.53 g, 4 mmol), (4-bromophenoxy)(*tert*-butyl)dimethylsilane (2.32 mL, 2.4 eq.) and sodium *tert*-butoxide (1.13 g, 3 eq.) in 10 mL of anhydrous toluene was added a solution of Pd(OAc)₂ (9 mg, 0.01 eq.) and tri-*tert*-butylphosphine (119 μL, 0.03 eq.) in 6 mL of anhydrous toluene, which has been stirred for 20 minutes at room temperature. The resulting reaction mixture was heated to 110 °C for 18 h. After cooling 10 mL of ethyl acetate was added, the mixture was washed 3 times with 20 mL of brine, dried over sodium sulphate and evaporated to dryness. The crude product was recrystallized from toluene (starting with 20 mL), filtered, washed 3 times with 10 mL of ethyl acetate and dried under vacuum to obtain compound **11** as white solid (2.02 g, 64 %).

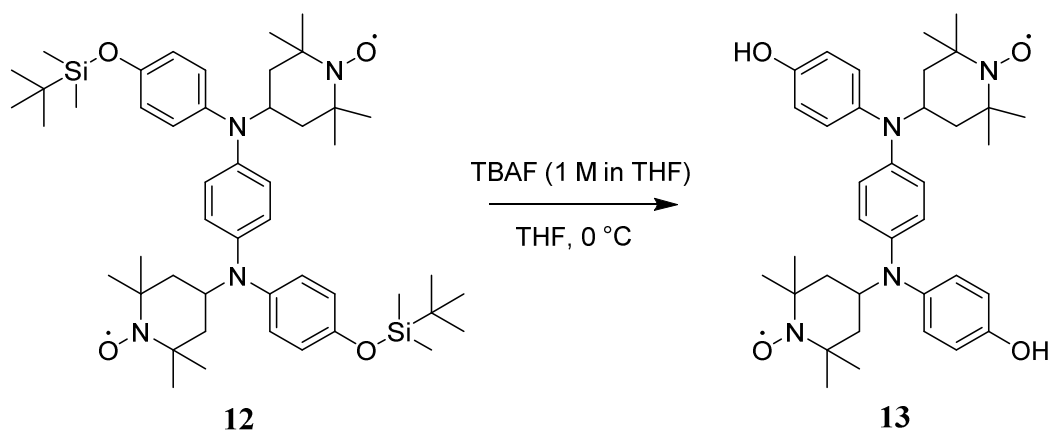
¹H NMR (300.36 MHz, CDCl₃, δ in ppm): 6.75 (s, 8H), 6.63 (s, 4H), 4.36-4.19 (m, 2H), 1.96-1.82 (m, 4H), 1.34 (s, 12H) 1.20-0.87 (m, 34H), 0.19 (s, 12H); ¹³C NMR (APT, 75.53 MHz, CDCl₃, δ in ppm): 150.97, 140.50, 140.12, 124.84, 122.12, 120.59, 51.81, 49.52, 43.62, 35.14, 28.63, 25.83, 18.30, -4.28; MALDI-MS: M⁺, m/z found: 798.5637 Da, calculated for C₄₈H₇₈N₄O₂Si₂: 798.5663 Da; 2927, 2856, 1602, 1499, 1388, 1362, 1253, 1161, 1095, 1070, 1009, 911, 870, 837, 780, 727, 658, 633, 536, 480 cm⁻¹

N,N'-bis(4-((*tert*-butyldimethylsilyl)oxy)phenyl)-*N,N'*-bis(2,2,6,6-tetramethylpiperidinyloxy-4-yl)-*p*-phenylenediamine (**12**)



Compound **11** (0.80 g, 1 mmol) was dissolved in 4 mL of anhydrous THF and cooled to 0 °C. 3.7 mL of 3-chloroperbenzoic acid in anhydrous THF (1.1 mmol/mL, 4.05 eq.) were added dropwise under stirring. 10 mL of ethyl acetate was added after 1.5 h and the mixture was washed with 10 mL of saturated NaHCO₃ and 10 mL of brine. The organic phase was dried over sodium sulphate and evaporated to dryness. After column chromatography on silica (eluent: cyclohexane/ethyl acetate = 5/1) compound **12** was obtained as slightly pink-white solid (0.52 g, 63 %).

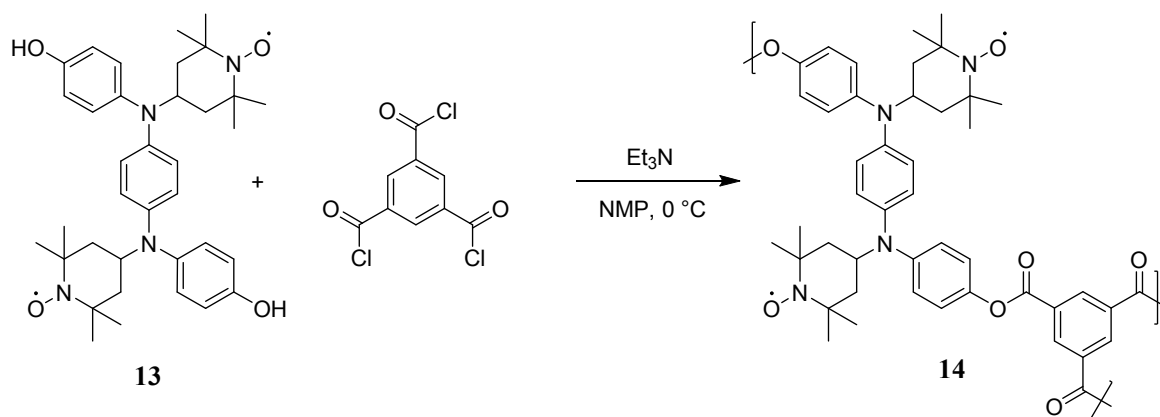
MALDI-MS: M⁺, m/z found: 828.5384 Da, calculated for C₄₈H₇₆N₄O₄Si₂: 828.5405 Da; IR: 2928, 2857, 1606, 1500, 1461, 1361, 1248, 1231, 1180, 1097, 1005, 913, 837, 778, 742, 703, 615, 561 cm⁻¹

N,N'-bis(4-phenol)-*N,N'*-bis(2,2,6,6-tetramethylpiperidinyloxy-4-yl)-*p*-phenylenediamine (**13**)

Monomer precursor **12** (1.88 g, 2.3 mmol) was dissolved in 11.3 mL of anhydrous THF and cooled to 0 °C. 7.9 mL of a solution of tetra-*n*-butylammonium fluoride in THF (1 M, 3.5 eq.) were added dropwise under stirring. The color of the reaction mixture immediately changed to deep blue. After 1 h 20 mL of saturated aqueous ammonium chloride was added to the reaction mixture. The mixture was extracted 3 times with 20 mL of ethyl acetate and washed 3 times with approximately 50 mL of brine. The organic phase was dried over sodium sulphate and evaporated to dryness. The crude product was dispersed in 50 mL of water and stirred for 2 h, filtered and dried under vacuum to obtain compound **13** as blue solid (1.24 g, 91 %).

MALDI-MS: M^+ , m/z found: 600.3684 Da, calculated for $C_{36}H_{48}N_4O_4$: 600.3676 Da

IR: 3236, 2973, 1733, 1593, 1499, 1462, 1355, 1298, 1263, 1225, 1175, 1076, 921, 881, 840, 821, 803, 753, 715, 649, 560, 521, 465 cm^{-1}

Polyester with TPPD- and TEMPO-units (14)

Monomer **13** (347.97 mg, 0.19 mmol) was dissolved in 2 mL of anhydrous NMP. Triethylamine (242 μ L, 3 eq.) was added and the reaction mixture was cooled to 0 °C. Benzene-1,3,5-tricarbonyl trichloride (103.05 mg, 0.667 eq.) was dissolved in 0.9 mL of anhydrous NMP and added dropwise upon stirring. After about 10 minutes gelation occurred. The gel was added to 40 mL of methanol, stirred for 1 h, filtered, washed 3 times with 10 mL of methanol and dried under vacuum to obtain polymer **14** as a greyish-blue solid (286.61 mg, 64 %).

IR: 2970, 1737, 1684, 1609, 1499, 1354, 1193, 1096, 912, 810, 731, 559, 469 cm^{-1}

4 Results and Discussion

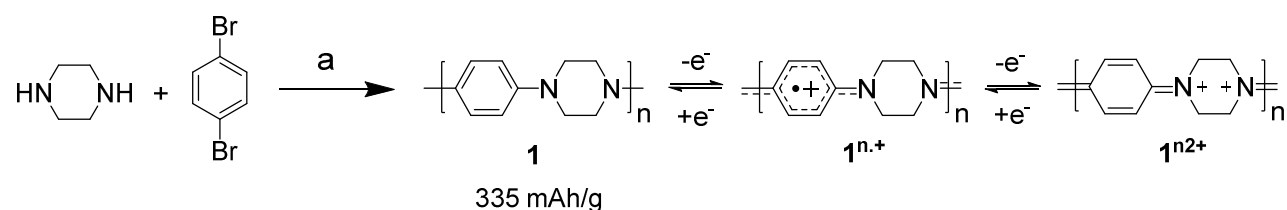
4.1 Polymers with TAPD-units

Polymers containing tetrasubstituted p-phenylenediamine (TSPD) units have been studied as electrochromic materials^{89–92} and a utilization as charge storage material has been described recently⁹⁴ (compare 2.3).

Polymers containing tetraalkyl-p-phenylenediamine (TAPD) groups can reach high theoretical capacities due to the low molecular weight of the repeating unit and the two-electron electrochemistry.

4.1.1 TAPD-units in the main-chain

Scheme 15 outlines the synthetic route for polymer **1** which was obtained via a Buchwald-Hartwig polycondensation of piperazine and 1,4-dibromobenzene as beige insoluble solid. It has a high theoretical capacity of 334.6 mAh/g. The anticipated redox reactions for charging are the formation of a radical-cationic ($\mathbf{1}^{n\cdot+}$) and a dicationic (quinone diimine, $\mathbf{1}^{n2+}$) species via two one-electron redox steps (Scheme 15).



Scheme 15: Synthetic route and redox couples for polymer **1** – (a) Pd(OAc)₂, P(t-Bu)₃, NaO-t-Bu, Toluene, 110 °C

Polymer **1** was not accessible for the most commonly used characterization techniques like NMR, SEC or cyclic voltammetry in solution because of its insolubility, resulting from the rigid structure. But a comparison of the ATR-IR-spectra of piperazine and polymer **1** shows the absence of the N-H stretch – peak for the polymer, indicating that a polycondensation took place (Figure 2).

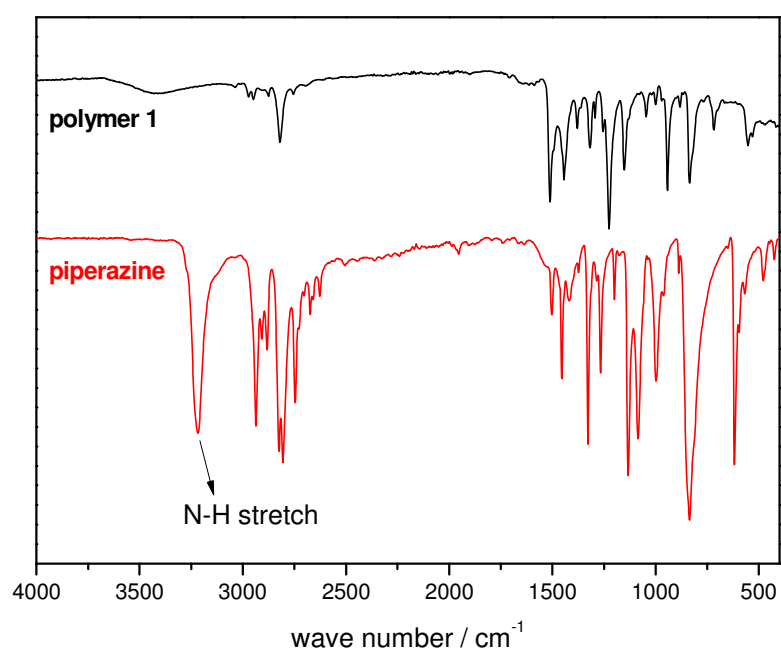


Figure 2: IR spectra of polymer **1** and piperazine

Composite cathodes containing 25 wt-% of polymer **1**, 20 wt-% PVdF and 55 wt-% Super P[®] were fabricated and characterized in half-cells (Swagelok[®]) with Lithium as counter and reference electrode according to general half-cell procedure (compare 3.1.2).

The cyclic voltammogram (CV) shows one irreversible oxidation peak at a potential of $E_{1,ox} = 3.43$ V vs. Li/Li^+ in the first scan (Figure 3). It is ascribed to the first oxidation-step of the TSPD-unit (formation of $\mathbf{1}^{n+}$), which should occur approximately at this potential vs. Li/Li^+ (compare 4.2, Figure 8). The second scan shows almost no electrochemical activity, indicating electrochemical instability of the TSPD-groups in polymer **1**. A possible explanation is the occurrence of side reactions/ rearrangements of the electrochemically formed radical cations.

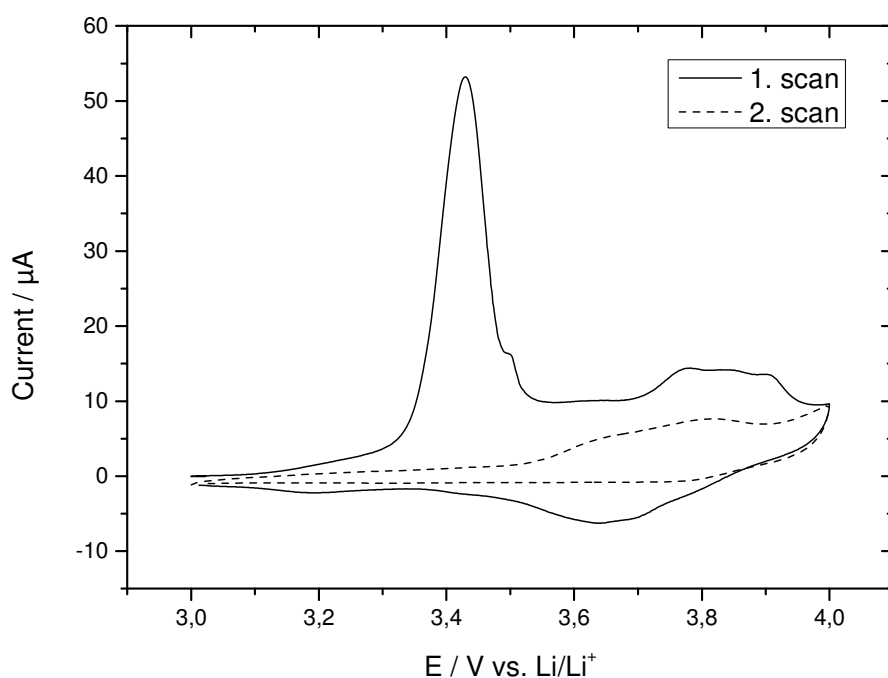


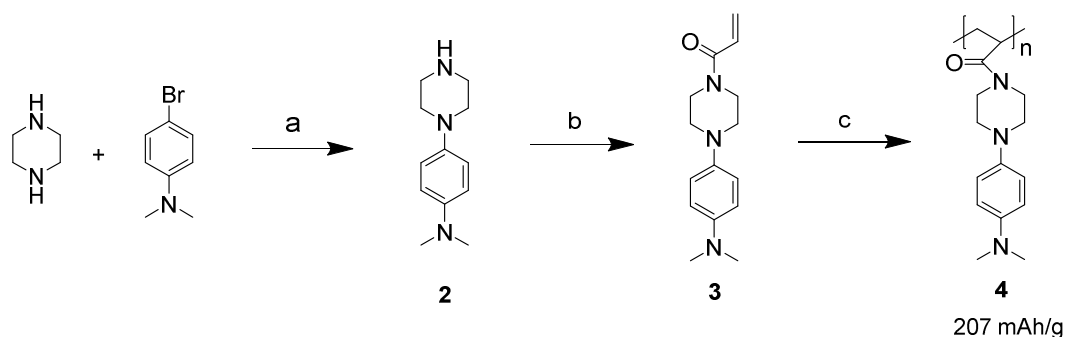
Figure 3: Cyclic voltammogram of a composite cathode containing polymer **1** as active material (scan rate $v = 0.1$ mV/s)

4.1.2 TAPD-units in the side-chain

As alternative approach a less rigid polymer with TAPD-units in the side-chain was synthesized due to the insolubility and unsatisfactory electrochemical properties of polymer **1**.

Scheme 16 outlines the synthetic route for polymer **4**. The first step was a Buchwald-Hartwig amination of piperazine with 4-bromo-N,N-dimethylaniline. In the next step a nucleophilic substitution with acryloyl chloride was used to synthesize monomer **3**, which was subsequently polymerized using 2,2'-Azobis(2-methylpropionitrile) (AIBN). The resulting polyacrylamide **4** has tetraalkyl-p-phenylenediamine (TAPD) units in side-chains, a theoretical capacity of 207 mAh/g, and is soluble in THF and chloroform.

The number and weight average molar masses (M_n and M_w) determined by size exclusion chromatography (SEC) were 20,000 and 36,000 g/mol (PDI = 1.8), respectively.



Scheme 16: Synthetic route for polymer **4** – (a) Pd(OAc)₂, P(t-Bu)₃, NaO-t-Bu, Toluene, 110 °C, (b) Acryloyl chloride, Et₃N, CH₂Cl₂, 0 °C, and (c) AIBN, Dioxan, 80 °C

Cyclic voltammetry of polymer **4** was performed according to general procedure (compare 3.1.1). The cyclic voltammogram of polymer **4** in solution at a scan rate (v) of 50 mV/s shows redox couples at formal potentials of $E^{O'}_1 = -0.08$ V and $E^{O'}_2 = 0.35$ V vs. Ag/AgNO₃ (Figure 4).

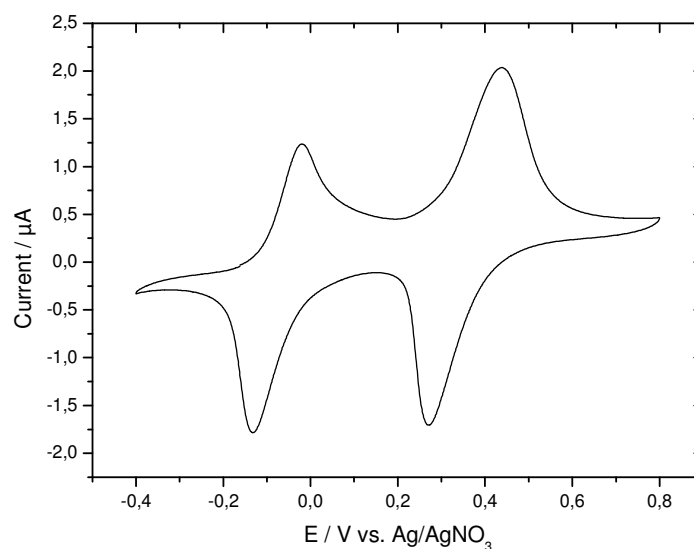
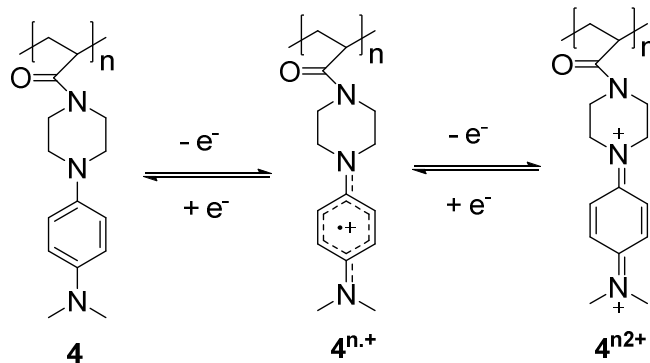


Figure 4: Cyclic voltammogram of polymer **4** in solution ($v = 50$ mV/s, 1 mM in CHCl_3 containing 0.1 M TBAP)

This behavior is characteristic for TSPD-units and corresponds to the formation of $\mathbf{4}^{n,+}$ and $\mathbf{4}^{n2+}$ (Scheme 17).



Scheme 17: Redox couples of polymer **4**

Cyclic voltammograms at lower scan rates revealed an irreversibility of the electrochemical behavior, indicated by a rapid decrease of peak currents over the first 5 scans (Figure 5a, $v = 20$

mV/s). In the solid state, this occurred already in the first scan and even at higher scan rates. Figure 5b shows the corresponding CV of polyacrylamide **4** spincoated on an ITO-coated glass substrate, which was used as working electrode (similar to the characterization of electrochromic polymers reported in the literature⁸⁹, compare 3.1.1).

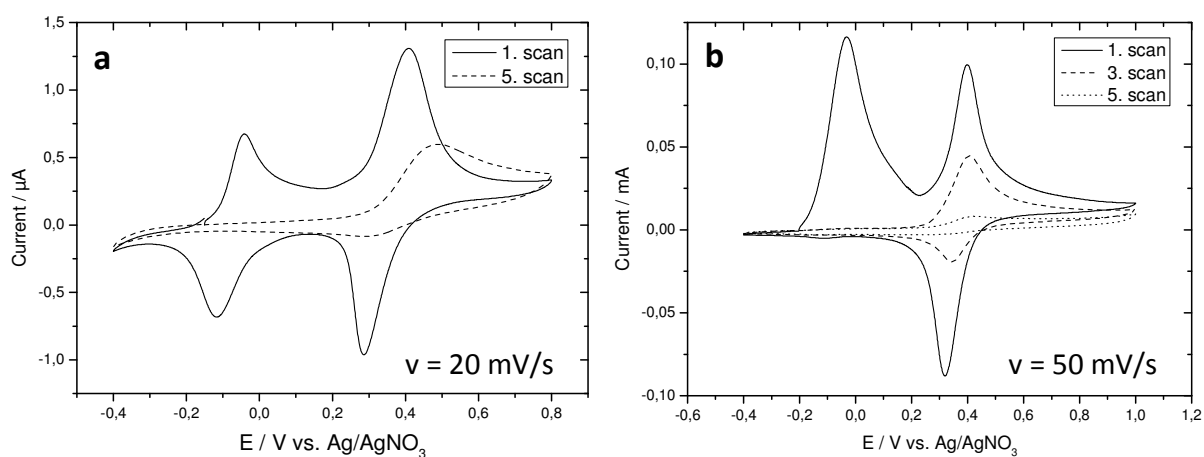


Figure 5: Cyclic voltammograms of polymer **4** (a) in solution ($v = 20$ mV/s, 1 mM in CHCl_3 containing 0.1 M TBAP) and (b) on ITO ($v = 50$ mV/s, electrolyte: 0.1 M TBAP in acetonitrile)

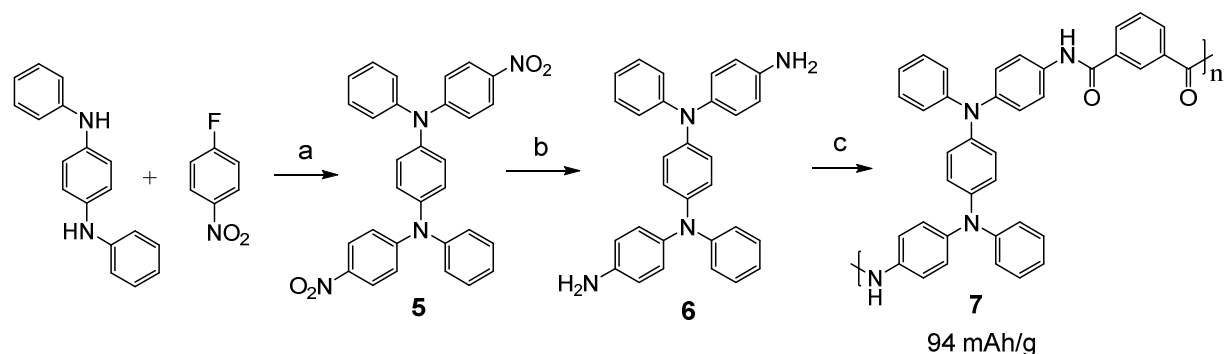
The irreversible behavior probably occurs due to side reactions/rearrangements of the electrochemically formed radical cations, that were not further investigated within this work.

4.2 Polymer with TPPD-units

Alternative structures with aromatic groups were considered due to the electrochemical instability of polymers **1** and **4**, which are based on tetraalkyl-p-phenylenediamine units. Examples for stable electrochromic polymers based on tetraphenyl-p-phenylenediamine (TPPD) units were found in the literature.^{89,91,92}

4.2.1 Synthesis of polymer **7**

Scheme 18 outlines the synthetic route for monomer **6** and the correspondent polyamide **7**, which were synthesized according to literature^{96,97}, with slight modifications. The first step was a double N-arylation of N,N'-diphenyl-p-phenylenediamine with 1-fluoro-4-nitrobenzene. The nitro groups of compound **5** were reduced with hydrazine hydrate and Pd/C, and subsequently a polycondensation with isophthaloyl dichloride yielded polyamide **7**, which has a theoretical capacity of 93.6 mAh/g. Polymer **7** is soluble in DMF, DMSO and NMP, but insoluble in ethylene carbonate (EC)/diethyl carbonate (DEC) (3/7 v/v), where only swelling was observed.



Scheme 18: Synthetic route for monomer **6** and polyamide **7** – (a) KO-t-Bu, DMSO, 90 °C, (b) H₂NNH₂*H₂O, Pd/C, EtOH, 80 °C, (c) isophthaloyl dichloride, NMP, 0 °C - RT

4.2.2 Electrochemical behavior of polymer **7**

An ITO-coated glass substrate was dropcoated with polyamide **7** (in DMF) and used as working electrode in cyclic voltammetry experiments according to general procedure (compare 3.1.1). The CV shows the two redox couples at formal potentials of $E^{0'}_1 = 0.21$ V and $E^{0'}_2 = 0.57$ V vs. Ag/AgNO₃ (Figure 6). It is important to note, that no changes were observed at lower scan rates (CVs not shown).

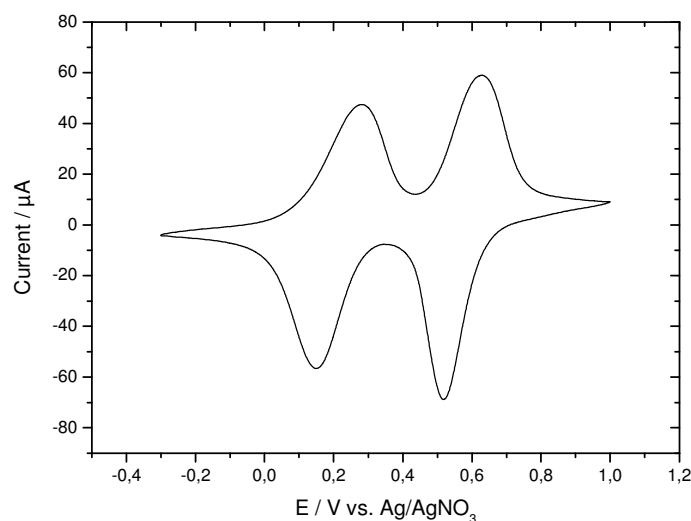
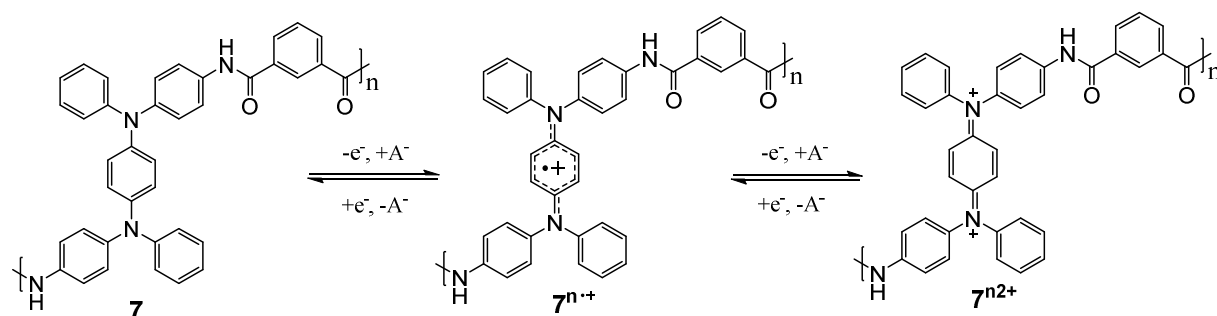


Figure 6: Cyclic voltammogram of polyamide **7** on ITO ($v = 50$ mV/s, 0.1 M TBAP in acetonitrile)

Upon charging the TPPD-groups are oxidized in two one-electron oxidation-steps resulting in the formation of a radical cationic ($\mathbf{7}^{n\cdot+}$) and dicationic (quinone diimine, $\mathbf{7}^{n2+}$) species, respectively (Scheme 19). This is accompanied by electrolyte salt anion A^- association to neutralize the charges. Upon discharging reduction of $\mathbf{7}^{n2+}$ to $\mathbf{7}^{n\cdot+}$ and $\mathbf{7}^{n\cdot+}$ to **7**, respectively, occurs and the anions A^- are ejected back into the electrolyte.



Scheme 19: Redox couples of polyamide **7** (A^- ...electrolyte salt anion)

4.2.3 Composite cathodes of polymer **7** - morphology

Composite cathodes containing 25 - 60 wt-% of polymer **7**, 10 - 20 wt-% PVdF and 30 - 70 wt-% Super P[®] were fabricated (Table 1) and characterized according to general half-cell procedure (compare 3.1.2).

Table 1: Cathode compositions

Composition	Active material / wt-%	PVdF / wt-%	Super P [®] / wt-%	Current collector
A	25	20	55	carbon-coated Al
B	20	10	70	Al
C	40	10	50	Al
D	60	10	30	Al

Scanning electron microscopy (SEM) was used to study the morphology of composite cathode **A** and Super P[®] (Figure 7), since the morphology is a crucial parameter for the application in secondary batteries.

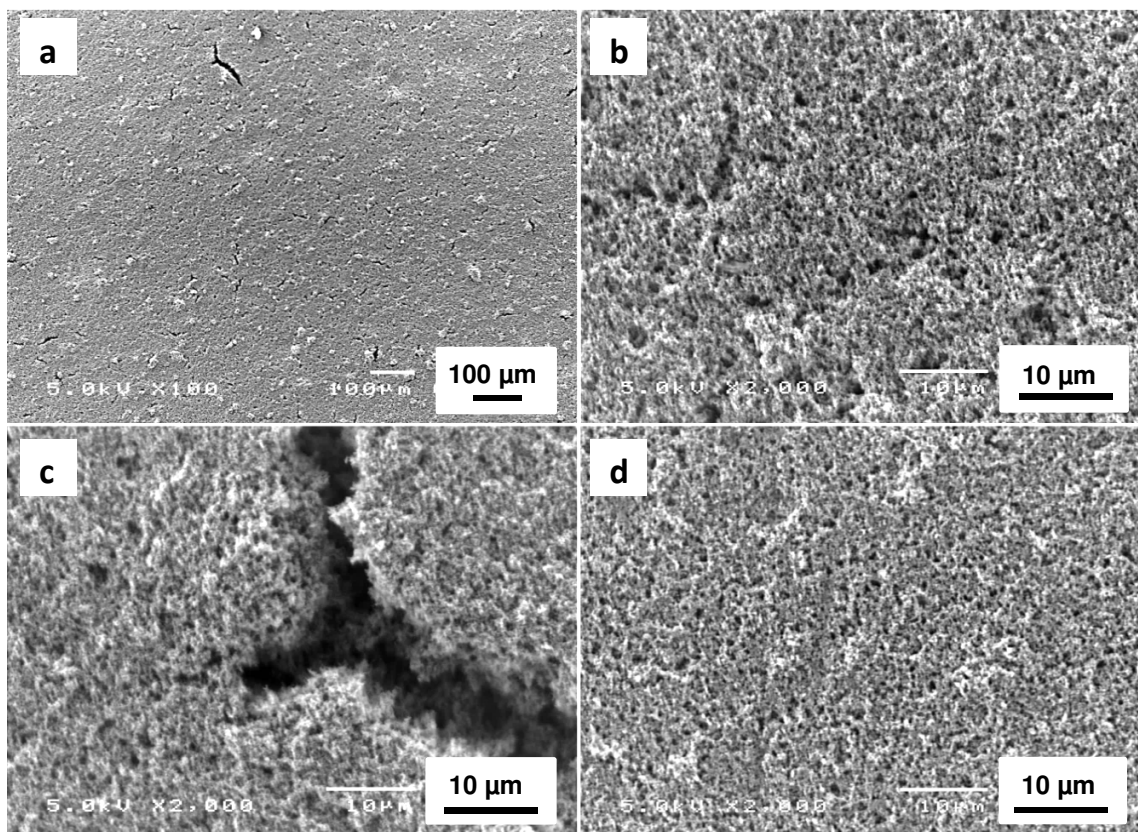


Figure 7: SEM images of (a-c) composite cathode **A** and (d) Super P®

The SEM images of composite cathode **A** show a porous structure (Figure 7a,b), with occasional cracks (Figure 7c). The morphology is mainly dominated by the conductive additive Super P® (Figure 7d). The ‘open structure’ with pores is promising because it facilitates electrolyte infiltration. The ions of the electrolyte salt (e.g. LiPF₆) neutralize the charges formed upon charging/oxidation of the polymer and play an important role in the charge transport processes.^{76,93} A porous structure is also attended by a higher surface area, which should assist good contacting between the polymer and the conductive additive.

4.2.4 Composite cathodes of polymer **7** – basic electrochemistry

The cyclic voltammogram of composite cathode **A** containing polyamide **7** as active material shows the characteristic redox couples at formal potentials of $E^{0'}_1 = 3.42$ V and $E^{0'}_2 = 3.78$ V vs. Li/Li⁺ (Figure 8).

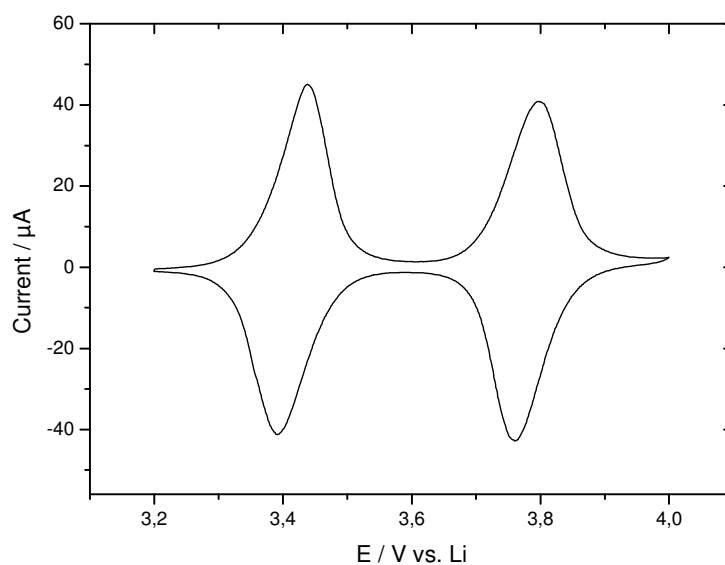


Figure 8: Cyclic voltammogram of composite cathode **A** containing polyamide **7** as active material ($\nu = 0.1$ mV/s)

The peak-potential separations ΔE_p were 48 mV for the first and 39 mV for the second redox step at a scan-rate of 0.1 mV/s, indicating fast electron transfer. This is promising for the application in secondary batteries because fast electron transfer is essential for fast charging/discharging of cells for high-power applications.

Thus, the electrochemical behavior was investigated in more detail. Cyclic voltammograms at different scan rates (0.1 – 22 mV/s) were recorded and are depicted in Figure 9.

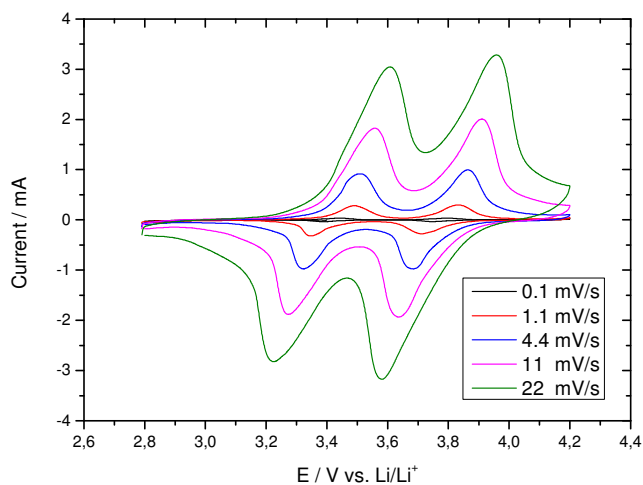


Figure 9: Cyclic voltammograms at different scan rates of composite cathode **A** containing polyamide **7** as active material

Table 2 gives the results obtained for ΔE_p as function of the scan rate. The peak-potential separation ΔE_p increases with increasing scan rate from 57 and 51 mV ($v = 0.1$ mV/s) to 387 and 379 mV ($v = 22$ mV/s) for the two redox couples.

This probably results from ionic resistance due to a limitation of counter ion mobility in the swollen active material layers, thus influencing the charge transport processes, as reported for gel electrodes containing polyradicals.⁷⁶

Table 2: Peak-potential separation ΔE_p at different scan rates

scan rate	ΔE_p / mV	
	1. redox couple	2. redox couple
0.1	57	51
0.2	99	73
1.1	143	119
2.2	150	141
4.4	185	183
11	286	275
22	387	379

The interpretation is also supported by cyclic voltammograms of a composite cathode **A** which was allowed to rest for 72 hours prior to measurement in comparison to one that was measured without a resting step (Figure 10, $v = 1.1$ mV/s).

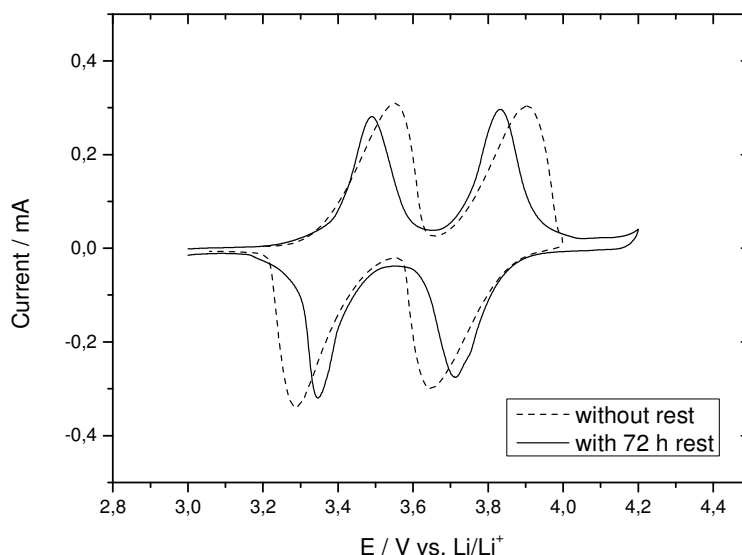


Figure 10: Cyclic voltammograms of composite cathodes **A** with and without a 72 hour resting step ($v = 1.1$ mV/s)

In this experiment, ΔE_p values for the two redox couples decreased from 266 and 258 mV, respectively, to 143 and 119 mV, respectively, after a resting step of 72 hours. The results indicate faster electron transfer, which can be ascribed to the higher counter ion mobility in the entirely electrolyte-swollen or gel-like polymer layers.

4.2.5 Composite cathodes of polymer 7 - battery testing

One of the advantages of (most) organic electrode materials in comparison to inorganic intercalation materials is the fast electron transfer, resulting in significantly better high-rate capabilities and thus higher power densities.

Polymer **7** (composition **A**) showed very good high-rate capability, as a test with rates of 1 to 100 C (charging/discharging of the half-cell in one hour at 1 C, 36 seconds at 100 C) revealed (3.2-4.0 V vs. Li/Li⁺, Figure 11). The specific discharge capacity at 1 C was 87.7 mAh/g (10th cycle), which corresponds to 94 % of the theoretical value. The capacity retention at 100 C (corresponding to a current density of approximately 2.3 mA/cm²) was 70 % compared to the capacity at 1 C. Note that the discharge capacities at 1 C taken at the end of the test corresponded well to those from the beginning. The results are summarized in Table 3.

Table 3: Discharge capacities at different C-rates

Rate	1 C	5 C	10 C	50 C	100 C
Discharge capacity / mAh/g (10 th cycle)	87.7	84.9	82.0	71.8	61.2
Percentage compared to 1 C	100	97	94	82	70

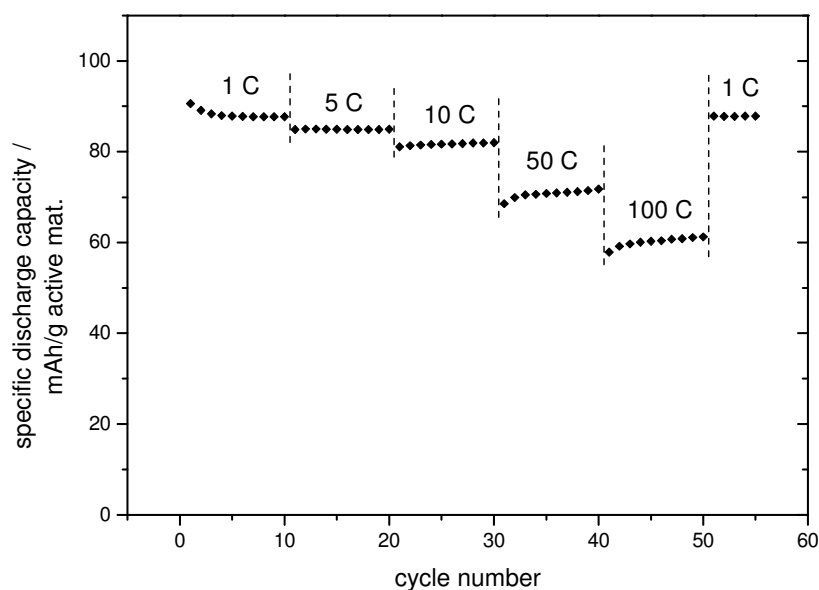


Figure 11: Rate capability test (3.2-4.0 V vs. Li/Li⁺) of composite cathode **A** containing polyamide **7** as active material

The great high-rate capability/capacity retention at high current rates of polymer **7** is comparable to very promising polymers applied in organic radical batteries.^{58,71}

Figure 12 depicts the corresponding charge/discharge curves at rates of 1, 10 and 100 C. At 1 and 10 C average charge/discharge potentials of approximately 3.4 and 3.8 V (vs. Li/Li⁺) were observed. This is in good agreement with the results from cyclic voltammetry shown in Figure 8. At 100 C the average discharge potentials drop to approximately 3.7 and 3.3 V, respectively, and the charge potentials increase to approximately 3.5 and 3.85 V, respectively. The voltage plateaus are less distinct.

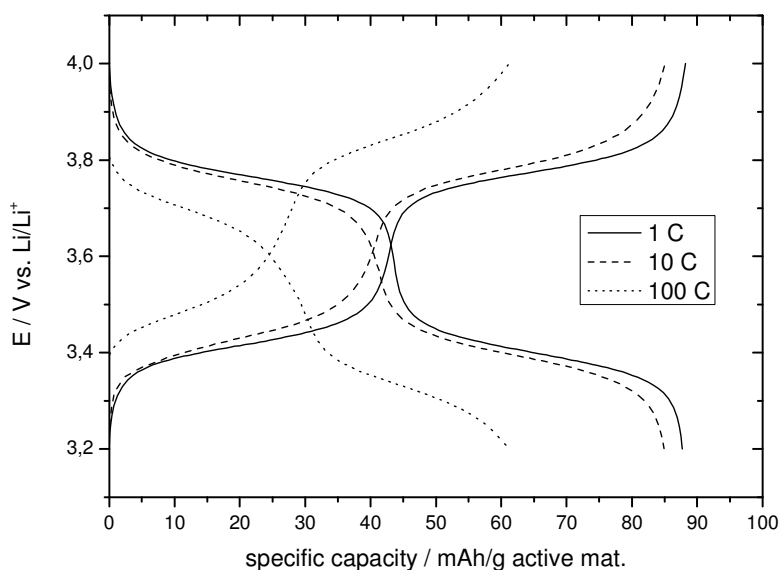


Figure 12: Charge/discharge curves at different C-rates of composite cathode **A** containing polyamide **7** as active material

The separations between the average charge and discharge potentials (ΔE_{ave}) at different C-rates are summarized in Table 4. At 1 C ΔE_{ave} values are very low with 14 mV for the first and 4

mV for the second redox step. ΔE_{ave} values at 100 C increase to 163 mV and 153 mV, respectively.

Table 4: Separation between the average charge and discharge potentials (ΔE_{ave})

C-rate	$\Delta E_{\text{ave}} / \text{mV}$	
	1. redox couple	2. redox couple
1	14	4
5	32	37
10	41	51
50	113	110
100	163	153

These low values of ΔE_{ave} further highlight the fast electron transfer resulting in high specific power densities for polymer **7**. Figure 13 depicts the ragone plots (energy vs. power density) for composite cathode **A** normalized to the weight of (a) the active material and (b) the composite.

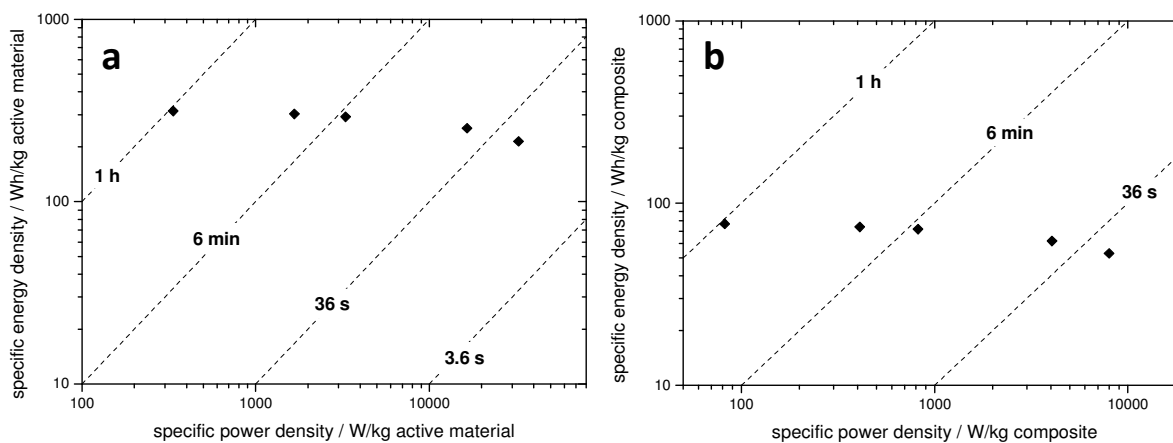


Figure 13: Ragone plots for composite cathode **A** containing polyamide **7** as active material normalized to the weight of (a) the active material and (b) the composite

At a charge rate of 100 C a specific discharge capacity of 61 mAh/g (70 % of that observed at 1 C) was obtained, corresponding to a specific power density of about 32.7 kW/kg with a specific

energy density of 212 Wh/kg, in reference to the active material content (Figure 13a). When normalized to the weight of the composite a specific power density of about 8 kW/kg (with a specific energy density of about 53 Wh/kg) was obtained (Figure 13b), which is high compared to Lithium-ion batteries (about 0.3 to 1 kW/kg) and comparable to electrochemical capacitors. The advantage over electrochemical capacitors is the higher specific energy density.

Constant current cycling of a half-cell (composition **A**) at 1 C (charging/discharging in one hour) between 3.2 and 4.0 V was performed and the results are shown in Figure 14.

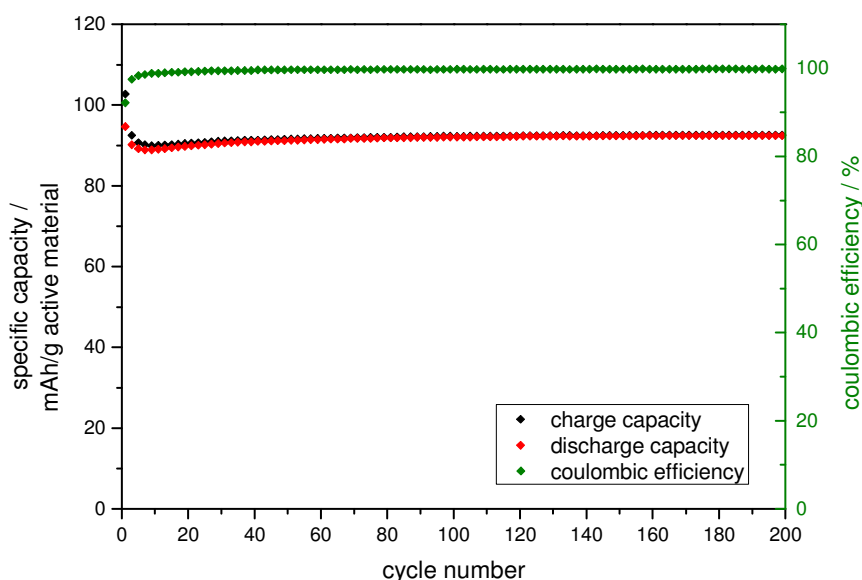


Figure 14: Constant current cycling at 1 C of composite cathode **A** containing polyamide **7** as active material

The initial specific discharge capacity was 94.7 mAh/g, which is a little bit higher than the theoretical value (93.6 mAh/g). A decrease to 88.9 mAh/g occurred during the first 10 cycles, which is interpreted as dissolution of low molecular weight fractions of the polymer into the electrolyte. After the 10th cycle the specific discharge capacity increases gradually to 92.5

mAh/g ($\approx 99\%$ of the theoretical value). The increase is ascribed to a better swelling of the polymer with repeated cycling. Coulombic efficiencies are $\geq 99\%$ after the 10th cycle and increase to $\geq 99.8\%$ after 100 cycles. This first test already shows the excellent reversibility and cycle stability of polymer **7**.

SEM images of the composite cathode before and after constant current cycling (200 cycles, 1 C) showed no major differences in morphology (Figure 15). The roughness and porosity appeared to be a bit higher after cycling, which is ascribed to swelling of the polymer in the electrolyte.

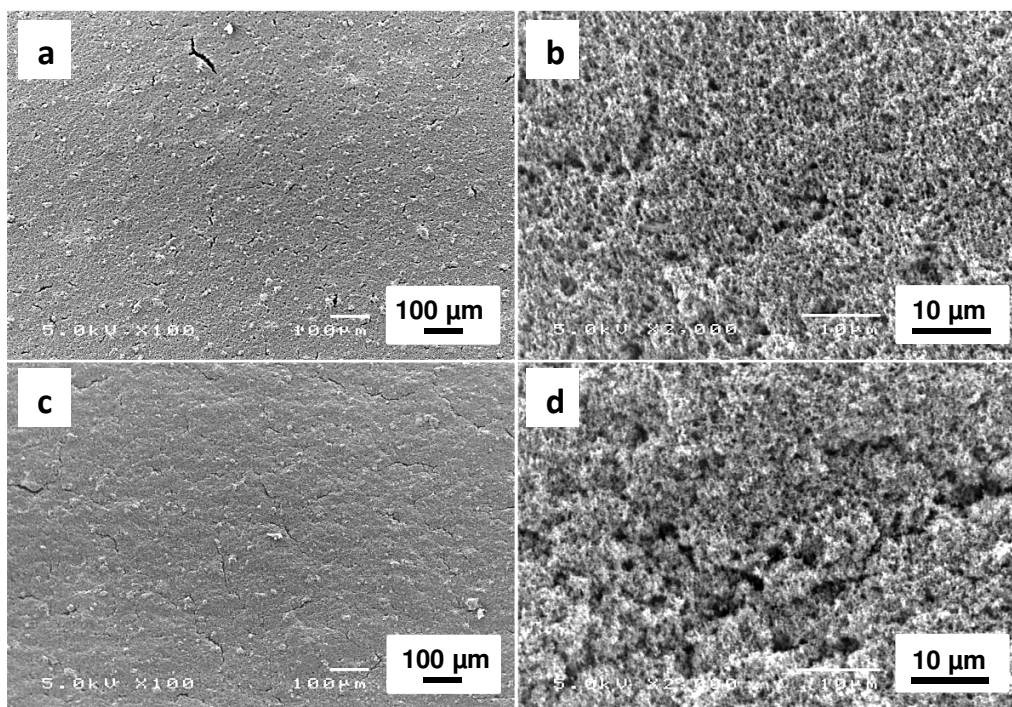


Figure 15: SEM images of composite cathode **A** (a+b) before and (c+d) after constant current cycling at 1 C for 200 cycles

Subsequently long-term constant current cycling at 10 C was performed to further test the cycle stability of polymer **7** (Figure 16). After an initial specific discharge capacity of 87.6 mAh/g a decrease over the first 20 cycles to 74.2 mAh/g was observed (Figure 16, inset), similar to the tests at 1 C (Figure 14). Upon further cycling an increase in capacity was observed, which reached a plateau of 79.0 mAh/g after about 1000 cycles. This value almost coincides with the value from the rate capability test (82 mAh/g at 10 C, Table 3).

The specific discharge capacity after 11,000 cycles was 70.5 mAh/g, which corresponds to 89 % of the plateau and 75 % of the theoretical value.

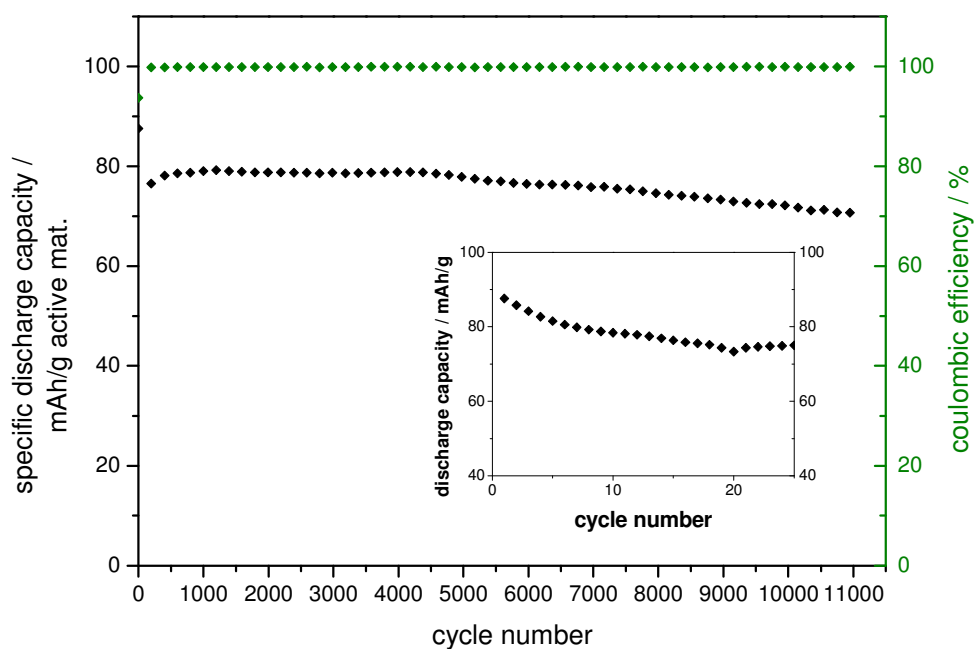


Figure 16: Constant current cycling at 10 C of a composite cathode **A** containing polyamide **7** as active material. The inset shows the first 25 cycles in more detail

The excellent cycle stability with almost 90 % of capacity retention after 11,000 cycles is remarkable when compared to inorganic electrode materials used, e.g. in Li-ion batteries, and is also high compared to other organic electrode materials like polyradicals.

Another important aspect for the evaluation of organic electrode materials is the electrochemical stability, especially when cycled to and held at high potentials. Potentials close/slightly above 4 V (vs. Li/Li⁺) can lead to a degradation of some organic electrode materials, e.g. conducting polymers.

IU-charging was performed for half-cells with composite cathodes **A** containing polyamide **7** as active material, and for comparison with a composite cathode containing polynorbornene substituted with TEMPO-units (**PN**, Scheme 10) as active material (**PN**/Super P[®]/binder = 10:80:10 wt-%). IU-charging combines constant current and constant voltage charging (CCCV). Battery cells are charged with a constant current until a cut-off potential is reached. The potential is held constant for a specified time or until the current decreases to a specified value.

In this experiment half-cells were charged with a constant current of 1 C until the cut-off potential of 4.0 V (vs. Li/Li⁺) was reached. The potential was held constant for 2 hours (polyamide **7**) and 1 hour (**PN**), respectively. The half-cells were discharged with a constant current of 1 C. Figure 17 depicts the current-voltage characteristics.

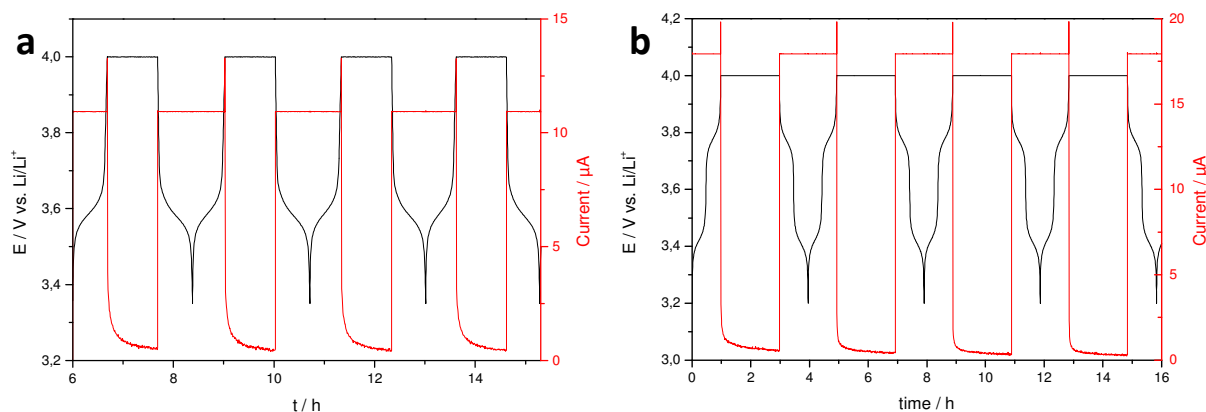


Figure 17: Current-voltage characteristic of IU-charging of half-cells with composite cathodes containing (a) **PN** (1 C, cut-off potential: 4.0 V vs. Li/Li⁺, 1h) and (b) polyamide **7** (1 C, cut-off potential: 4.0 V vs. Li/Li⁺, 2h) as active material (composition **A**)

Composite cathodes containing **PN** as active material showed a decrease of capacity to about 20 % over the first 20 cycles (Figure 18). This clearly indicates that degradation takes place under the IU-charging conditions. The behavior is assigned to an electrochemical instability of either the polymer backbone or the TEMPO-units when held at high potentials vs. Li/Li^+ .

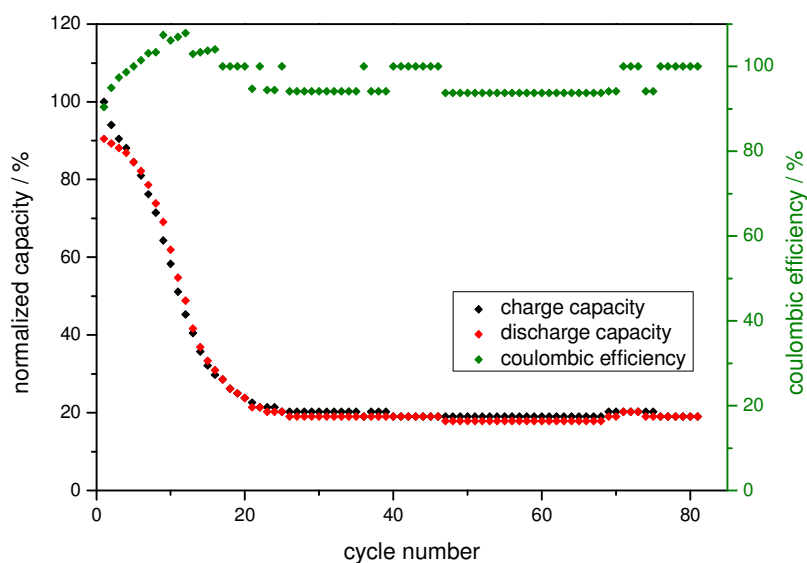


Figure 18: IU-charging (1 h, 4.0 V vs Li/Li^+) and discharging at 1 C of a composite cathode containing polynorbornene with TEMPO-units (**PN**) as active material (**PN**:Super P®:binder = 10:80:10 wt-%)

Composite cathodes **A** containing polyamide **7** as active material on the other hand exhibited great stability under the IU-charging conditions (Figure 19). Coulombic efficiencies of $\geq 99\%$ were reached after the 15th cycle and the specific capacity increases upon further cycling, similar to half-cells dis-/charged under constant current conditions (Figure 14 and Figure 16). These results demonstrate the superior electrochemical stability of polymer **7**.

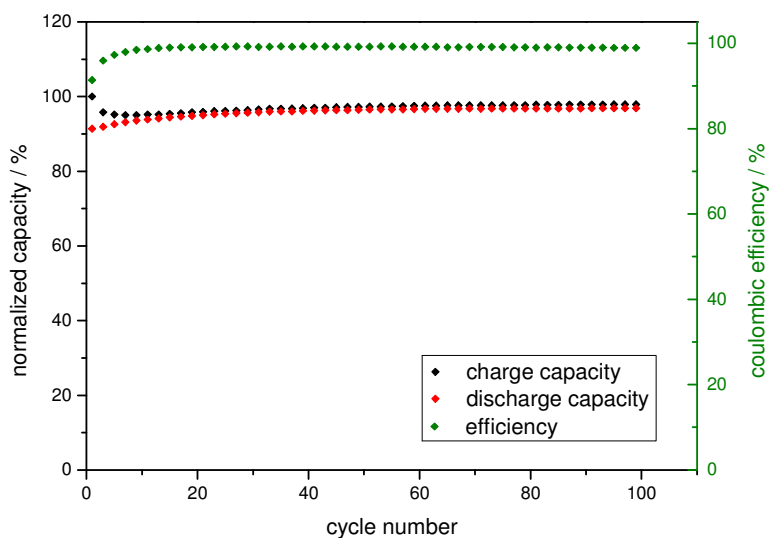


Figure 19: IU-charging (2 h, 4.0 V vs Li/Li⁺) and discharging at 1 C of composite cathode **A** containing polyamide **7** as active material

4.2.6 Influence of the cathode composition on the morphological and electrochemical properties

Morphology

Composite cathodes containing 20 to 60 wt-% of polymer **7**, 10 wt-% PVdF and 30 to 70 wt-% Super P[®] were fabricated (Table 1, **B**, **C** and **D**) according to general half-cell procedure (compare 3.1.2) and characterized with respect to their electrochemical and morphological properties.

First the morphologies were studied with Scanning Electron Microscopy (SEM). The corresponding images are depicted in Figure 20.

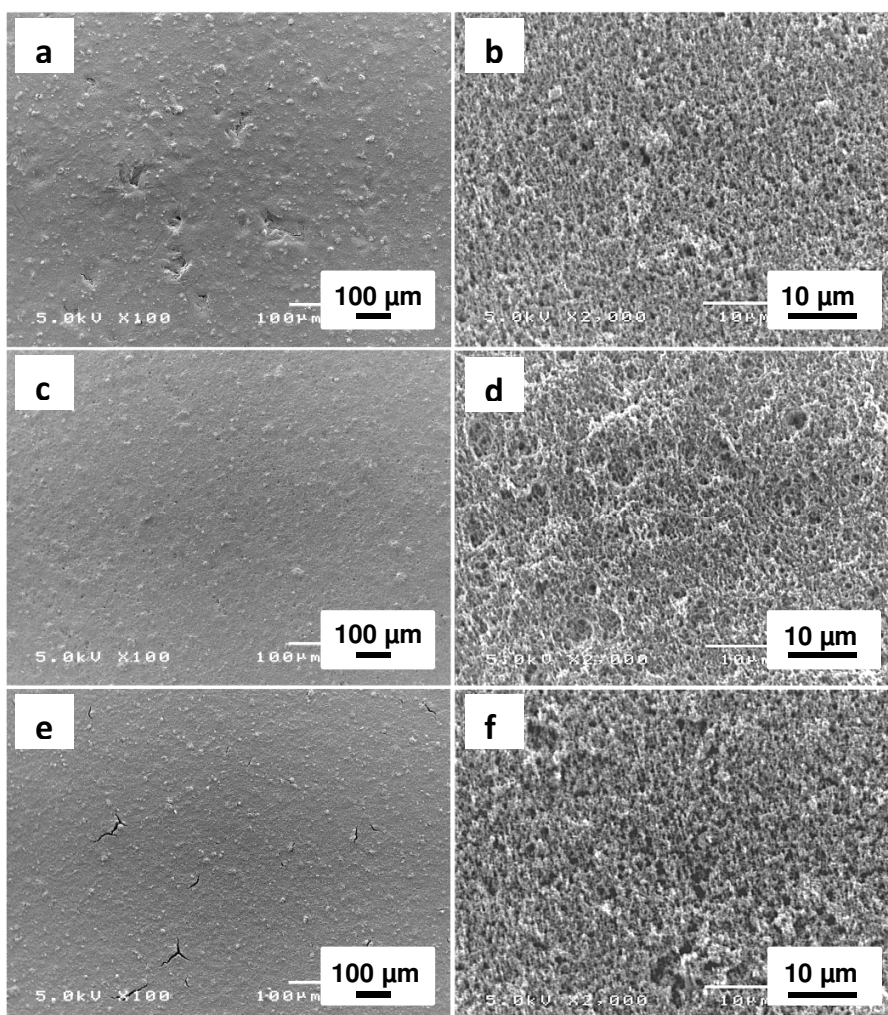


Figure 20: SEM images of composite cathodes with different compositions – active material content of (a+b) 20 wt-% (**B**), (c+d) 40 wt-% (**C**) and (e+f) 60 wt-% (**D**)

The morphologies of composite cathodes **C** and **D** with 40 and 60 wt-% active material content (Figure 20c,e) appear to be a bit smoother in comparison to cathodes **B** with 20 wt-% active material content (Figure 20a). Images with higher magnification (Figure 20b, d, f) show in principle no differences with respect to porosity, and the morphology is more or less

dominated by the conductive additive Super P® (compare Figure 7d), even for cathodes **D** with only 30 wt-% of Super P®.

Electrochemical properties

Cyclic voltammograms show an increase in peak-potential separation (ΔE_p) with increasing amount of active material (Figure 21).

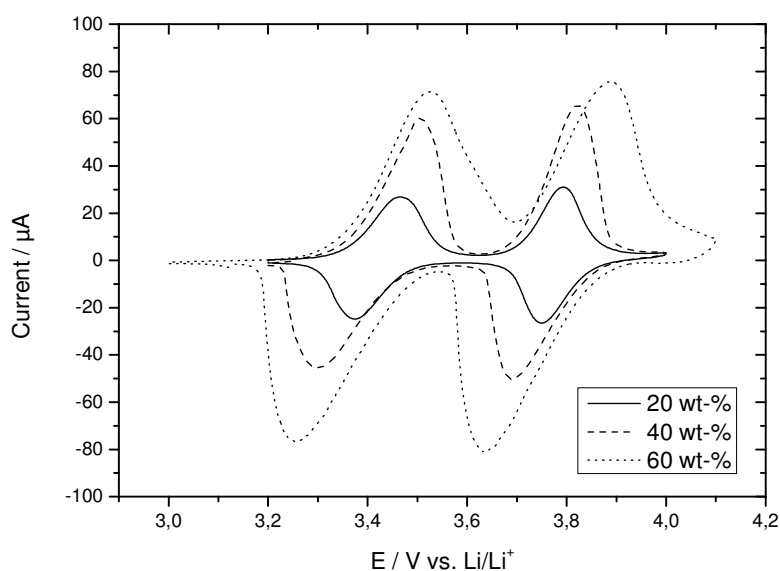


Figure 21: Cyclic voltammograms of composite cathodes **B**, **C** and **D** with increasing amount of active material (20, 40 and 60 wt-%, respectively) ($\nu = 0.1 \text{ mV/s}$)

ΔE_p values of the two redox couples increase from 94 and 44 mV, respectively, for composite cathode **B** to 270 and 252 mV, respectively, for composite cathode **D** (Table 5). This is attributed to higher electronic and ionic resistances for composites **C** and **D**. The electronic resistance increases due to a lower conductive additive content. Counter ion mobility inside the electrolyte-swollen/gel-like polymer plays an important role in the electrochemical behavior (as

discussed earlier). Thus also the ionic resistances for composites **C** and **D** increase because the ions have to pass thicker layers of the polymer.

Table 5: Peak-potential separations ΔE_p of composite cathodes with increasing active material content

Active material content / wt-%	ΔE_p / mV	
	1. redox couple	2. redox couple
20	94	44
40	209	135
60	270	252

Rate capability tests in a potential window from 3.0 to 4.2 V (vs. Li/Li⁺) and with rates between 0.2 and 50 C were performed with composite cathodes **B**, **C** and **D** (Figure 22a-c).

At a C-rate of 0.5 a specific discharge capacity (10th cycle) of 92.2 mAh/g was obtained for composite cathode **B** (20 wt-% active material). The capacity corresponds to almost 99 % of the theoretical value of 93.6 mAh/g. The active material utilization decreased with increasing amount of polymer. Values of

- 84.7 mAh/g, 90 % of the theoretical value (cathode **C**, 40 wt-% active material) and
- 79.0 mAh/g, 84 % of the theoretical value (cathode **D**, 60 wt-% active material)

were obtained at 0.5 C. This is ascribed to the low Super P[®] content, which leads to a less interpenetrating conducting network in the composites, and consequently some parts of the polymer will be 'electronically inaccessible'.

Composite cathode **B** showed great high-rate capability with specific discharge capacities of

- 89.7 mAh/g at 20 C (corresponding to 97 % of the value at 0.5 C) and
- 87.6 mAh/g at 50 C (95 %) (Figure 22a).

The capacity retention at higher current rates was significantly lower for cathode **C**, showing specific discharge capacities of

4 Results and Discussion

- 47.3 mAh/g at 20 C (60 % compared to 0.5 C) and
- 5.5 mAh/g at 50 C (7 %) (Figure 22b).

Cathode D exhibited no electroactivity in the tested potential window at rates higher than 2 C. The ohmic polarization or internal impedance (ionic, electronic and contact resistances) gets so high that the potential necessary to charge cathode D at rates higher than 2 C lies outside of the tested potential window. This results in charge/discharge capacities of zero. The results are summarized in Table 6.

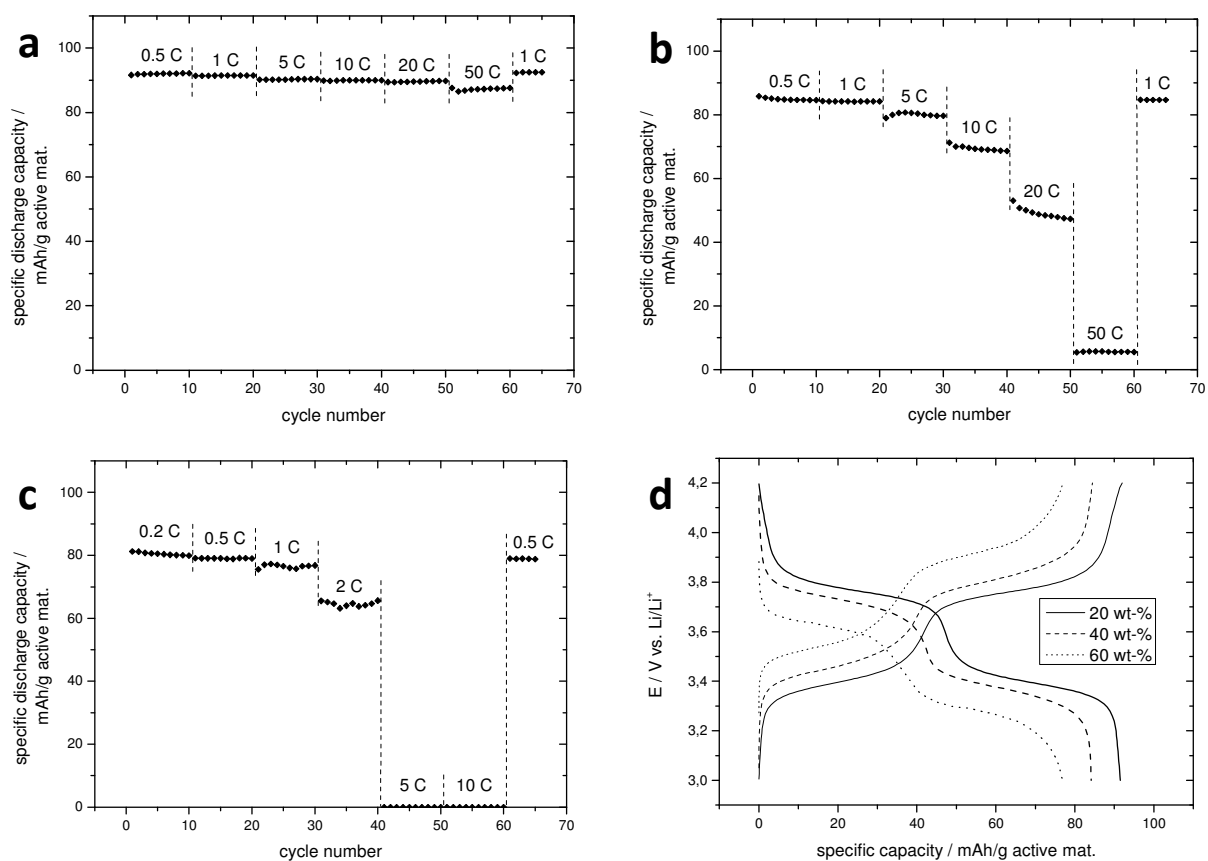
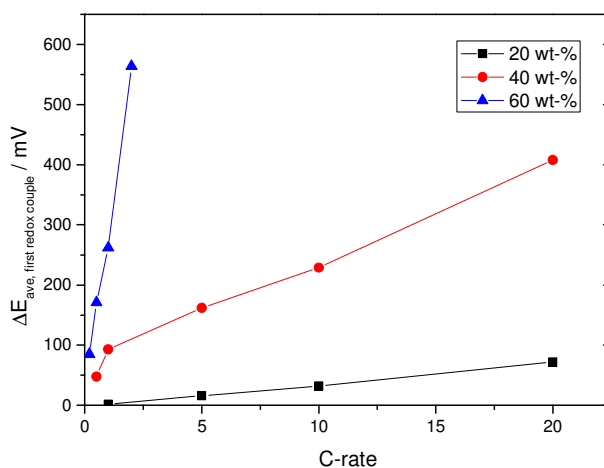


Figure 22: Rate capability tests (3.0-4.2 V vs. Li/Li⁺) of composite cathodes with active materials contents of (a) 20 wt-% (B), (b) 40 wt-% (C), (c) 60 wt-% (D) and (d) corresponding charge/discharge curves at a rate of 1 C

Table 6: Specific discharge capacities (10th cycle) of half-cells with composite cathodes **B**, **C** and **D** (3.0-4.2 V vs Li/Li⁺)

Polymer content / wt-%	Specific discharge capacities at different C-rates / mAh/g active mat.							
	0.2 C	0.5 C	1 C	2 C	5 C	10 C	20 C	50 C
20	n.d. ^b	92.2	91.5	n.d.	90.4	90.0	89.7	87.6
40	n.d.	84.7	84.1	n.d.	79.6	68.6	47.3	5.5
60	79.9	79.0	76.8	65.6	0 ^c	0	n.d.	n.d.

Figure 22d depicts the corresponding charge and discharge curves at 1 C, which show an increase in separation between the average charge and discharge potentials with increasing amount of active material. At 1 C ΔE_{ave} values for the first redox couple increased from 2 mV (cathode **B**) to 93 mV (**C**) and 262 mV (**D**). Figure 23 gives the ΔE_{ave} values at different C-rates for the three composite cathodes.

**Figure 23:** ΔE_{ave} values at different C-rates for composite cathodes **B**, **C** and **D** of varying active material content (3.0-4.2 V vs Li/Li⁺)

Composite cathode **B** exhibited the lowest ΔE_{ave} values and the smallest change with increasing C-rate. Cathode **D** exhibited the highest ΔE_{ave} values and the steepest increase. Thus the active

^b Not determined^c No electroactivity in the tested potential window (3.0 – 4.0 V vs. Li/Li⁺)

material content has a significant influence on ohmic polarization or internal impedance of the cell and thus the electron transfer rate.

Figure 24a shows a Ragone plot to compare the energy densities that the composites can deliver at varying current densities or discharge loads (power densities). Composite cathode **B** (20 wt-% active material) showed almost no change in energy density with increasing current density (approximately 65 Wh/kg for power densities of 20 to 3000 W/kg). Composite cathode **C** showed a higher specific energy density (approximately 120 Wh/kg) due to the higher active material content (40 wt-%), but also a significant decrease at higher current densities (approximately 65 Wh/kg for a power density of about 2000 W/kg). The energy density of composite cathode **D** (60 wt-% active material) is approximately 170 Wh/kg. At higher current densities (> 2 C) no electroactivity in the tested potential window (3.0-4.2 V vs. Li/Li^+) was observed.

The difference in the performance of the composites becomes more evident when the specific energy and power densities are normalized to the weight of the active material. The Ragone plot (Figure 24b) shows that the active material utilization is lower, and the energy densities at high power densities decrease more significantly, with increasing amount of active material.

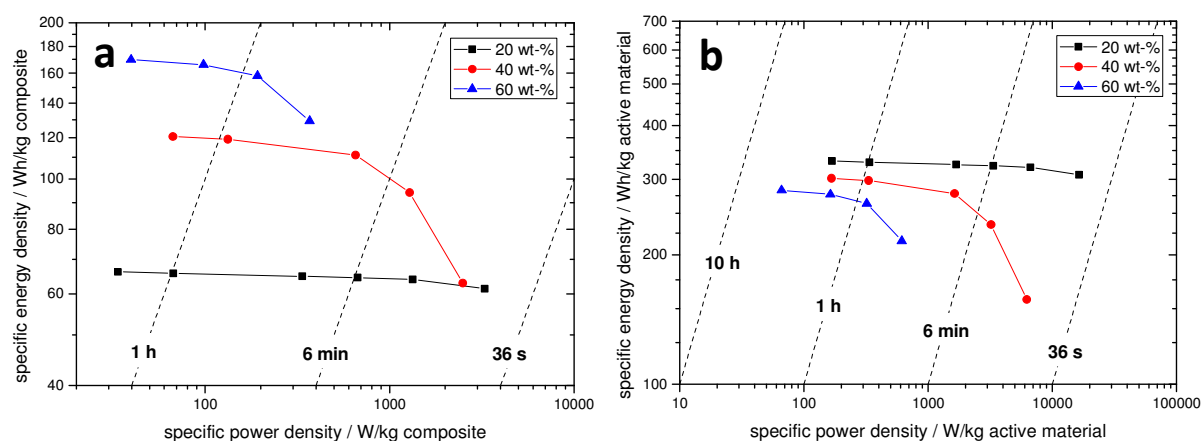


Figure 24: Ragone plot for composite cathodes **B**, **C** and **D** (3.0-4.2 V vs Li/Li^+) normalized to the weight of (a) the composite and (b) the active material

The results clearly indicate a major influence of the cathode composition (amount of active material) on the electrochemical properties. At high active material loadings polymer **7** loses its advantageous properties (fast charging/discharging, high power densities) and is clearly inferior to inorganic active materials due to the lower specific and volumetric energy densities. Maintaining these properties at high active material contents is of high priority, making an optimization of the composite architecture necessary.

Cyclic voltammetry in solution was performed according to general procedure (compare 3.1.1) to characterize the electrochemical properties of model compound **10**. For comparison, cyclic voltammograms (CVs) of N,N,N',N'-tetraphenyl-p-phenylenediamine (TPPD) and 4-acetamido-TEMPO have been recorded (Figure 25).

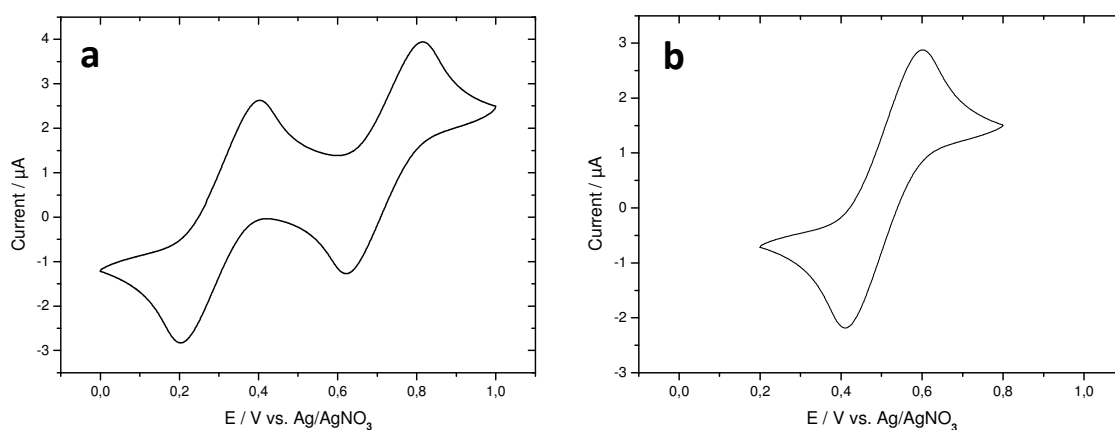


Figure 25: Cyclic voltammograms of (a) N,N,N',N'-tetraphenyl-p-phenylenediamine and (b) 4-acetamido-TEMPO in solution ($v = 50$ mV/s, 1mM in chloroform containing 0.1 M TBAP)

The CV of TPPD shows the two characteristic redox couples with formal potentials of $E^0_{1a} = 0.30$ V and $E^0_{2a} = 0.72$ V (Figure 25a), while the formal potential observed for 4-acetamido-TEMPO was $E^0_{1b} = 0.51$ V (Figure 25b) vs. Ag/AgNO₃.

The CV of model compound **10** shows 3 redox couples at $E^0_{1c} = 0.26$ V, $E^0_{2c} = 0.56$ V and $E_{3c,anodic} = 0.91$ V^d (Figure 26) which can be assigned to the different redox reactions via comparison with the CVs of TPPD and 4-acetamido-TEMPO.

^d Anodic peak potential

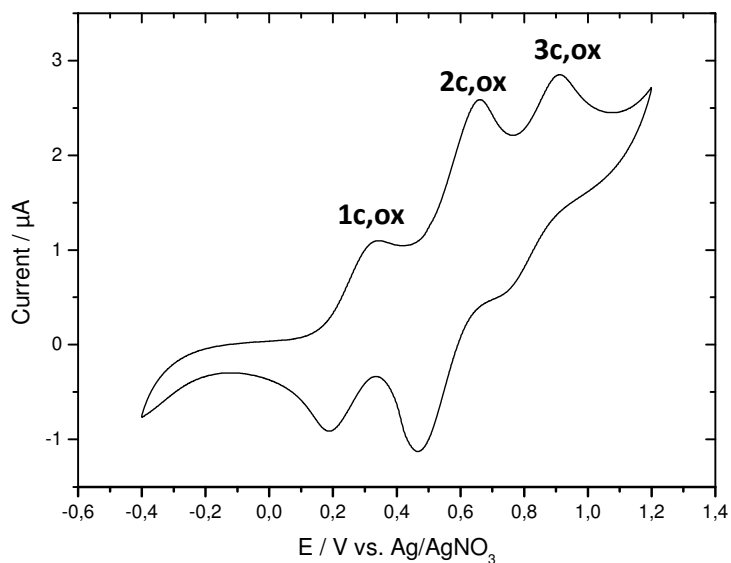
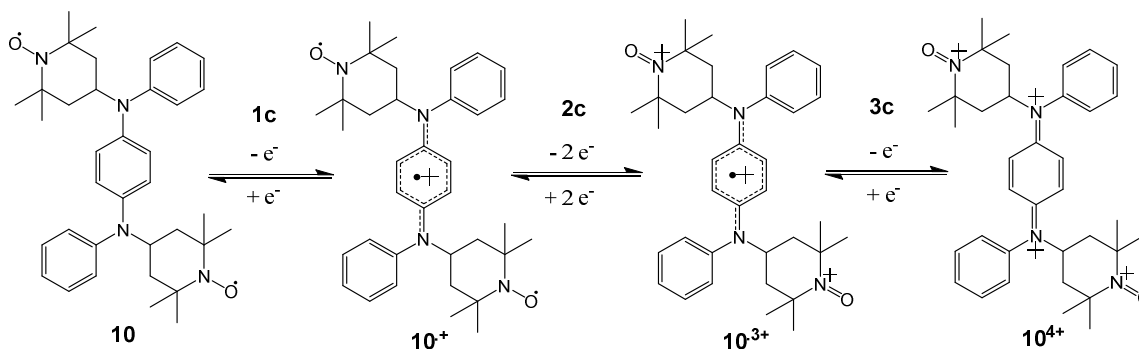


Figure 26: Cyclic voltammogram of model compound **10** in solution ($v = 50$ mV/s, 1mM in chloroform containing 0.1 M TBAP)

Scheme 21 outlines the proposed redox reactions. The first oxidation peak (Figure 26, 1c,ox) represents the formation of the radical cation of the tetrasubstituted p-phenylenediamine (TSPD) moiety ($10^{+\bullet}$). In the next step the oxidation of the TEMPO-units occurs (Figure 26, 2c,ox, formation of 10^{3+}), and finally the second oxidation step of the TSPD-unit can be observed (Figure 26, 3c,ox), leading to the formation of a tetracationic species (10^{4+}).



Scheme 21: Proposed redox reactions for model compound **10**

Upon further scans, no decrease of peak currents occurred, indicating electrochemical compatibility of the two different electroactive groups. It is important to note, that no changes were observed at lower scan rates (CVs not shown).

The EPR-spectrum of model compound **10** is depicted in Figure 27. Although there are two radical centers in the molecule, it shows the characteristics of a single TEMPO-(mono)radical. This indicates that the two radical centers do not interact with each other (on the time scale of the EPR experiment). The spectrum displays a triplet hyperfine structure (hyperfine coupling constant $a_N = 1.56$ mT) corresponding to the interaction of an electron spin of the unpaired electron ($s = \frac{1}{2}$) with a nuclear spin of a nitrogen nucleus ^{14}N ($I = 1$).⁹⁹

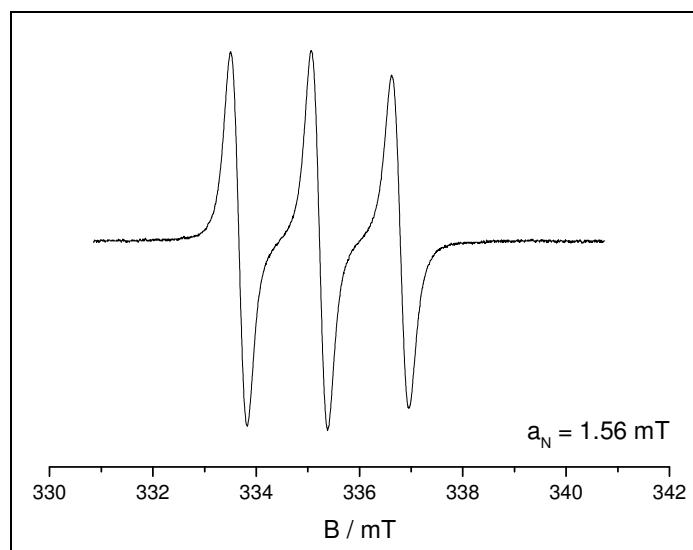
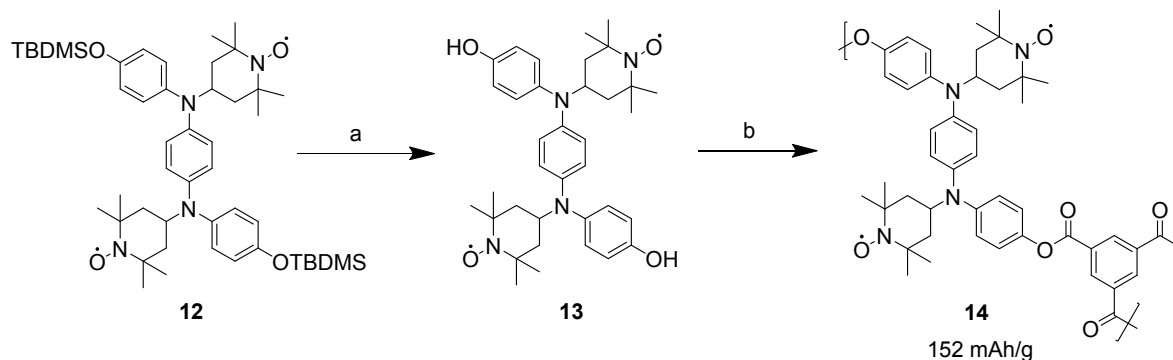


Figure 27: EPR-spectrum of model compound **10**

4.3.2 Polymer

To convert model substance **10** into a polymerizable compound, additional functional groups were introduced. The synthetic route for monomer precursor **12** was already outlined in Scheme 20. (4-bromophenoxy)-*tert*-butyldimethylsilane was used instead of bromobenzene to introduce two protected hydroxy functionalities. After cleavage of the protecting groups with tetrabutylammonium fluoride, monomer **13** was obtained (Scheme 22). The polycondensation of monomer **13** and benzene-1,3,5-tricarbonyl trichloride was carried out in NMP to yield insoluble polymer **14**, a material containing TSPD- as well as TEMPO-units (Scheme 22).



Scheme 22: Synthetic route for monomer **13** and polymer **14** – (a) TBAF, THF, 0 °C, (b) benzene-1,3,5-tricarbonyl trichloride, NMP, 0 °C

Polymer **14** has a significantly higher theoretical capacity (152.1 mAh/g) in comparison to polymer **7** (93.6 mAh/g), due to the additional TEMPO-units.

The EPR-spectra of monomer **13** and polymer **14** are reproduced in Figure 28. The spectrum of monomer **13** (Figure 28a) has the same characteristics as those obtained for model compound **10**. This confirms, together with the MALDI-MS data, that the cleavage of the TBDMS-groups

does not affect the radical groups. Polymer **14** also shows a triplet hyperfine structure, indicating that even in the polymer the TEMPO-radicals do not interact, which would result in a different shape of the EPR-spectrum.

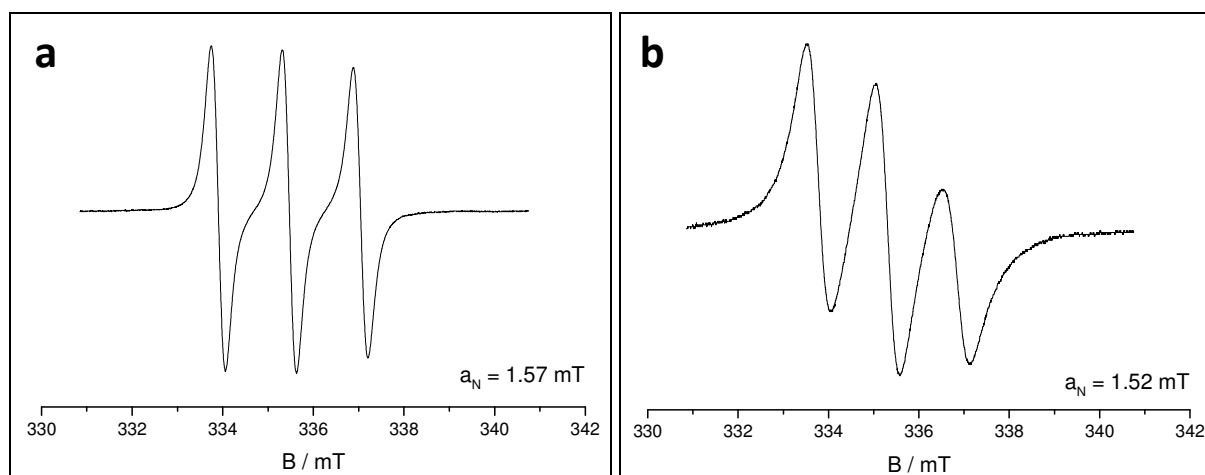


Figure 28: EPR-spectra of (a) monomer **13** and (b) polymer **14**

Composite cathodes containing 25 wt-% of polymer **14**, 20 wt-% PVdF and 55 wt-% Super P[®] were fabricated according to general half-cell procedure (compare 3.1.2) and characterized.

In the first scan of the cyclic voltammogram (Figure 29) peaks for the three redox steps (similar to the CV of model compound **10**, Figure 26) with formal potentials of $E^{0'}_1 = 3.41$ V, $E^{0'}_2 = 3.65$ V and $E^{0'}_3 = 3.98$ V (vs. Li/Li⁺) were observed. In subsequent scans a decrease of the peak current for the oxidation of the TEMPO-unit occurred. A cyclic voltammogram in a smaller potential window (3.2-3.8 V vs. Li/Li⁺) was recorded and a significant decrease of the peak currents over the first 6 scans was observed (Figure 30). The results indicate electrochemical instability of polymer **14**.

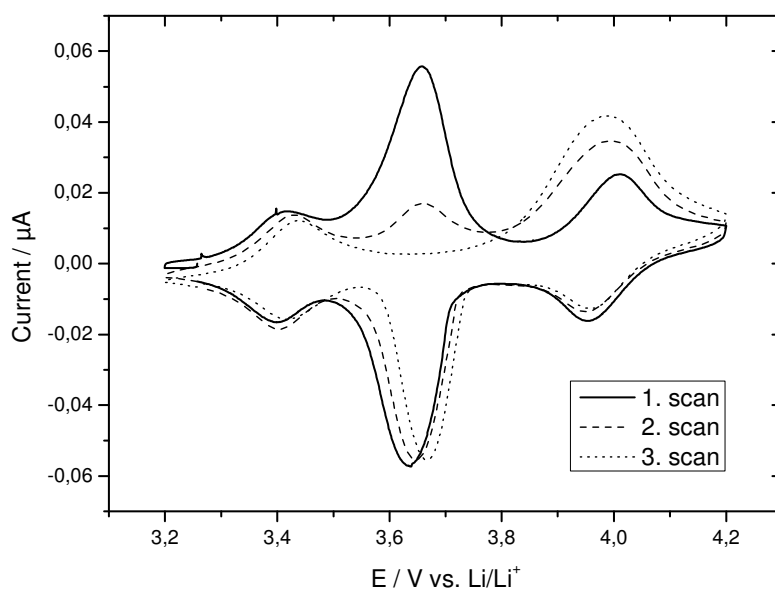


Figure 29: Cyclic voltammogram of a composite cathode with polymer **14** as active material (3.2-4.2 V vs. Li/Li⁺, $v = 0.1$ mV/s)

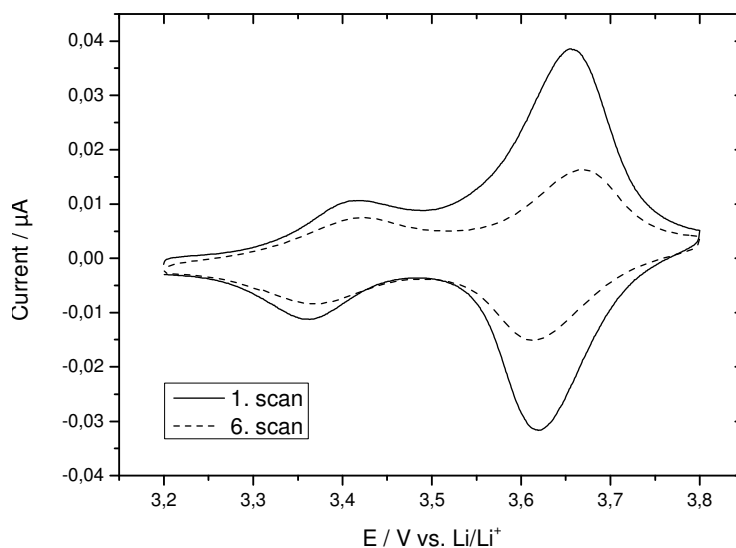


Figure 30: Cyclic voltammogram of a composite cathode with polymer **14** as active material in a smaller potential window (3.2-3.8 V vs. Li/Li⁺, $v = 0.1$ mV/s)

Charging/discharging at constant current (1 C, 3.2-4.2 V) showed a significant decrease in specific discharge capacity from 110 to about 50 mAh/g over the first 20 cycles (Figure 31).

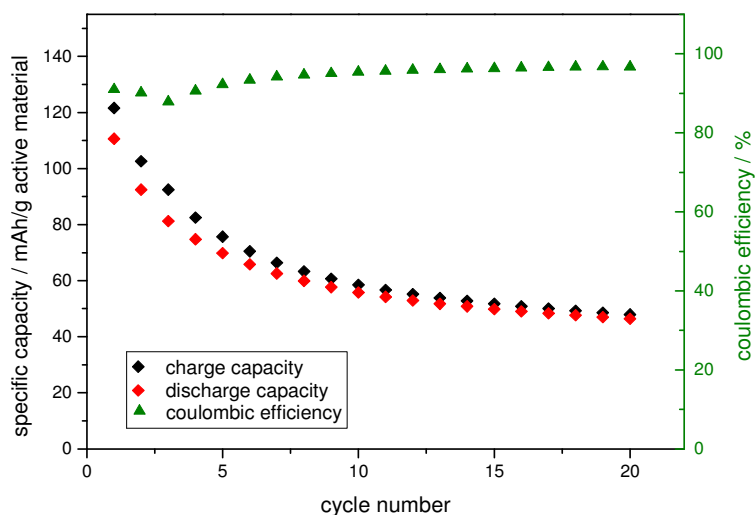


Figure 31: Constant current cycling at 1 C of a composite cathode with polymer **14** as active material

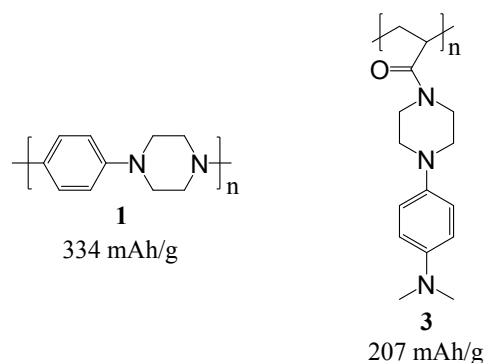
Two substituents of the p-phenylenediamine unit of polymer **14** are non-aromatic (TEMPO-units). The electrochemical instability is ascribed to the occurrence of side reactions/rearrangements of the electrochemically formed radical cations, similar to polymers **1** and **3**, and possibly also the TEMPO-units. It appears that the nature of the substituents is critical for electrochemical stability. This is supported by the fact that polymer **7** with tetraphenyl-p-phenylenediamine-units showed remarkable stability when applied as cathode-active material.

5 Summary and outlook

Organic electrode materials are currently a heavily researched topic due to potentially providing higher specific energy and power densities, higher safety, better processability, easier disposal/recyclability and lower cost compared to inorganic electrode materials.

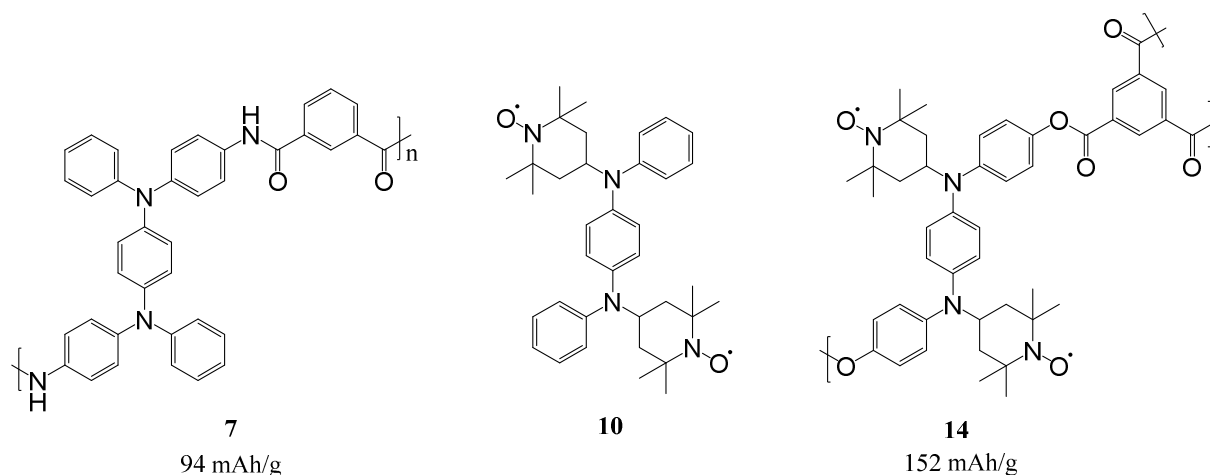
In the course of this work, novel redox-active polymers based on tetrasubstituted p-phenylenediamine (TSPD) units, as well as the corresponding precursors were synthesized, characterized and tested as cathode-active materials in secondary batteries with lithium as counter electrode. TSPD-units can exchange two electrons in two one-electron redox steps via the formation of a radical cationic and a dicationic (quinone diimine) species.

The repeating unit of polymers based on tetraalkyl-p-phenylenediamine (TAPD) units has typically low molecular weight. Thus high theoretical capacities can be reached. Two polymers were synthesized, polymer **1** with TAPD-units in the main-chain and polymer **3** with TAPD-units in the side-chain (Scheme 23). Electrochemical characterizations revealed irreversible redox-behavior, probably resulting from side-reactions/rearrangements of the radical cations formed during oxidation/charging.



Scheme 23: Structures and theoretical capacities of polymer **1** and **3**

A model compound containing TSPD- and TEMPO-units was synthesized (**10**, Scheme 24). Three reversible redox peaks were observed during cyclic voltammetry in solution indicating an electrochemical compatibility of the two redox-active groups. The corresponding polymer **14** (Scheme 24) was tested as active material in a half-cell but showed irreversible redox behavior. The results suggest that the critical factor for electrochemical stability of polymers based on TSPD-units appears to be the character of the substituents (aromatic vs. non-aromatic). This is supported by the fact that polymer **7** (Scheme 24), with tetraphenyl-p-phenylenediamine (TPPD) units, showed remarkable electrochemical stability in comparison to polymers **1**, **3** and **14**.



Scheme 24: Structures and theoretical capacities of polymer **7**, model compound **10** and polymer **14**

Polymer **7** was synthesized by a polycondensation of N,N'-bis(4-aminophenyl)-N,N'-diphenyl-p-phenylenediamine with isophthaloyl dichloride.

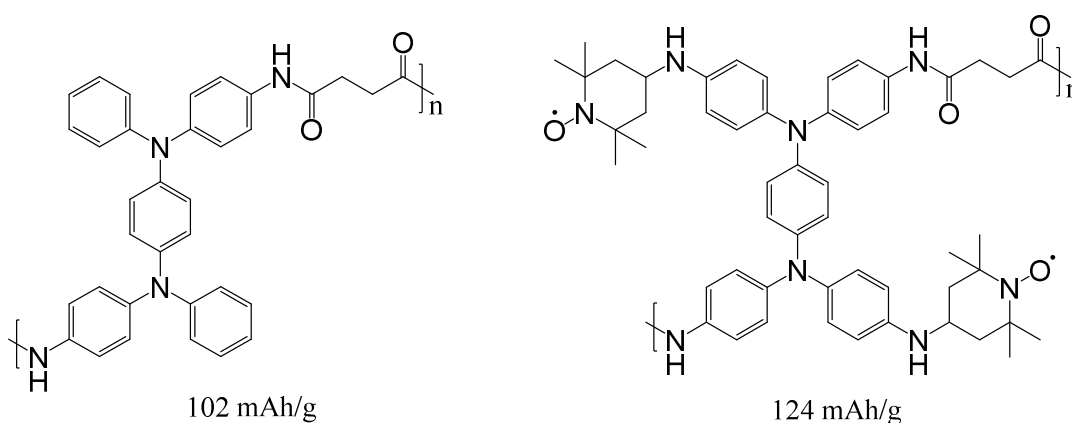
Composite cathodes with polymer **7** as active material (polymer/conductive additive/binder = 25:55:20 wt-%) showed great electrode utilization, with capacities of up to 92.5 mAh/g_{act.mat.} at 1 C, corresponding to 99 % of the theoretical value.

Polymer **7** also exhibited great electrochemical stability during constant current charging/discharging tests at 10 C. The capacity retention was approximately 89 % after 11,000 cycles, which exceeds the cycle stability of inorganic electrode materials significantly and is comparable to electrolytic capacitors. Even when cycled to and held at high potentials vs. Li/Li⁺ no degradation of the polymer was observed. This is an advantage in comparison to other organic electrode materials like conducting polymers or polyradicals.

Polymer **7** also showed great high-rate capability. A capacity retention of about 70 % was observed when comparing the capacity at 100 C (current density of approximately 2.3 mA/cm²) to the capacity at 1 C. This results in a high specific power density of 32.7 kW/kg. (with a specific energy density of 212 Wh/kg), in reference to the active material content. The biggest drawback was the electronic insulating nature of the polymer, making the addition of a significant amount of conductive additive necessary. This reduced the overall energy and power densities.

The influence of the polymer content on the morphological and electrochemical properties was investigated for composite cathodes containing 20 to 60 wt-% of active material. Scanning electron microscopy revealed no major morphological differences. Electrochemical characterizations showed that the active material utilization is lower, and that the energy densities at high power densities decrease significantly with increasing active material content. At high active material loadings polymer **7** loses its advantageous properties (fast charging/discharging, high power density) compared to inorganic electrode materials. Maintaining these properties at high active material contents is of high priority, making further research regarding the optimization of the composite architecture and composition necessary.

Compared to other organic electrode materials the capacity of polymer **7** is rather low. Nevertheless, some modifications to increase capacity will be part of future work due to the otherwise excellent electrochemical performance. Scheme 25 shows some potential polymer structures with higher capacities. Possibilities for modification are the substitution of isophthaloyl chloride with monomers with lower molecular weight (e.g. succinyl dichloride) and/or the incorporation of other electroactive moieties like TEMPO (in *m*- or *p*-position of the phenyl-groups).



Scheme 25: Potential polymer structures with higher theoretical capacities

6 References

- (1) Thejo Kalyani, N.; Dhoble, S. J. *Renew. Sustain. Energy Rev.* **2012**, *16*, 2696.
- (2) Bundgaard, E.; Krebs, F. *Sol. Energy Mater. Sol. Cells* **2007**, *91*, 954.
- (3) Novák, P.; Müller, K.; Santhanam, K. S. V.; Haas, O. *Chem. Rev.* **1997**, *97*, 207.
- (4) Liang, Y.; Tao, Z.; Chen, J. *Adv. Energy Mater.* **2012**, *2*, 742.
- (5) Song, Z.; Zhou, H. *Energy Environ. Sci.* **2013**, *6*, 2280.
- (6) Poizot, P.; Dolhem, F. *Energy Environ. Sci.* **2011**, *4*, 2003.
- (7) Williams, D. L.; Byrne, J. J.; Driscoll, J. S. *J. Electrochem. Soc.* **1969**, *116*, 2.
- (8) Shirakawa, H.; Louis, E. J.; MacDiarmid, A. G.; Chiang, C. K.; Heeger, A. J. *J. Chem. Soc. Chem. Commun.* **1977**, 578.
- (9) Chiang, C.; Fincher, C.; Park, Y.; Heeger, A.; Shirakawa, H.; Louis, E.; Gau, S.; MacDiarmid, A. *Phys. Rev. Lett.* **1977**, *39*, 1098.
- (10) Nigrey, P. J.; MacInnes, D. J.; Nairns, D. P.; MacDiarmid, A. G.; Heeger, A. J. *J. Electrochem. Soc.* **1981**, *128*, 1651.
- (11) MacInnes, D.; Druy, M. A.; Nigrey, P. J.; Nairns, D. P.; MacDiarmid, A. G.; Heeger, A. J. *J. Chem. Soc. Chem. Commun.* **1981**, 317.
- (12) Kitani, A.; Kaya, M.; Sasaki, K. *J. Electrochem. Soc.* **1986**, *133*, 1069.
- (13) MacDiarmid, A. .; Yang, L. .; Huang, W. .; Humphrey, B. . *Synth. Met.* **1987**, *18*, 393.
- (14) Mermilliod, N.; Tanguy, J. *J. Electrochem. Soc.* **1986**, *133*, 1073.
- (15) Kaneto, K.; Yoshino, K.; Inuishi, Y. *Jpn. J. Appl. Phys.* **1983**, *22*, L567.
- (16) Snook, G. a.; Kao, P.; Best, A. S. *J. Power Sources* **2011**, *196*, 1.

- (17) Visco, S. J.; Mailhe, C. C.; De Jonghe, L. C.; Armand, M. B. *J. Electrochem. Soc.* **1989**, *136*, 661.
- (18) Visco, S. J.; Liu, M.; De Jonghe, L. C. *J. Electrochem. Soc.* **1990**, *137*, 1191.
- (19) Liu, M.; Visco, S. J.; De Jonghe, L. C. *J. Electrochem. Soc.* **1989**, *136*, 2570.
- (20) Liu, M.; Visco, S. J.; De Jonghe, L. C. *J. Electrochem. Soc.* **1991**, *138*, 1891.
- (21) Deng, S.-R.; Kong, L.-B.; Hu, G.-Q.; Wu, T.; Li, D.; Zhou, Y.-H.; Li, Z.-Y. *Electrochim. Acta* **2006**, *51*, 2589.
- (22) Oyama, N.; Tatsuma, T.; Sato, T.; Sotomura, T. *Nature* **1995**, *373*, 598.
- (23) Oyama, N.; Kiya, Y.; Hatozaki, O.; Morioka, S.; Abruña, H. D. *Electrochem. Solid-State Lett.* **2003**, *6*, A286.
- (24) Naoi, K.; Kawase, K.; Mori, M.; Komiyama, M. *J. Electrochem. Soc.* **1997**, *144*, L173.
- (25) Peover, M. E. *J. Chem. Soc.* **1962**, 4540.
- (26) Alt, H.; Binder, H.; Köhling, A.; Sandstede, G. *Electrochim. Acta* **1972**, *17*, 873.
- (27) Tobishima, S.; Yamaki, J. I.; Yamaji, A. *J. Electrochem. Soc.* **1984**, *131*, 57.
- (28) Pasquali, M.; Pistoia, G.; Boschi, T.; Tagliatesta, P. *Solid State Ionics* **1987**, *23*, 261.
- (29) Foos, J. S.; Erker, S. M.; Rembetsy, L. M. *J. Electrochem. Soc.* **1986**, *133*, 836.
- (30) Häring, D.; Novak, P.; Haas, O.; Piro, B.; Pham, M. C. *J. Electrochem. Soc.* **1999**, *146*, 2393.
- (31) Choi, W.; Harada, D.; Oyaizu, K.; Nishide, H. *J. Am. Chem. Soc.* **2011**, *133*, 19839.
- (32) Nokami, T.; Matsuo, T.; Inatomi, Y.; Hojo, N.; Tsukagoshi, T.; Yoshizawa, H.; Shimizu, A.; Kuramoto, H.; Komae, K.; Tsuyama, H.; Yoshida, J. *J. Am. Chem. Soc.* **2012**, *134*, 19694.
- (33) Song, Z.; Zhan, H.; Zhou, Y. *Chem. Commun. (Camb)*. **2009**, 448.
- (34) Song, Z.; Zhan, H.; Zhou, Y. *Angew. Chem. Int. Ed. Engl.* **2010**, *49*, 8444.

- (35) Kakuta, T.; Shirota, Y.; Mikawa, H. *J. Chem. Soc. Chem. Commun.* **1985**, *12*, 553.
- (36) Iwakura, C.; Kawai, T.; Nojima, M.; Yoneyama, H. *J. Electrochem. Soc.* **1987**, *134*, 791.
- (37) Feng, J. K.; Cao, Y. L.; Ai, X. P.; Yang, H. X. *J. Power Sources* **2008**, *177*, 199.
- (38) Lebedev, O. L.; Kazarnovskii, S. N. *Zhur. Obs. Khim.* **1960**, *30*, 1631.
- (39) Tebben, L.; Studer, A. *Angew. Chem. Int. Ed. Engl.* **2011**, *50*, 5034.
- (40) Golubev, V. A.; Voronina, G. N.; Rozantsev, E. G. *Bull. Acad. Sci. USSR Div. Chem. Sci.* **1970**, *19*, 2449.
- (41) Lucio Anelli, P.; Biffi, C.; Montanari, F.; Quici, S. *J. Org. Chem.* **1987**, *52*, 2559.
- (42) Hubbell, W. L.; McConnell, H. M. *Proc. Natl. Acad. Sci. U. S. A.* **1968**, *61*, 12.
- (43) Georges, M. K.; Veregin, R. P. N.; Kazmaier, P. M.; Hamer, G. K. *Macromolecules* **1993**, *26*, 2987.
- (44) Hawker, C. J. *J. Am. Chem. Soc.* **1994**, *116*, 11185.
- (45) Korshak, Y. V.; Medvedeva, T. V.; Ovchinnikov, A. A.; Spector, V. N. *Nature* **1987**, *326*, 370.
- (46) Nishide, H.; Kaneko, T.; Igarashi, M.; Tsuchida, E.; Yoshioka, N.; Lahti, P. M. *Macromolecules* **1994**, *27*, 3082.
- (47) Rajca, A. *Chemistry* **2002**, *8*, 4834.
- (48) Semmelhack, M. F.; Chou, C. S.; Cortes, D. A. *J. Am. Chem. Soc.* **1983**, *105*, 4492.
- (49) Merz, A.; Bachmann, H. *J. Am. Chem. Soc.* **1995**, *117*, 901.
- (50) Nakahara, K.; Iwasa, S.; Satoh, M.; Morioka, Y.; Iriyama, J.; Suguro, M.; Hasegawa, E. *Chem. Phys. Lett.* **2002**, *359*, 351.
- (51) Nishide, H.; Iwasa, S.; Pu, Y.-J.; Suga, T.; Nakahara, K.; Satoh, M. *Electrochim. Acta* **2004**, *50*, 827.

- (52) Nakahara, K.; Iriyama, J.; Iwasa, S.; Suguro, M.; Satoh, M.; Cairns, E. J. *J. Power Sources* **2007**, *165*, 398.
- (53) Nakahara, K.; Iriyama, J.; Iwasa, S.; Suguro, M.; Satoh, M.; Cairns, E. J. *J. Power Sources* **2007**, *163*, 1110.
- (54) Kim, J.; Cheruvally, G.; Choi, J.; Ahn, J.; Lee, S.; Choi, D.; Song, C. *Solid State Ionics* **2007**, *178*, 1546.
- (55) Kim, J.-K.; Cheruvally, G.; Ahn, J.-H.; Seo, Y.-G.; Choi, D. S.; Lee, S.-H.; Song, C. E. *J. Ind. Eng. Chem.* **2008**, *14*, 371.
- (56) Kim, J.-K.; Ahn, J.-H.; Cheruvally, G.; Chauhan, G. S.; Choi, J.-W.; Kim, D.-S.; Ahn, H.-J.; Lee, S. H.; Song, C. E. *Met. Mater. Int.* **2009**, *15*, 77.
- (57) López-Peña, H. a.; Hernández-Muñoz, L. S.; Cardoso, J.; González, F. J.; González, I.; Frontana, C. *Electrochem. commun.* **2009**, *11*, 1369.
- (58) Nakahara, K.; Iriyama, J.; Iwasa, S.; Suguro, M.; Satoh, M.; Cairns, E. J. *J. Power Sources* **2007**, *165*, 870.
- (59) Janoschka, T.; Teichler, A.; Krieg, A.; Hager, M. D.; Schubert, U. S. *J. Polym. Sci. Part A Polym. Chem.* **2012**, *50*, 1394.
- (60) Suguro, M.; Iwasa, S.; Nakahara, K. *Macromol. Rapid Commun.* **2008**, *29*, 1635.
- (61) Bugnon, L.; Morton, C. J. H.; Novak, P.; Vetter, J.; Nesvadba, P. *Chem. Mater.* **2007**, *19*, 2910.
- (62) Suga, T.; Pu, Y.; Kasatori, S.; Nishide, H. *Macromolecules* **2007**, *40*, 3167.
- (63) Suga, T.; Ohshiro, H.; Sugita, S.; Oyaizu, K.; Nishide, H. *Adv. Mater.* **2009**, *21*, 1627.
- (64) Dahms, H. *J. Phys. Chem.* **1968**, *72*, 362.
- (65) Ruff, I.; Friedrich, V. *J. Phys. Chem.* **1971**, *75*, 3297.
- (66) Andrieux, C. P.; Savéant, J. M. *J. Electroanal. Chem. Interfacial Electrochem.* **1980**, *111*, 377.

- (67) Oyaizu, K.; Ando, Y.; Konishi, H.; Nishide, H. *J. Am. Chem. Soc.* **2008**, *130*, 14459.
- (68) Yonekuta, Y.; Oyaizu, K.; Nishide, H. *Chem. Lett.* **2007**, *36*, 866.
- (69) Guo, W.; Yin, Y.-X.; Xin, S.; Guo, Y.-G.; Wan, L.-J. *Energy Environ. Sci.* **2012**, *5*, 5221.
- (70) Koshika, K.; Sano, N.; Oyaizu, K.; Nishide, H. *Chem. Commun. (Camb)*. **2009**, 836.
- (71) Komaba, S.; Tanaka, T.; Ozeki, T.; Taki, T.; Watanabe, H.; Tachikawa, H. *J. Power Sources* **2010**, *195*, 6212.
- (72) Katsumata, T.; Satoh, M.; Wada, J.; Shiotsuki, M.; Sanda, F.; Masuda, T. *Macromol. Rapid Commun.* **2006**, *27*, 1206.
- (73) Qu, J.; Katsumata, T.; Satoh, M.; Wada, J.; Masuda, T. *Macromolecules* **2007**, *40*, 3136.
- (74) Katsumata, T.; Qu, J.; Shiotsuki, M.; Satoh, M.; Wada, J.; Igarashi, J.; Mizoguchi, K.; Masuda, T. *Macromolecules* **2008**, *41*, 1175.
- (75) Koshika, K.; Sano, N.; Oyaizu, K.; Nishide, H. *Macromol. Chem. Phys.* **2009**, *210*, 1989.
- (76) Nakahara, K.; Oyaizu, K.; Nishide, H. *J. Mater. Chem.* **2012**, *22*, 13669.
- (77) Janoschka, T.; Hager, M. D.; Schubert, U. S. *Adv. Mater.* **2012**, *24*, 6397.
- (78) Oyaizu, K.; Nishide, H. *Adv. Mater.* **2009**, *21*, 2339.
- (79) Wurster, C. *Berichte der Dtsch. Chem. Gesellschaft* **1888**, *21*, 921.
- (80) Michaelis, L.; Hill, E. S. *J. Am. Chem. Soc.* **1933**, *55*, 1481.
- (81) Michaelis, L.; Schubert, M. P.; Granick, S. *J. Am. Chem. Soc.* **1939**, *61*, 1981.
- (82) Albrecht, A. C.; Simpson, W. T. *J. Am. Chem. Soc.* **1955**, *77*, 4454.
- (83) Fernández, H.; Zón, M. A. *J. Electroanal. Chem.* **1992**, *332*, 237.
- (84) Grampp, G.; Kelterer, A.-M.; Landgraf, S.; Sacher, M.; Niethammer, D.; Telo, J. P.; Dias, R. M. B.; Vieira, A. J. S. C. *Monatshefte für Chemie - Chem. Mon.* **2005**, *136*, 519.

- (85) Kovacs, Ni. *Nature* **1956**, *178*, 703.
- (86) Halpert, G.; Surampudi, S.; Shen, D.; Huang, C.-K.; Narayanan, S.; Vamos, E.; Perrone, D. J. *Power Sources* **1994**, *47*, 287.
- (87) Richardson, T. J. *J. Electrochem. Soc.* **1996**, *143*, 3992.
- (88) Richardson, T. J.; Ross, P. N. *J. Power Sources* **1999**, *84*, 1.
- (89) Liou, G.; Chang, C. *Macromolecules* **2008**, *41*, 1667.
- (90) Hsiao, S.-H.; Liou, G.-S.; Kung, Y.-C.; Yen, H.-J. *Macromolecules* **2008**, *41*, 2800.
- (91) Yen, H.-J.; Liou, G.-S. *Chem. Mater.* **2009**, *21*, 4062.
- (92) Huang, L.; Yen, H.; Chang, C.; Liou, G. *J. Polym. Sci. Part A Polym. Chem.* **2010**, *48*, 4747.
- (93) Yen, T.-L.; Lo, H.-C.; Liou, G.-S.; Ho, K.-C. *Sol. Energy Mater. Sol. Cells* **2008**, *92*, 146.
- (94) Conte, S.; Rodríguez-Calero, G. G.; Burkhardt, S. E.; Lowe, M. a.; Abruña, H. D. *RSC Adv.* **2013**, *3*, 1957.
- (95) Gottlieb, H. E.; Kotlyar, V.; Nudelman, A. *J. Org. Chem.* **1997**, *62*, 7512.
- (96) Davis, M. C.; Chafin, A. C.; Sathrum, A. J. *Synth. Commun.* **2005**, *35*, 2085.
- (97) Liou, G.-S.; Hsiao, S.-H.; Ishida, M.; Kakimoto, M.; Imai, Y. *J. Polym. Sci. Part A Polym. Chem.* **2002**, *40*, 2810.
- (98) Sato, S.; Sakamoto, T.; Miyazawa, E.; Kikugawa, Y. *Tetrahedron* **2004**, *60*, 7899.
- (99) Dupeyre, R. M.; Lemaire, H.; Rassat, A. *J. Am. Chem. Soc.* **1965**, *87*, 3771.

7 Appendix

7.1 Abbreviations

a	hyperfine coupling constant
AIBN	2,2'-Azobis(2-methylpropionitrile)
APT	attached proton test
ATR-IR	attenuated total reflectance – infrared (spectroscopy)
B	Magnetic field (in mT)
c	theoretical specific capacity (in mAh/g)
C-rate	charge rate (1 C \triangleq full charging/discharging of the cell in 1 h)
CV	cyclic voltammogram
DEC	diethyl carbonate
DMSO	dimethyl sulfoxide
E	potential (in V)
EC	ethylene carbonate
EI-MS	electron impact mass spectrometry
EPR	electron paramagnetic resonance
I	nuclear spin
MALDI-MS	matrix-assisted laser desorption/ionization mass spectrometry
M_n	number average molar mass
M_w	weight average molar mass
n	degree of polymerization
NMP	N-methyl-2-pyrrolidone
NMR	nuclear magnetic resonance
PDI	polydispersity index (PDI = M_w/M_n)
s	spin quantum number
SEC	size exclusion chromatography
SEM	scanning electron microscopy
TAPD	tetraalkyl-p-phenylenediamine

TBAP	tetrabutylammonium perchlorate
TOF	time-of-flight
TPPD	tetraphenyl-p-phenylenediamine
TSPD	tetrasubstituted p-phenylenediamine
ν	scan rate in mV/s
x	doping level of conducting polymers
δ	chemical shift in ppm relative to tetramethylsilane (internal standard)
ΔE_{ave}	separation between average charge and discharge potential
ΔE_p	peak-potential separation

7.2 Characterization

Poly(1,4-piperazinediyl-1,4-phenylene) (15)

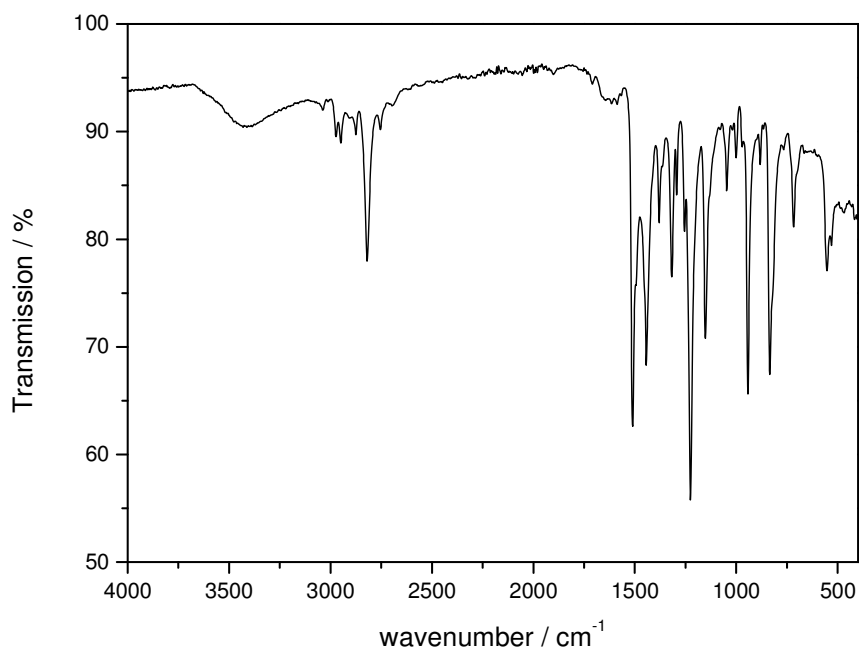
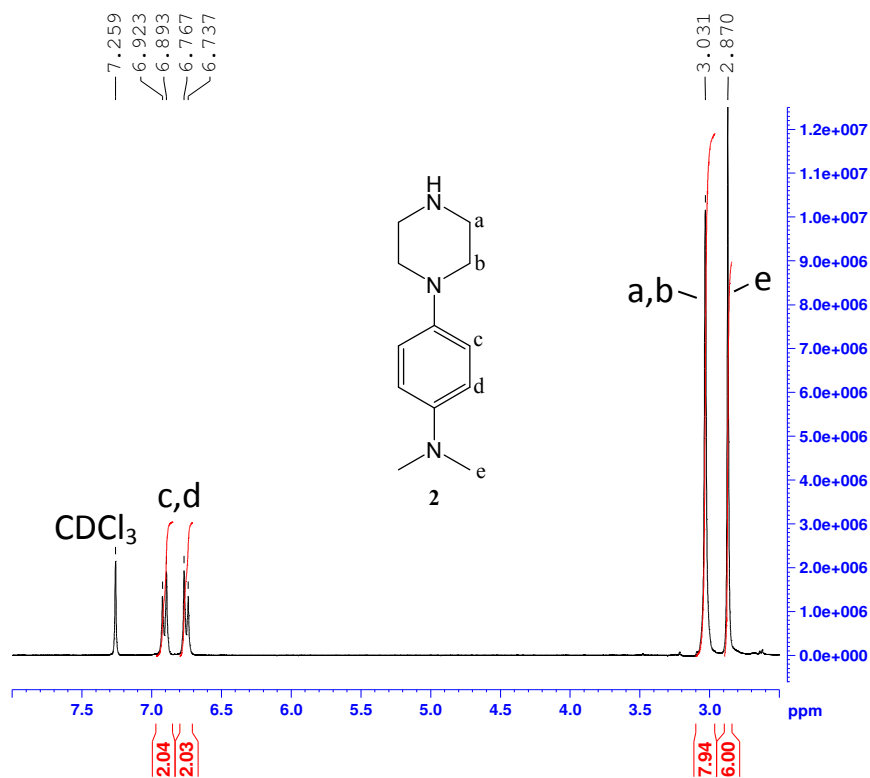
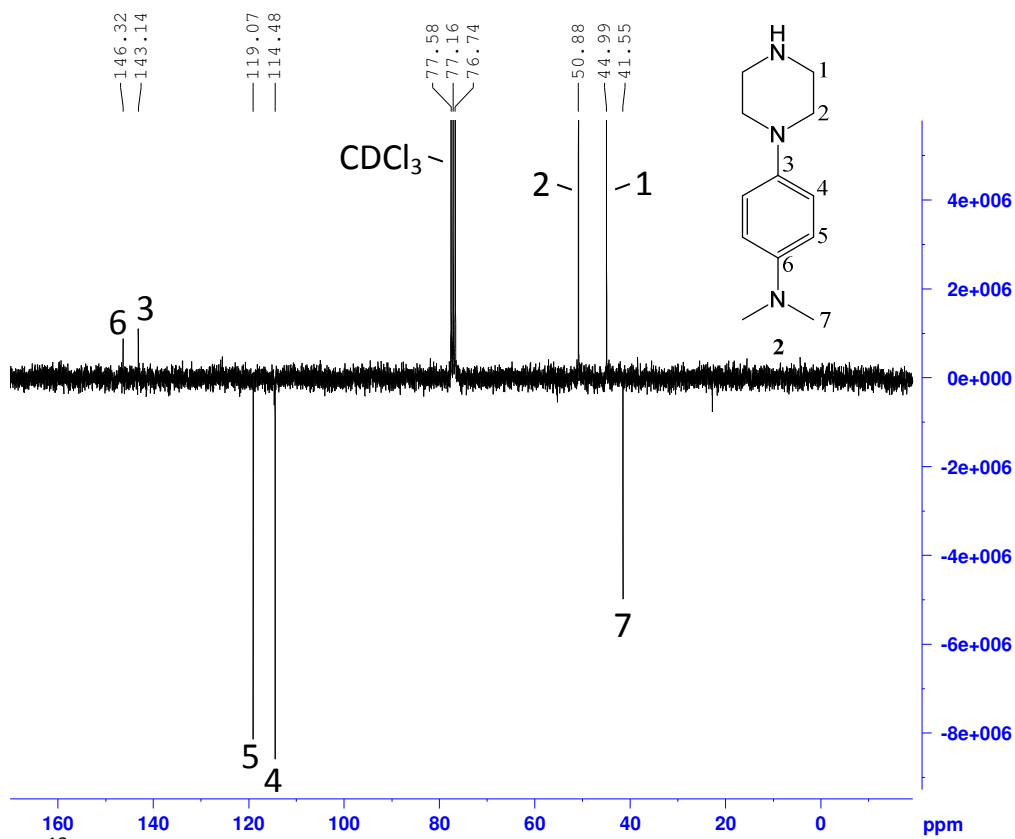


Figure 32: IR-spectrum of polymer **1**

N,N-dimethyl-4-(piperazin-1-yl)aniline (**2**)Figure 33: ¹H NMR spectrum of compound **2**Figure 34: ¹³C NMR (APT) spectrum of compound **2**

split100

David_polyWu 2a 2004 (10.812) Cm (2004:2005-1991:1992)

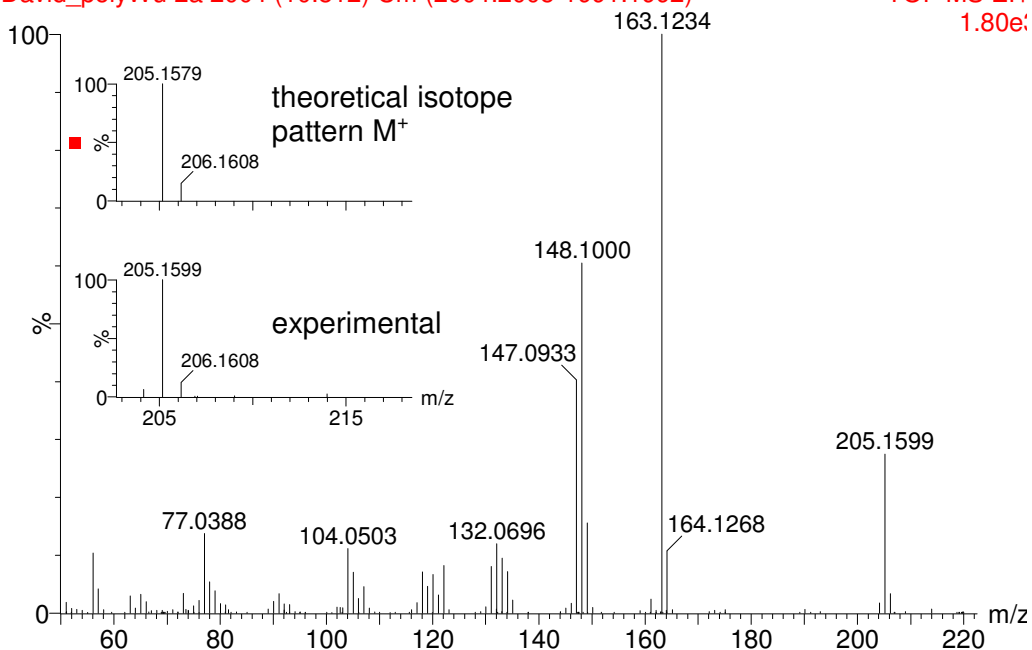
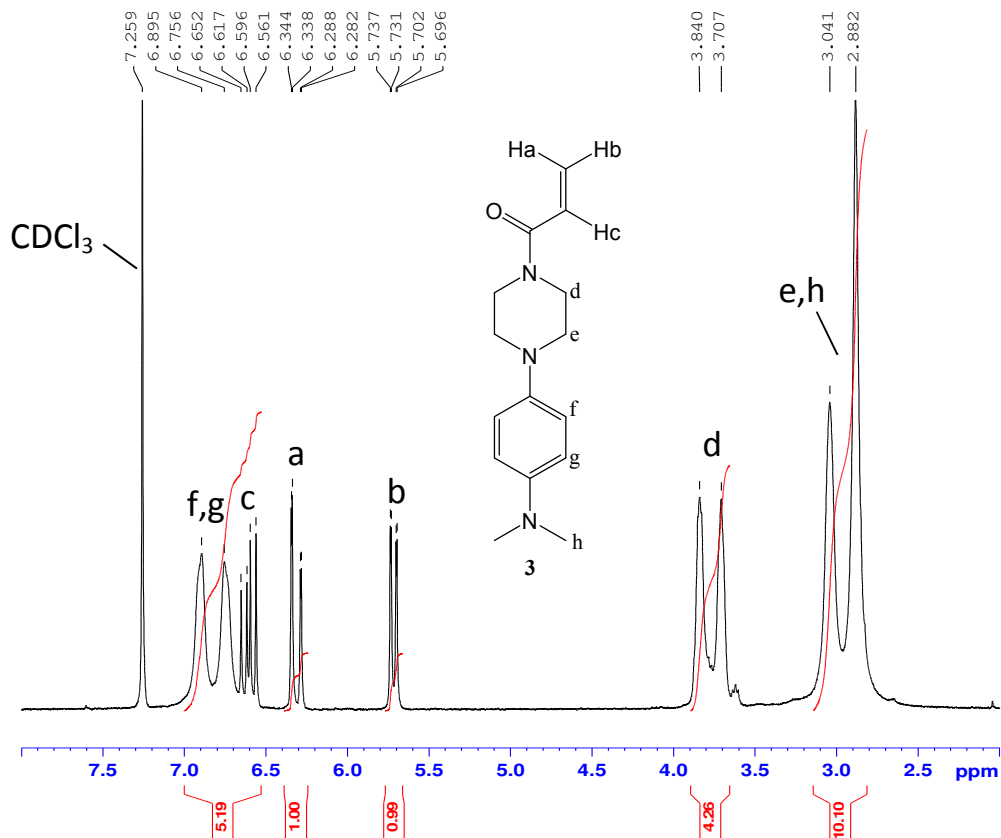
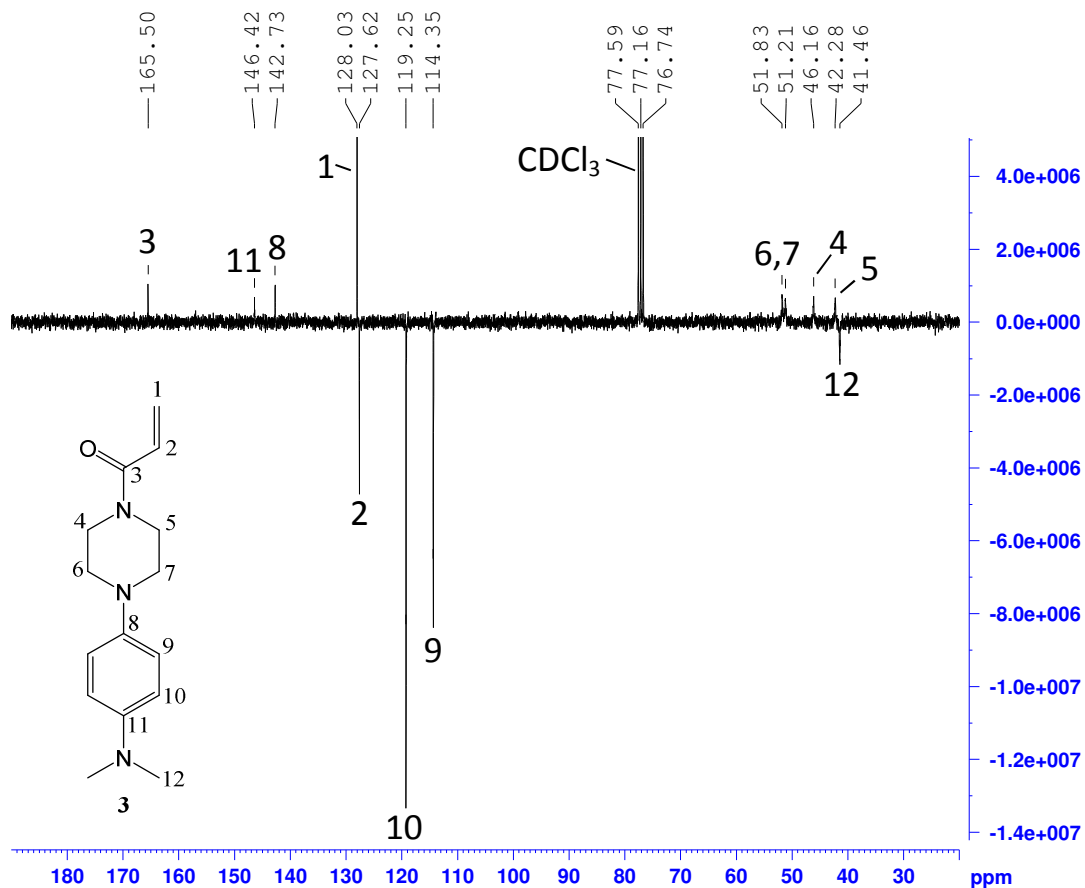
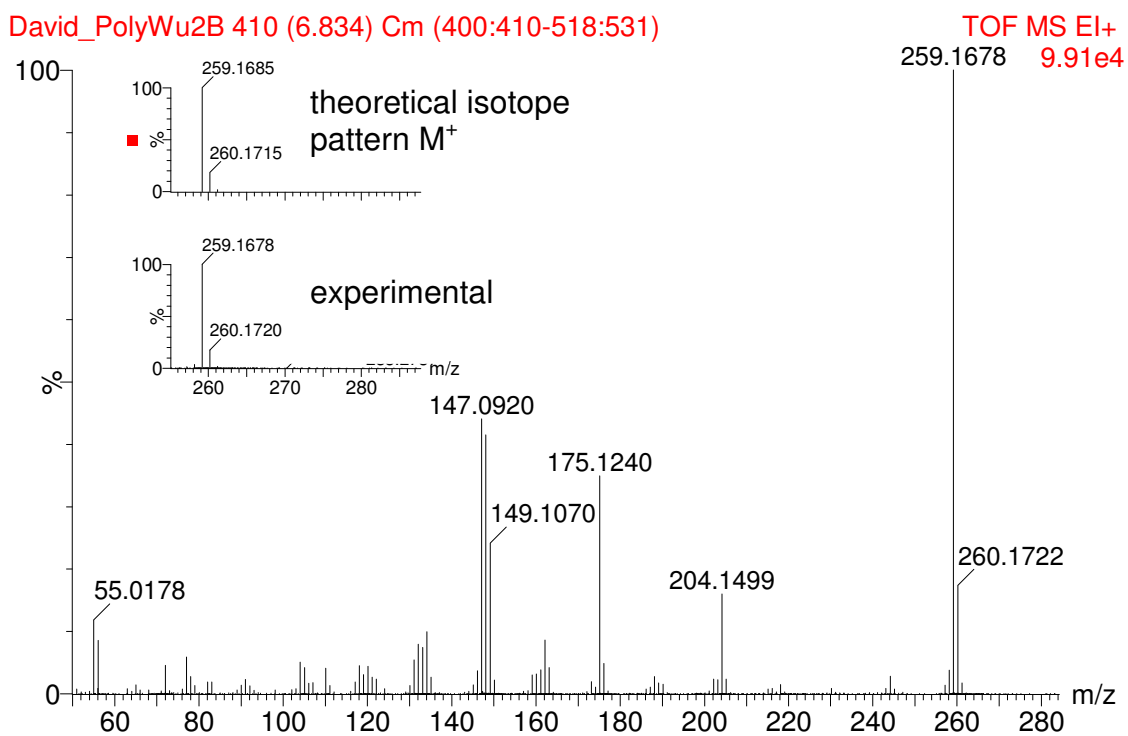
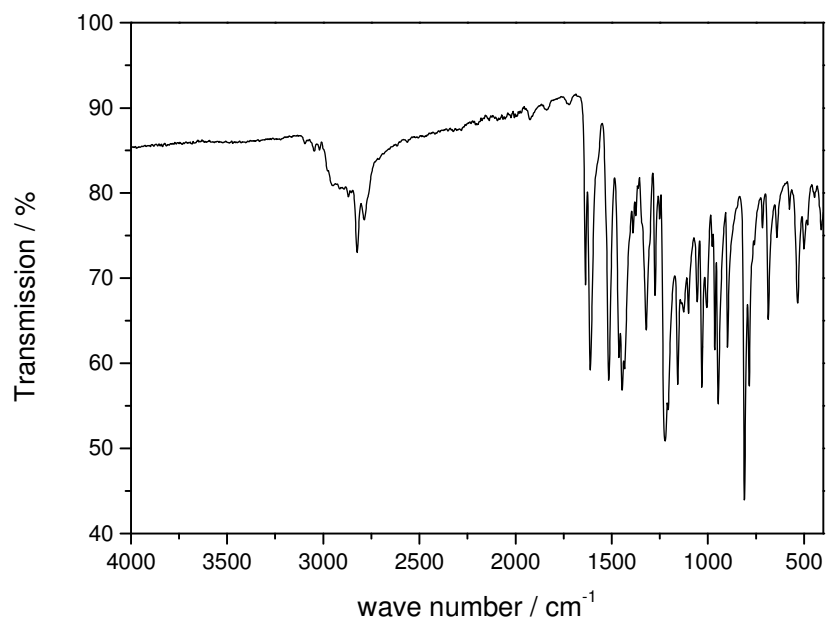
TOF MS EI+
1.80e⁶

Figure 35: GC/EI-MS spectrum of compound 2

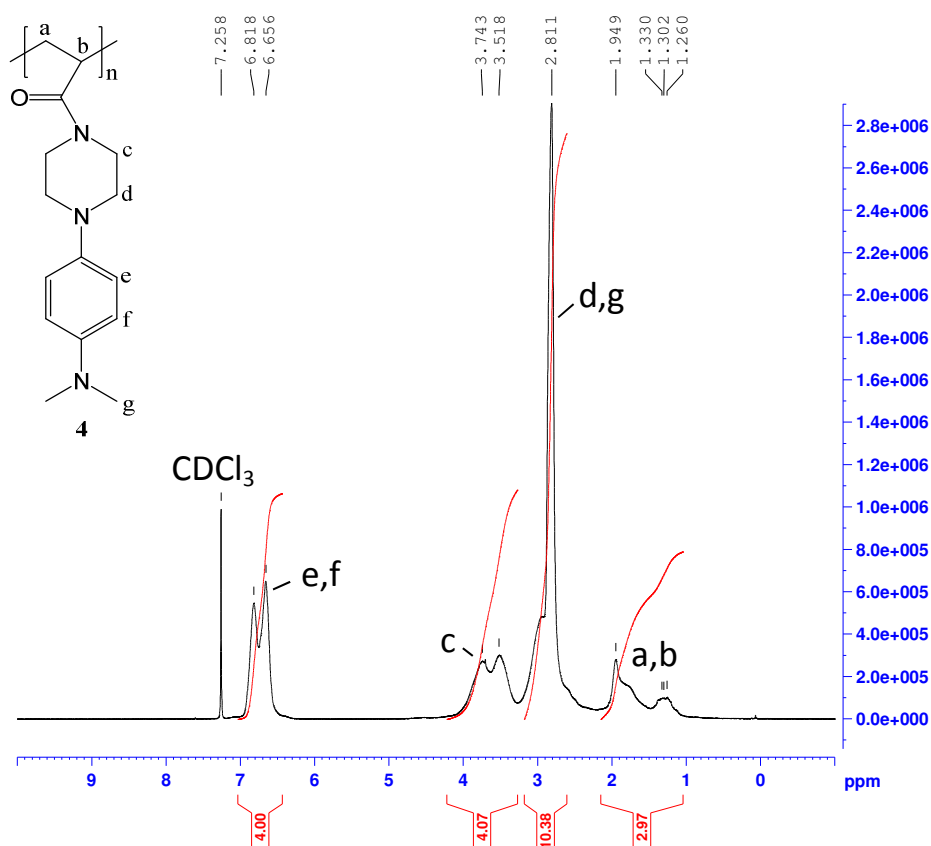
1-(4-(4-(dimethylamino)phenyl)piperazin-1-yl)prop-2-en-1-one (3)

Figure 36: ¹H NMR spectrum of compound 3

Figure 37: ^{13}C NMR (APT) spectrum of compound **3**Figure 38: EI-MS spectrum of monomer **3**

**Figure 39:** IR-spectrum of compound **3**

Poly[1-(4-(4-(dimethylamino)phenyl)piperazin-1-yl)acrylamide] (4)

**Figure 40:** ¹H NMR spectrum of polymer **4**

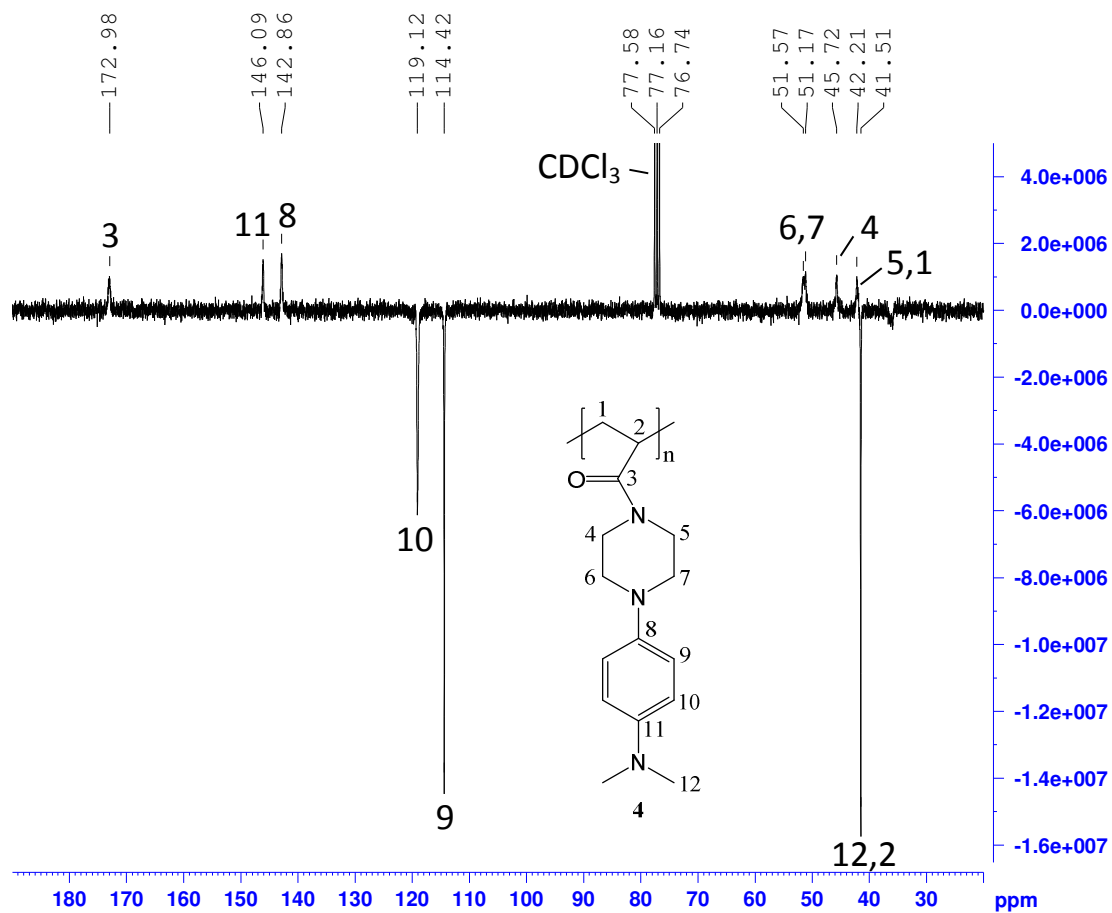


Figure 41: ^{13}C NMR (APT) spectrum of polymer 4

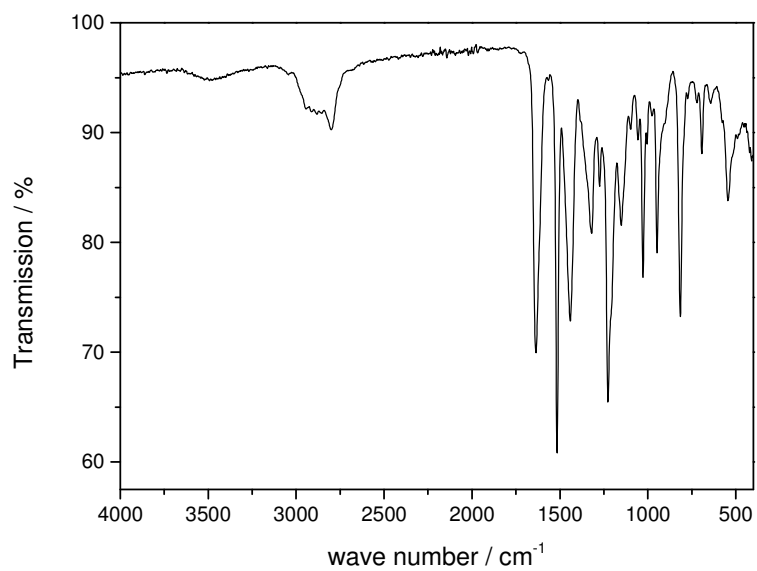
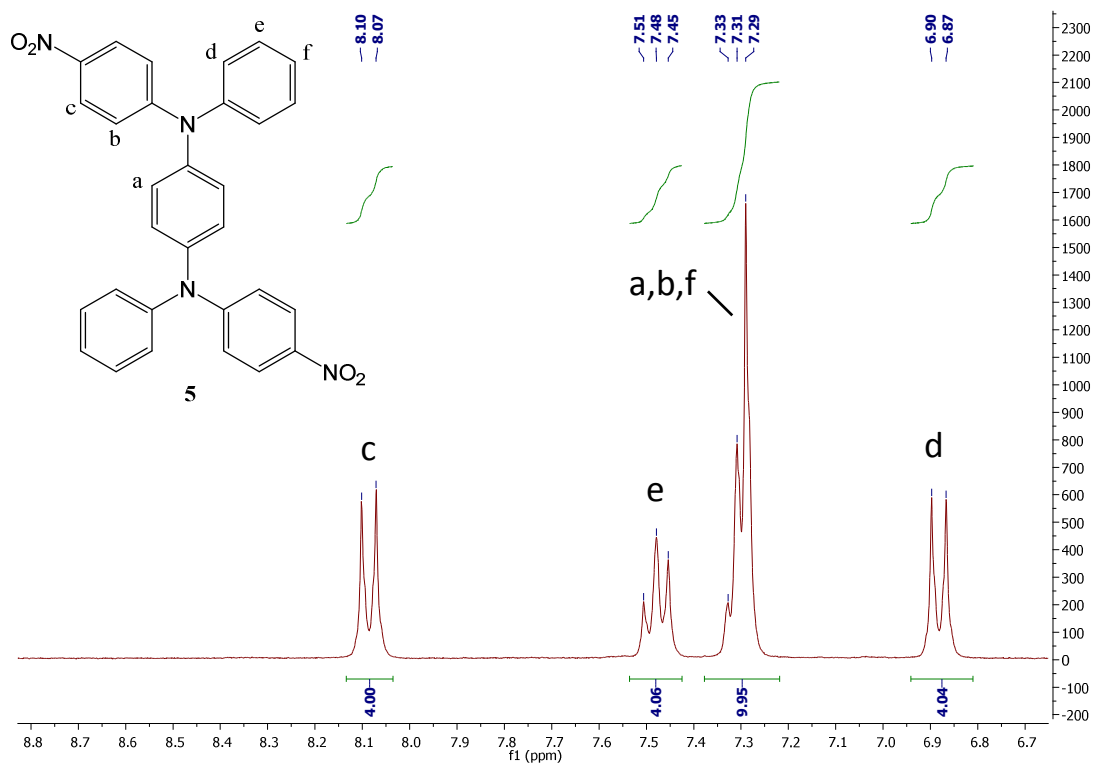
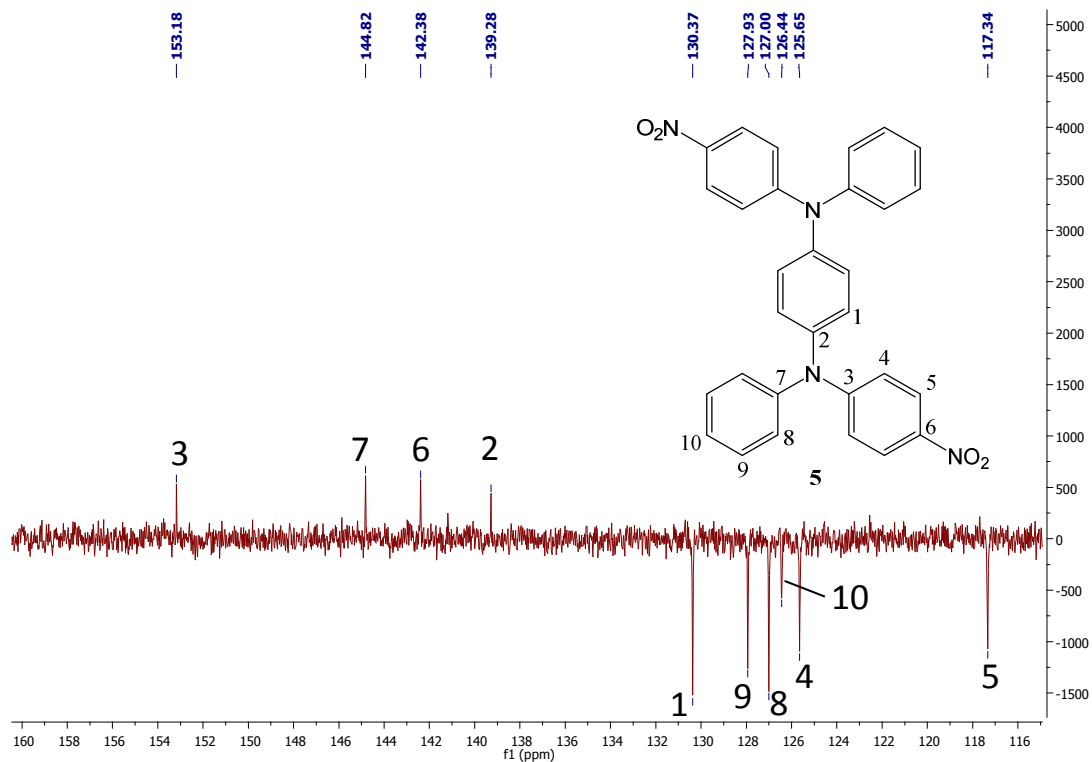


Figure 42: IR-spectrum of polymer 4

N,N'-bis(4-nitrophenyl)-*N,N'*-diphenyl-*p*-phenylenediamine (**5**)Figure 43: ^1H NMR spectrum of compound **5**Figure 44: ^{13}C NMR (APT) spectrum of compound **5**

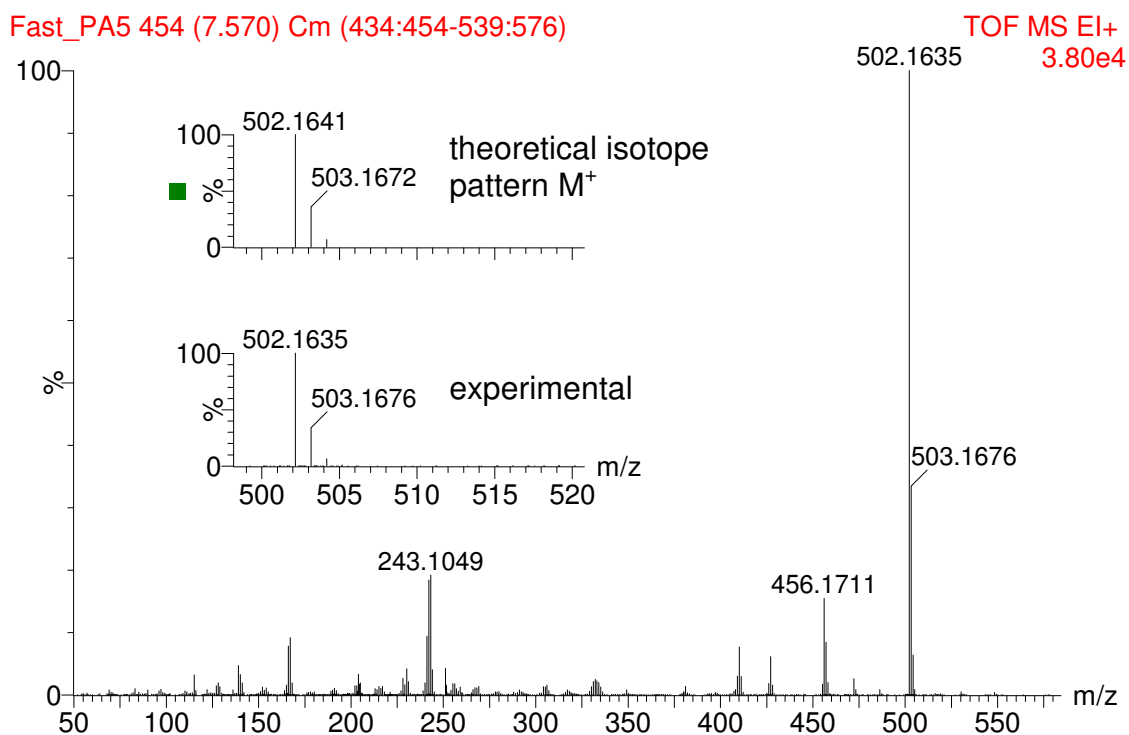


Figure 45: EI-MS spectrum of compound 5

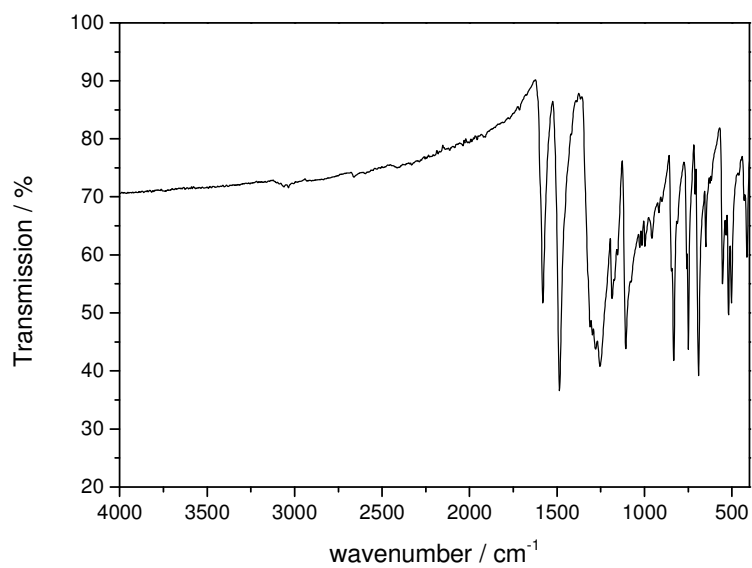
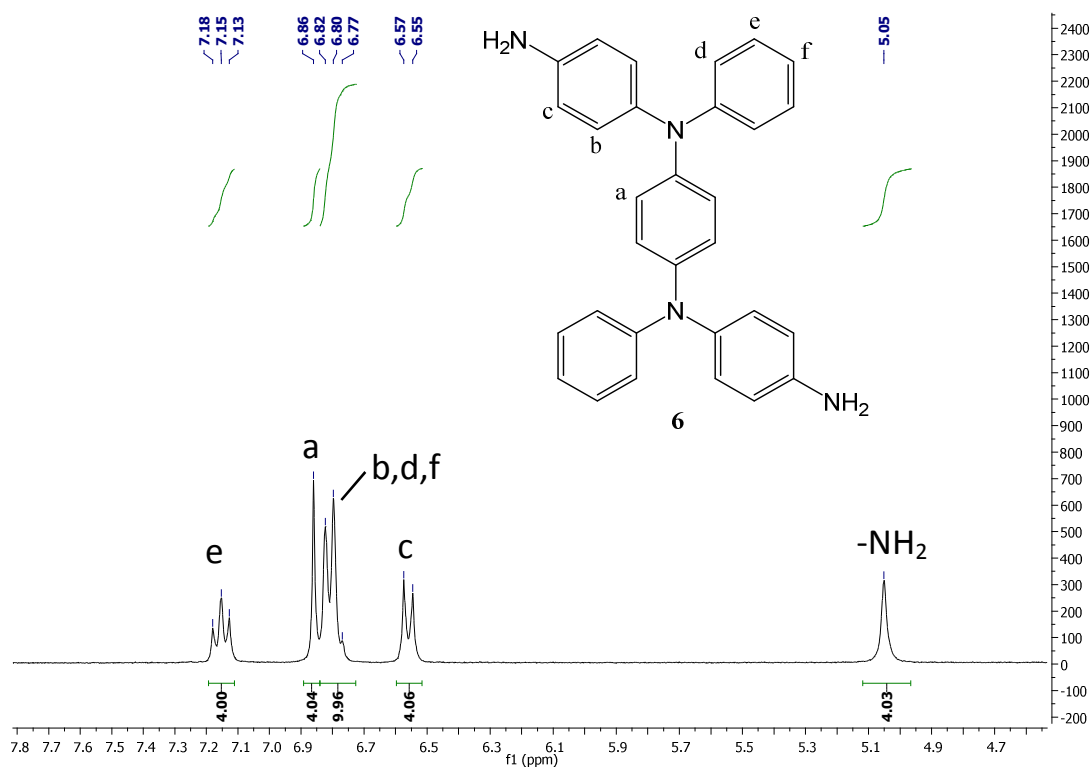
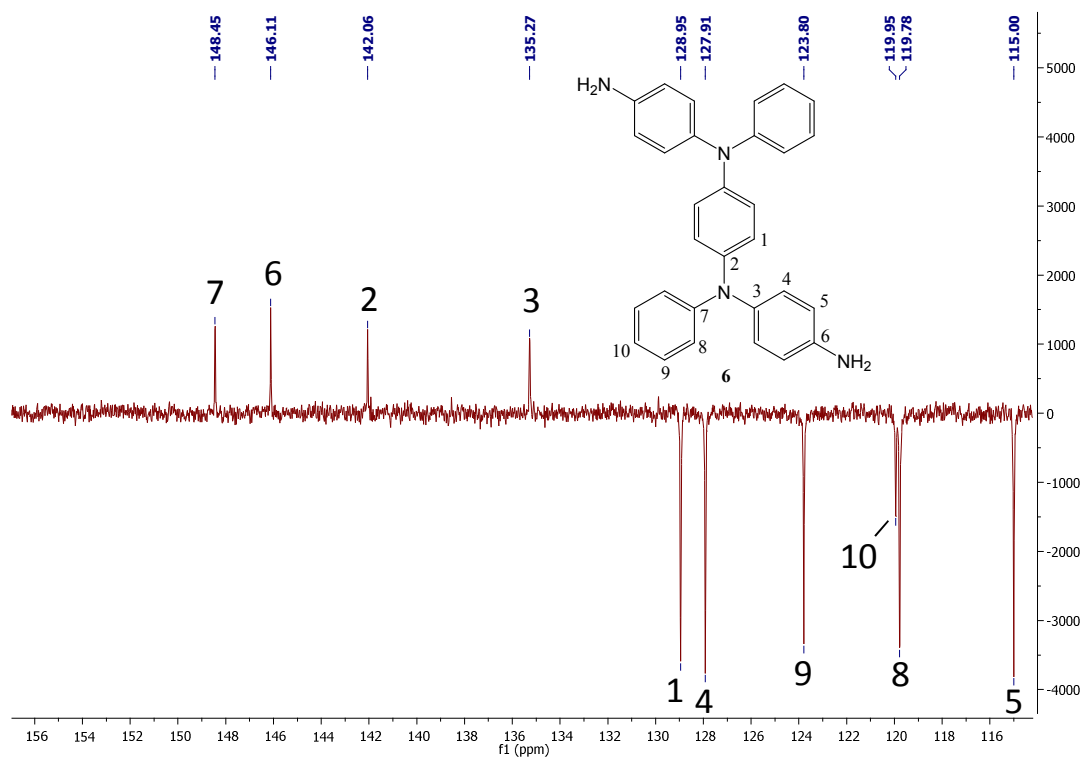


Figure 46: IR-spectrum of compound 5

N,N'-bis(4-aminophenyl)-*N,N'*-diphenyl-*p*-phenylenediamine (**6**)Figure 47: ¹H NMR spectrum of monomer **6**Figure 48: ¹³C NMR (APT) spectrum of monomer **6**

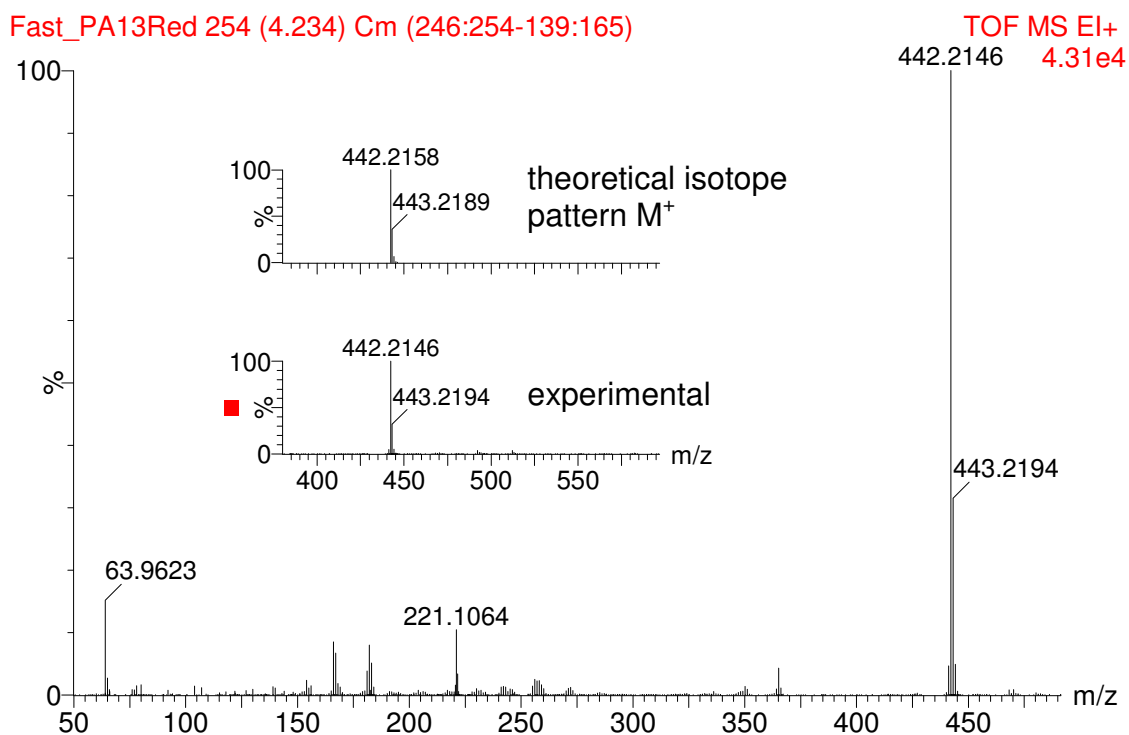


Figure 49: EI-MS spectrum of monomer 6

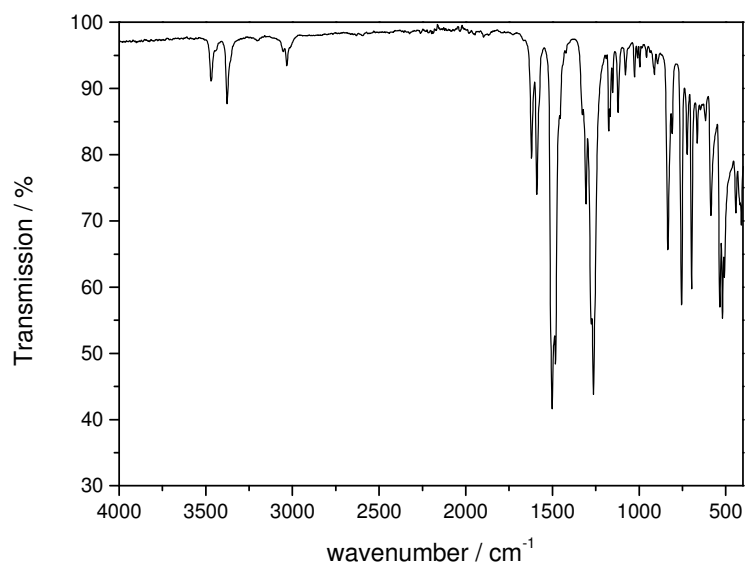
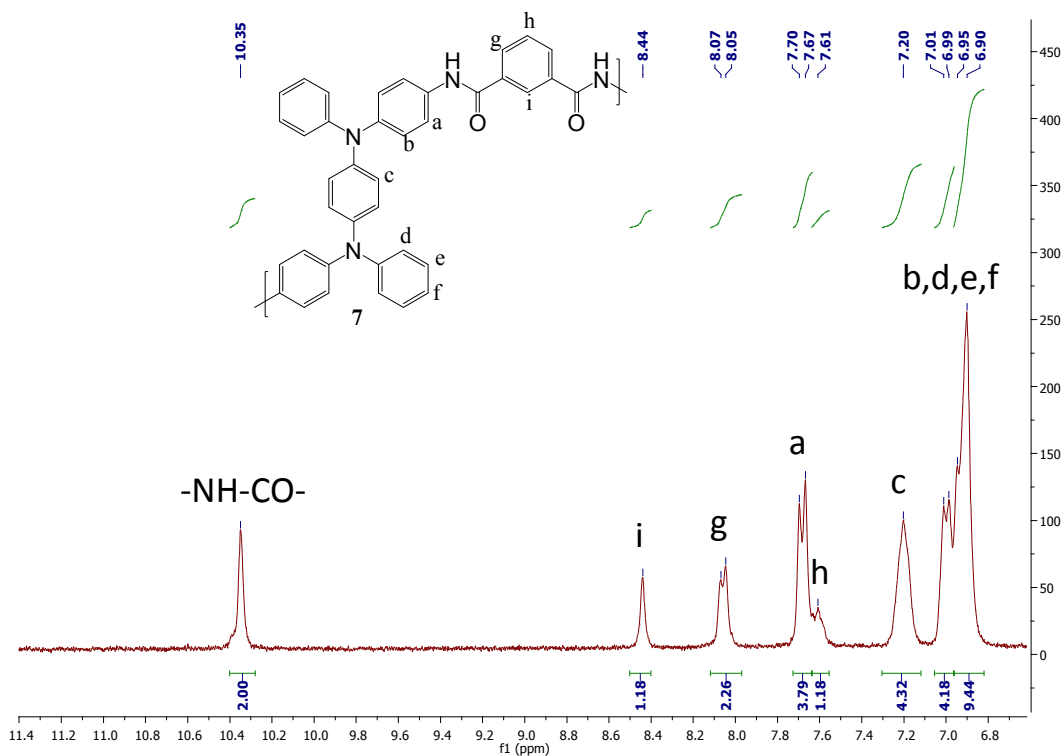
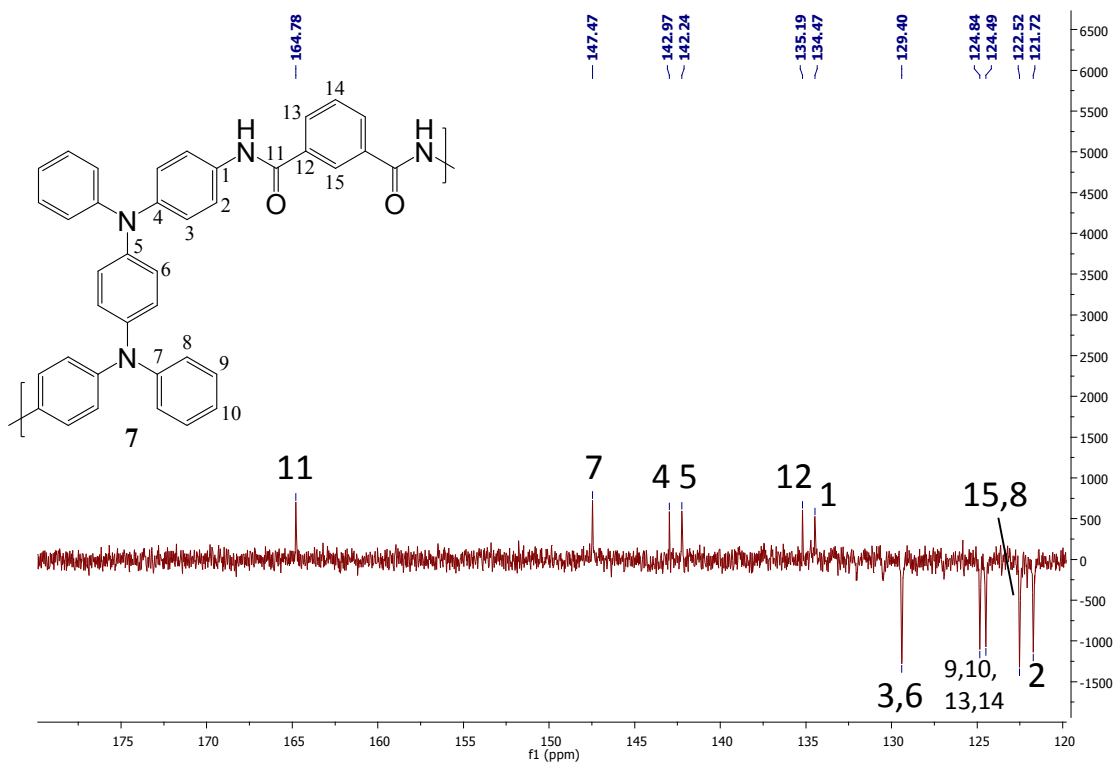


Figure 50: IR-spectrum of monomer 6

Polyamide with TPPD-units (**7**)Figure 51: ^1H NMR spectrum of polyamide **7**Figure 52: ^{13}C NMR (APT) spectrum of polyamide **7**

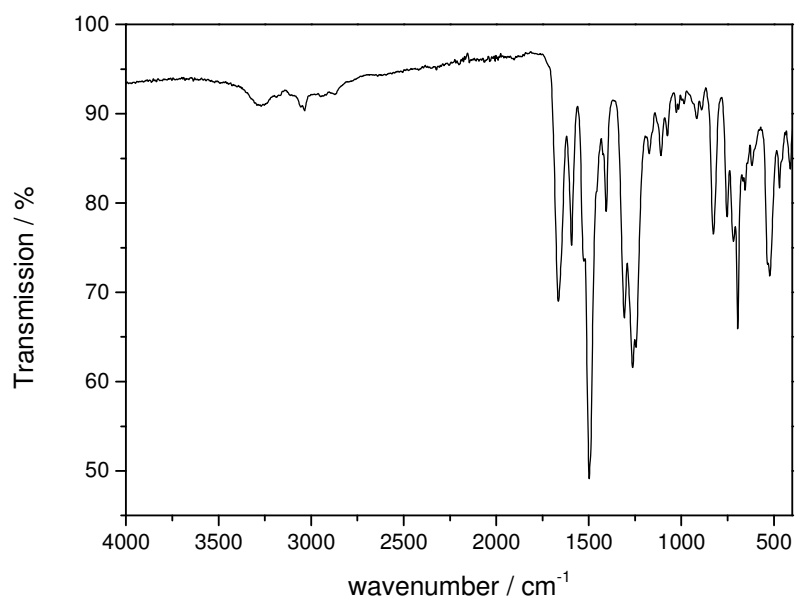
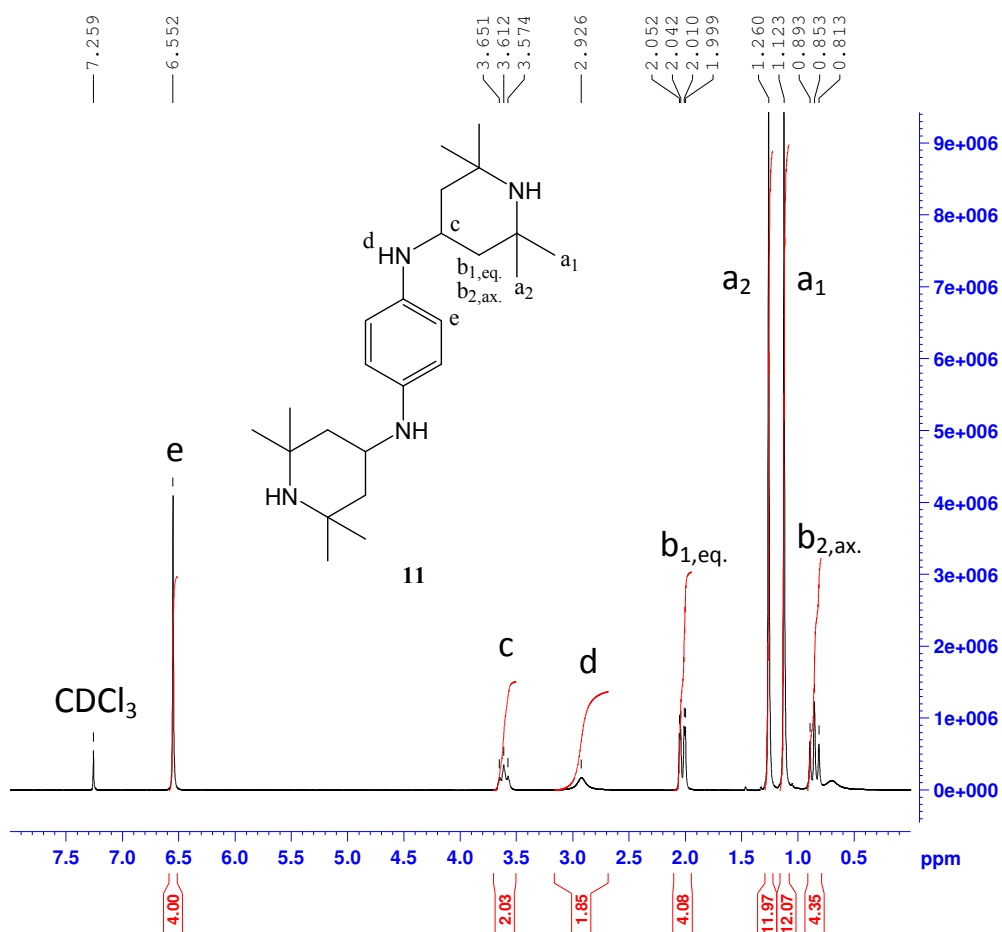


Figure 53: IR-spectrum of polyamide 7

N,N'-bis(2,2,6,6-tetramethylpiperidin-4-yl)-*p*-phenylenediamine (**8**)Figure 54: ^1H NMR spectrum of compound 8

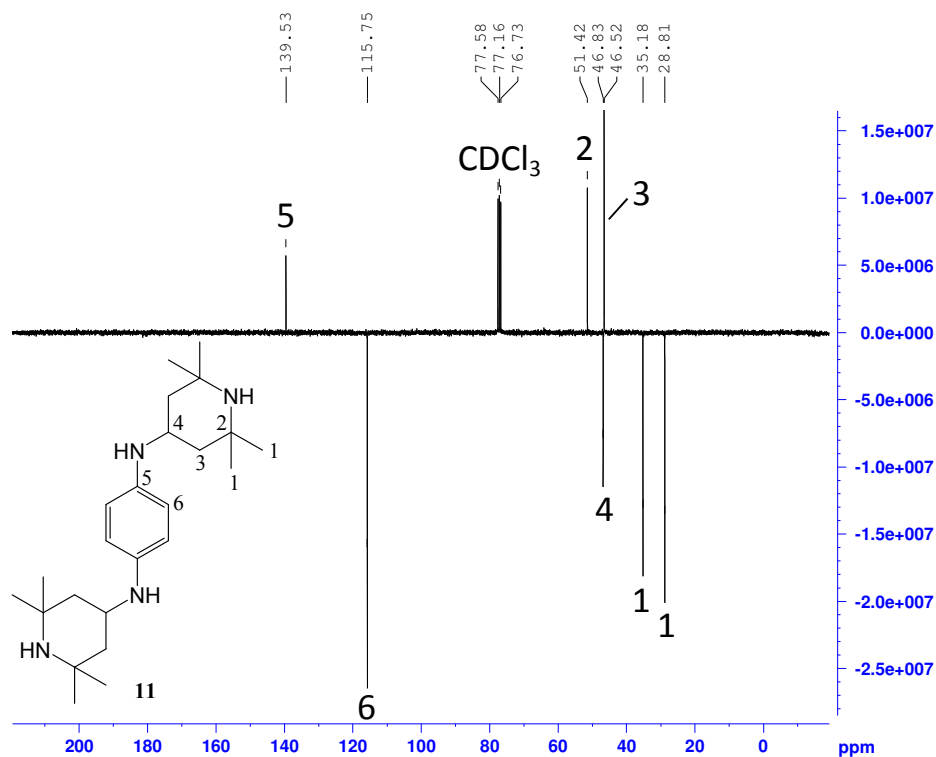
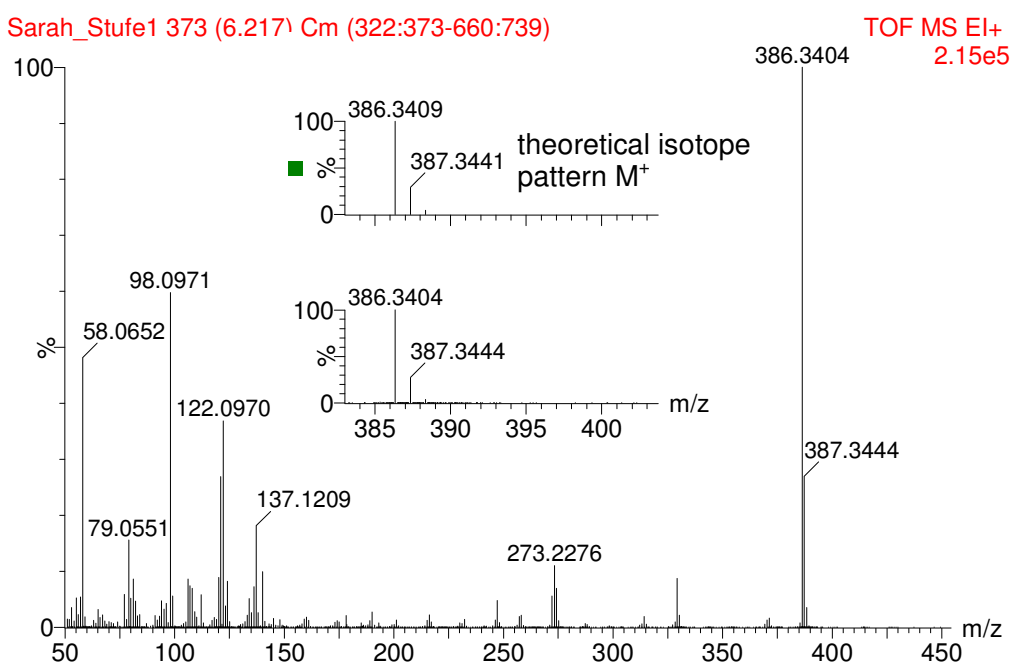
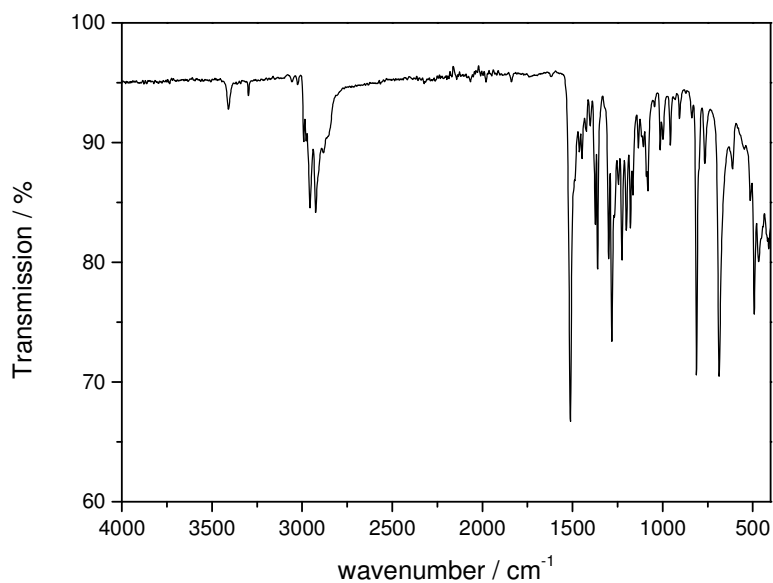
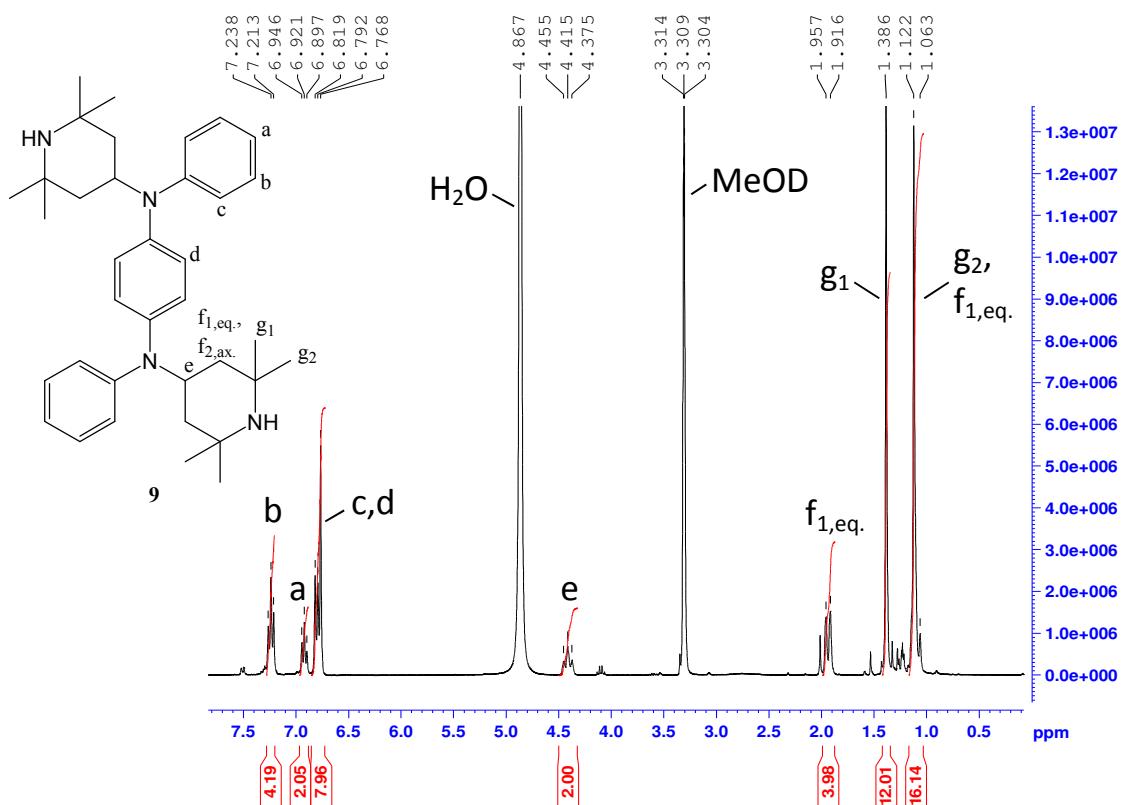
Figure 55: ^{13}C NMR (APT) spectrum of compound 8

Figure 56: EI-MS spectrum of compound 8

**Figure 57:** IR-spectrum of compound **8**

N,N'-diphenyl-*N,N'*-bis(2,2,6,6-tetramethylpiperidin-4-yl)*p*-phenylenediamine (**9**)

**Figure 58:** ¹H NMR spectrum of compound **9**

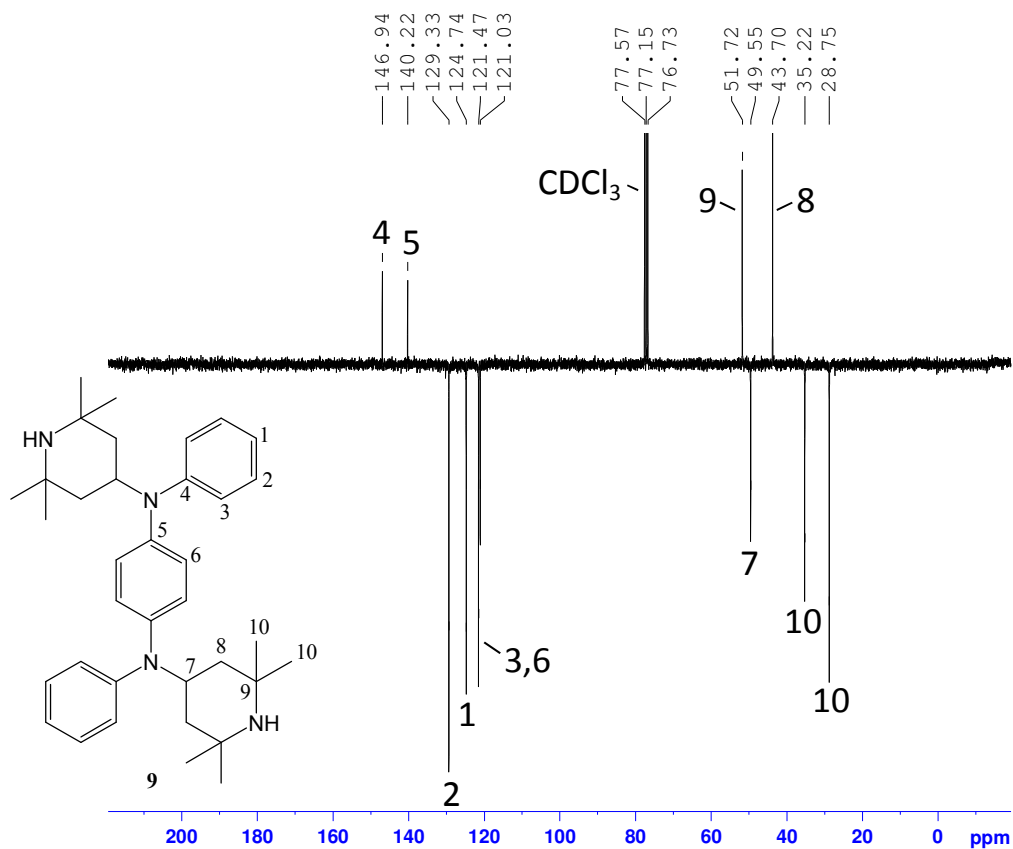
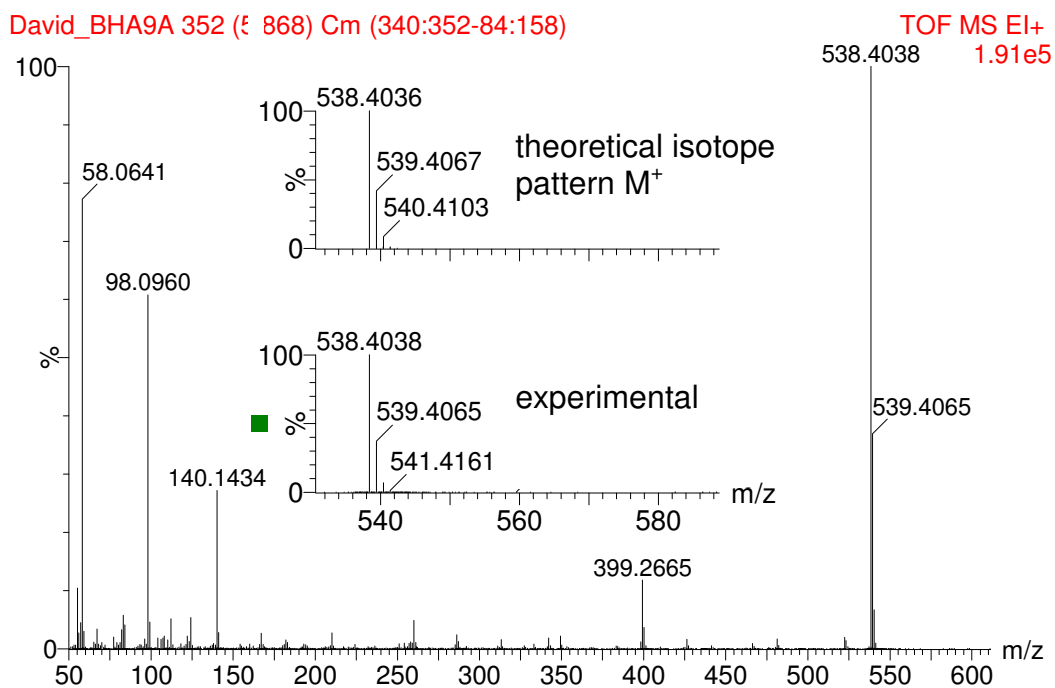
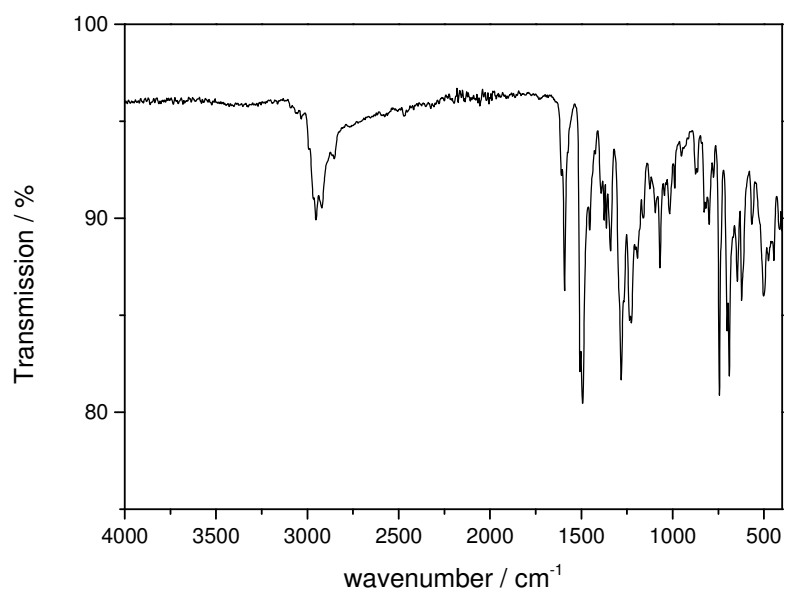
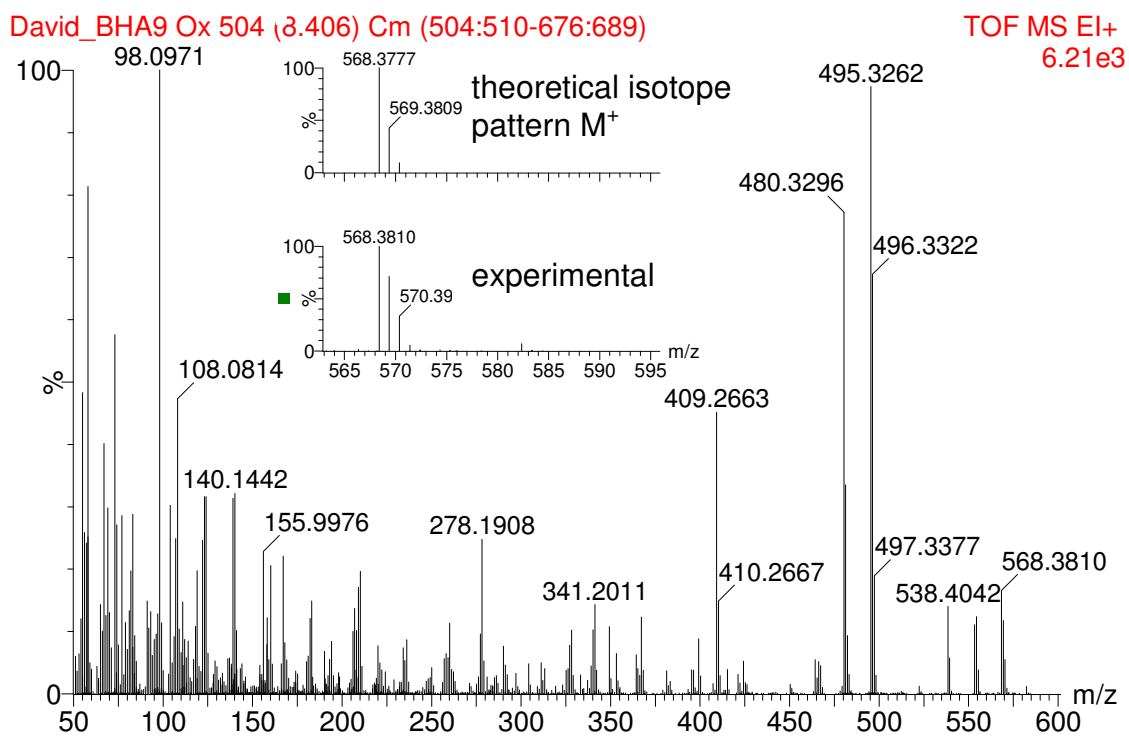
Figure 59: ^{13}C NMR (APT) spectrum of compound 9

Figure 60: EI-MS spectrum of compound 9

**Figure 61:** IR-spectrum of compound **9**

N,N'-diphenyl-*N,N'*-bis(2,2,6,6-tetramethylpiperidinyloxy-4-yl)-*p*-phenylenediamine (**10**)

**Figure 62:** EI-MS spectrum of model compound **10**

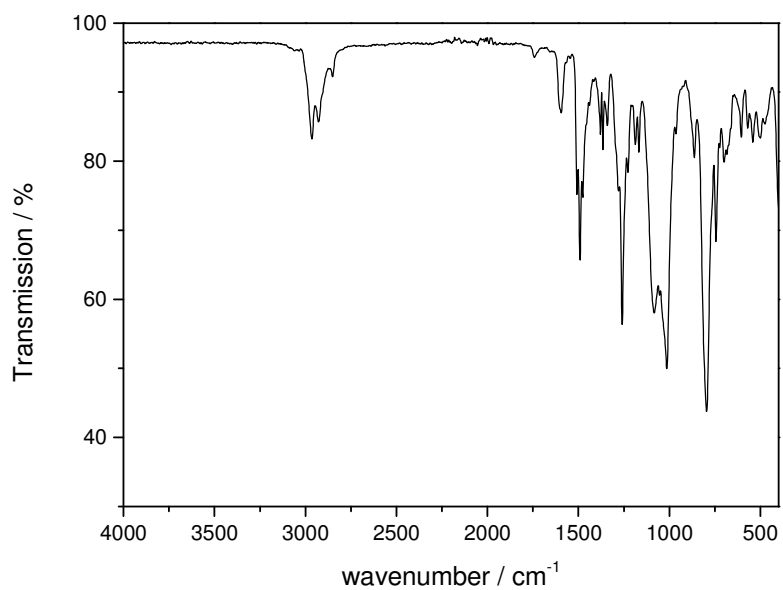


Figure 63: IR-spectrum of model compound **10**

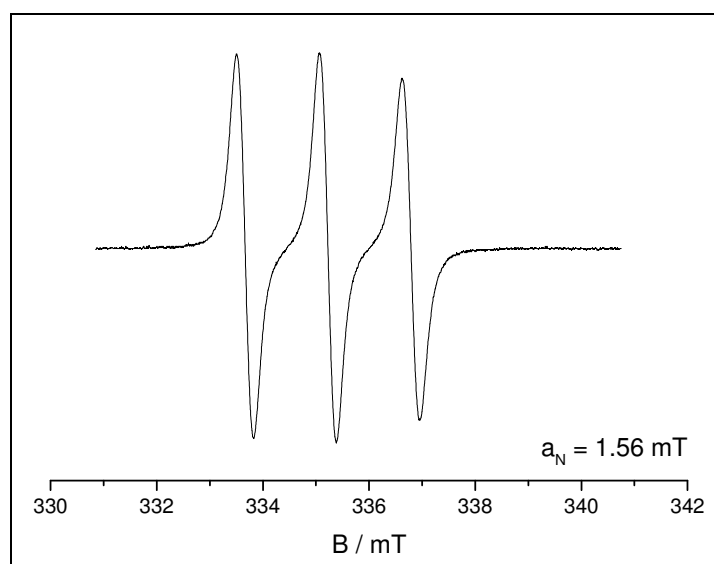


Figure 64: EPR-spectrum of model compound **10**

N,N'-bis(4-((*tert*-butyldimethylsilyl)oxy)phenyl)-*N,N'*-bis(2,2,6,6-tetramethylpiperidin-4-yl)-*p*-phenylenediamine (**11**)

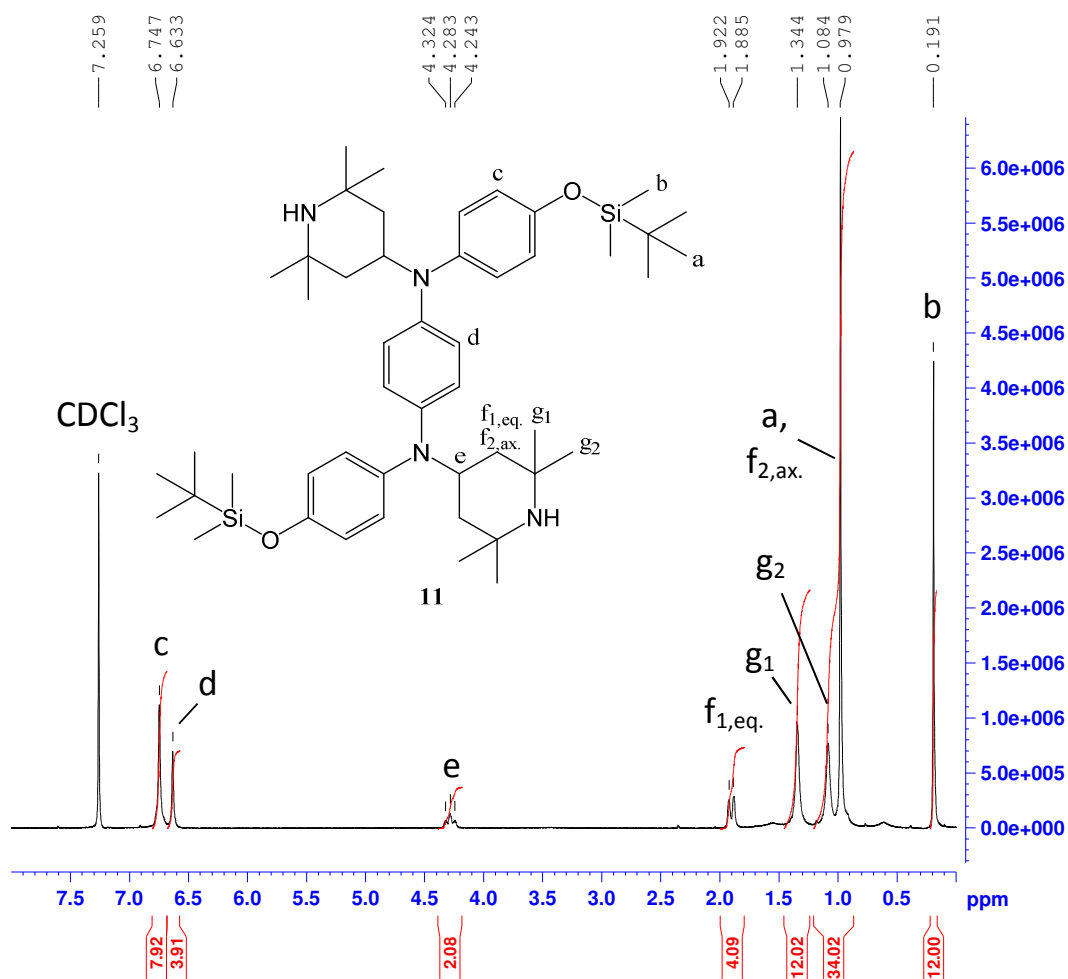
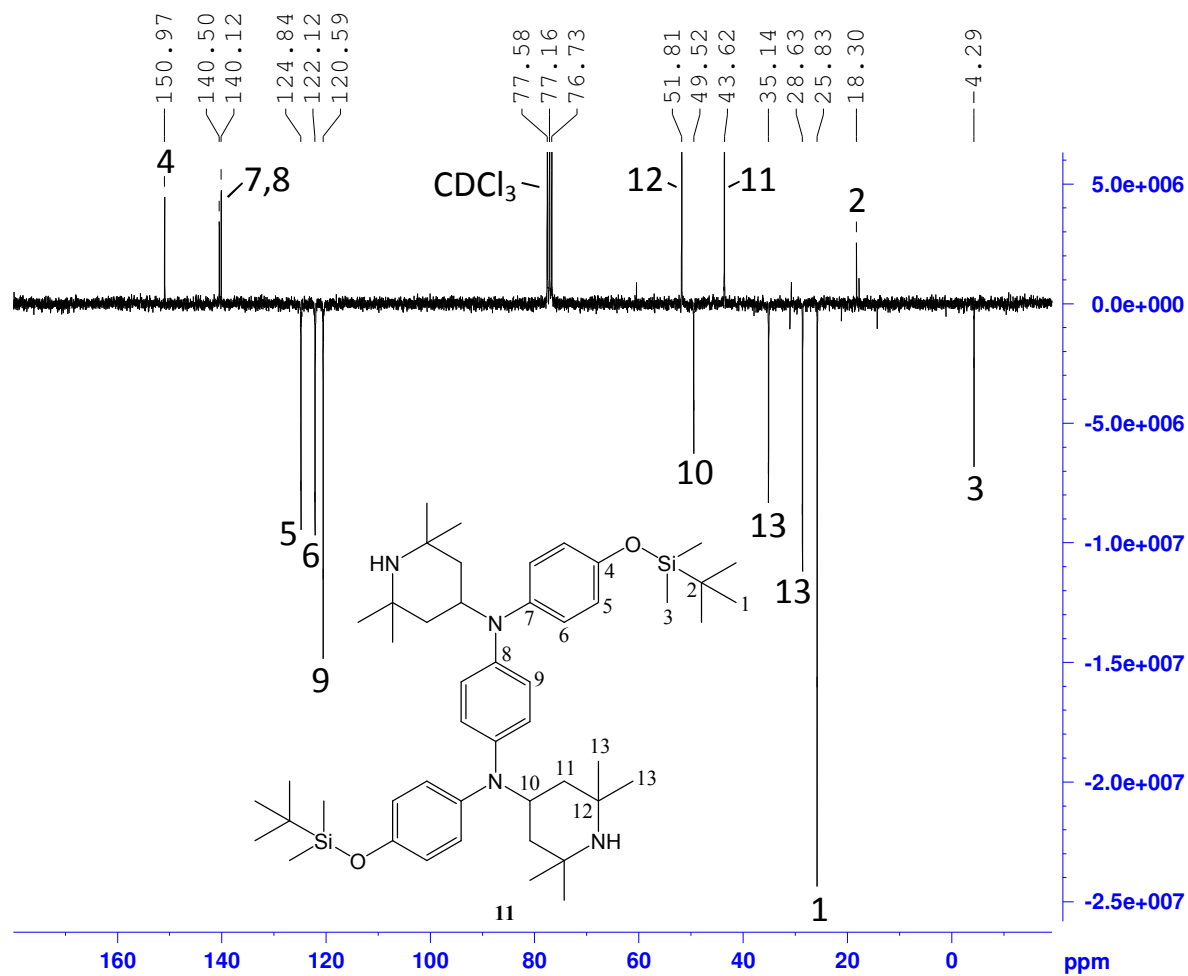


Figure 65: ^1H NMR spectrum of compound **11**



david m22 2 15 (0.658) Sb (99,30.00) ; Cm (1:37)

TOF LD+
2.44e4

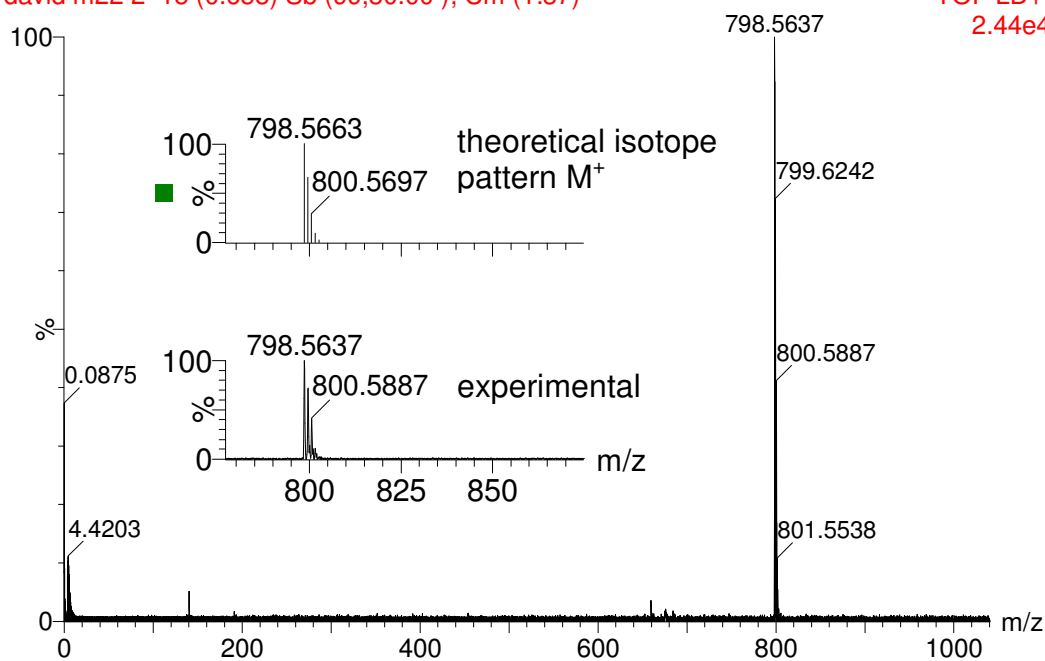


Figure 67: MALDI-MS spectrum of compound **11**

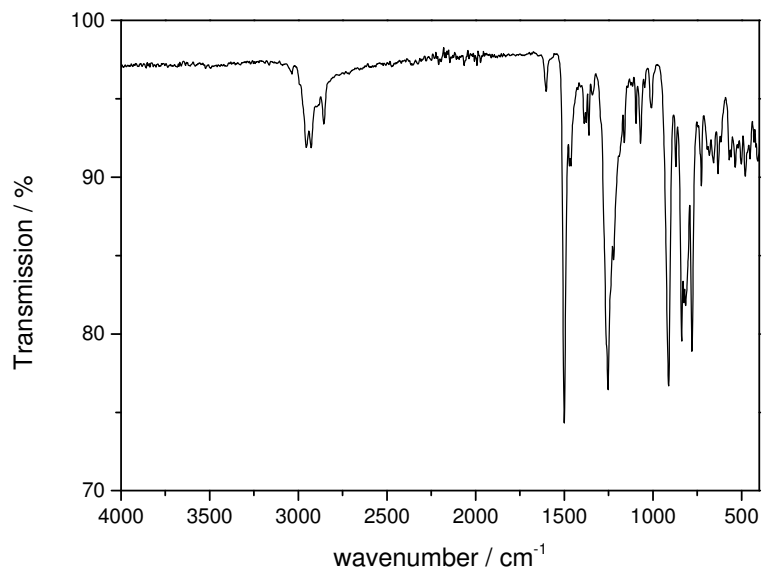


Figure 68: IR-spectrum of compound **11**

N,N'-bis(4-((*tert*-butyldimethylsilyl)oxy)phenyl)-*N,N'*-bis(2,2,6,6-tetramethylpiperidinyloxy-4-yl)-*p*-phenylenediamine (**12**)

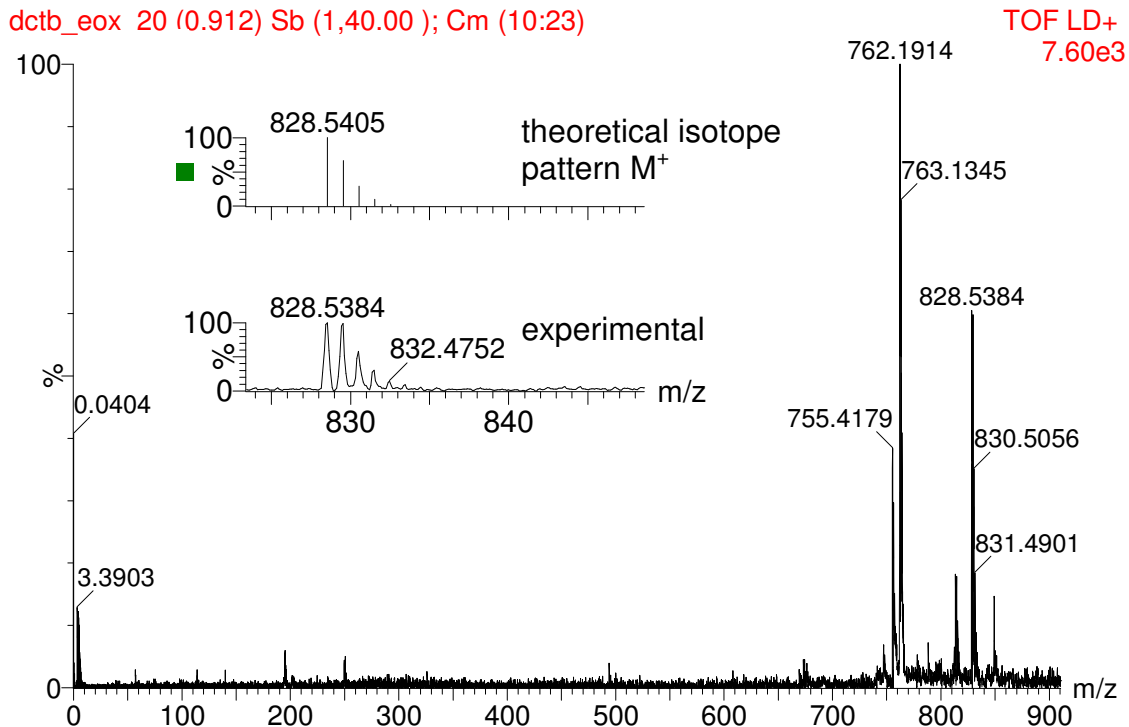


Figure 69: MALDI-MS spectrum of monomer precursor **12**

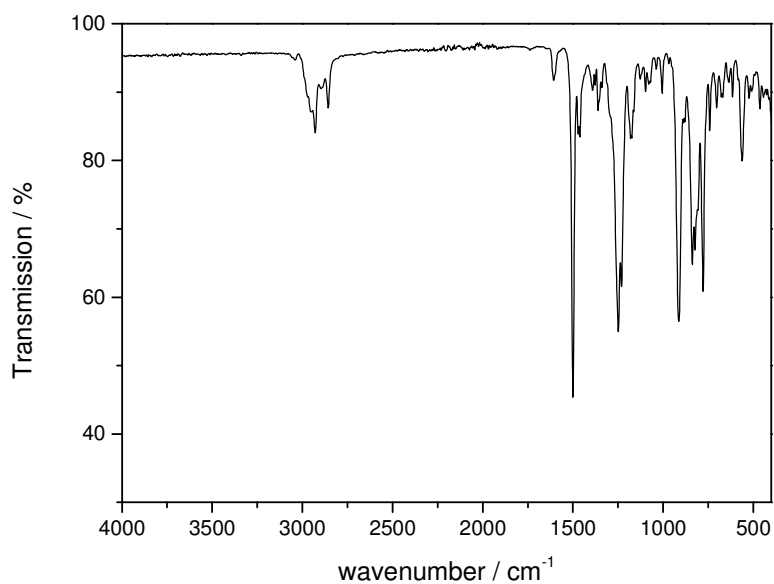


Figure 70: IR-spectrum of monomer precursor **12**

N,N'-bis(4-phenol)-*N,N'*-bis(2,2,6,6-tetramethylpiperidinyloxy-4-yl)-*p*-phenylenediamine (**13**)

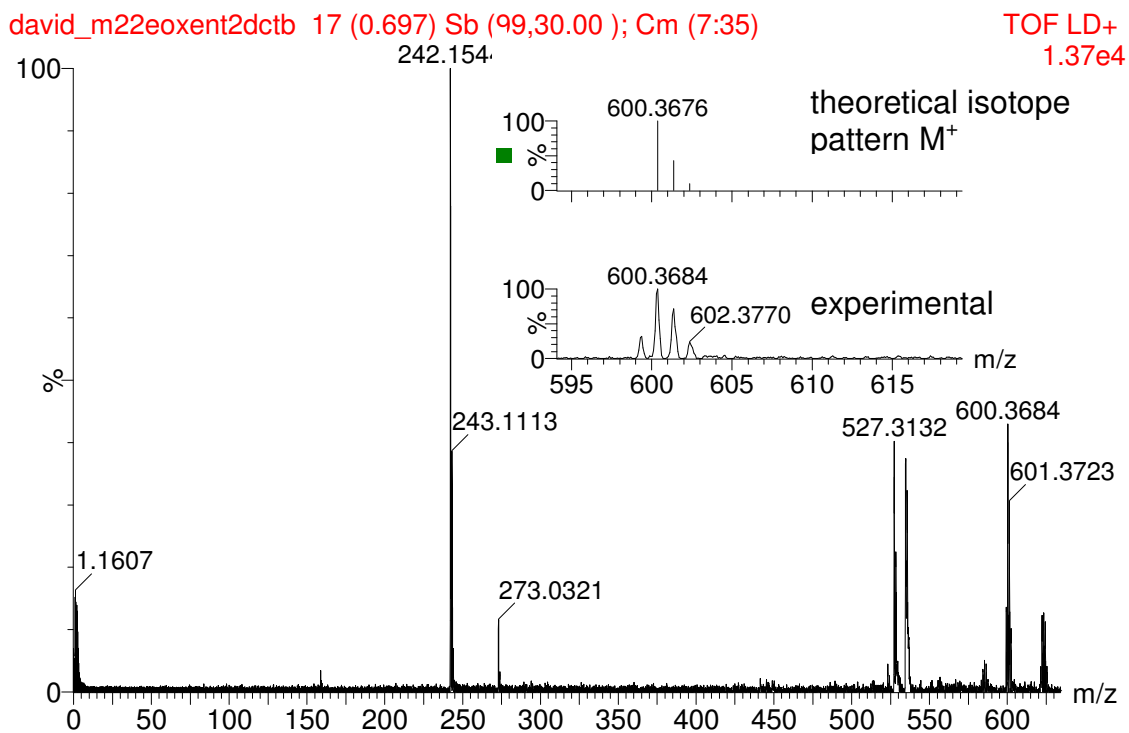


Figure 71: MALDI-MS spectrum of monomer **13**

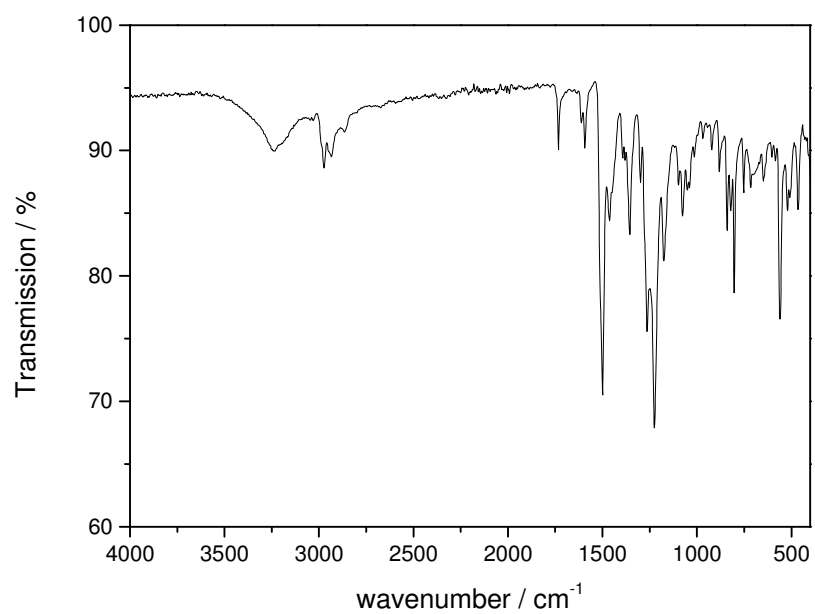


Figure 72: IR-spectrum of monomer **13**

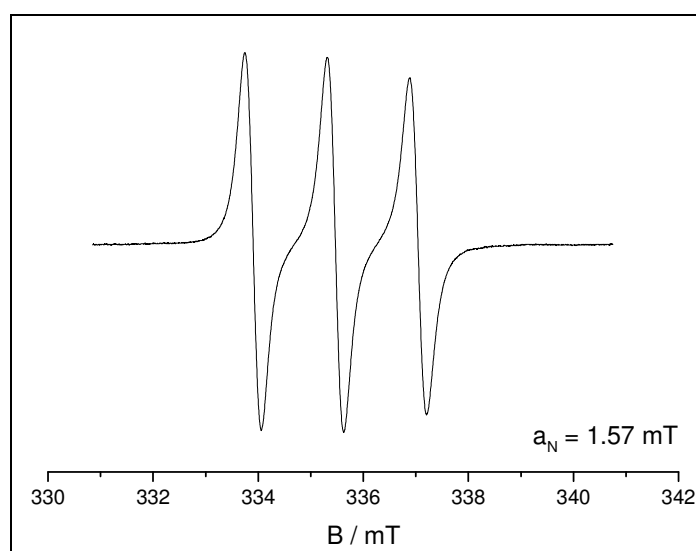
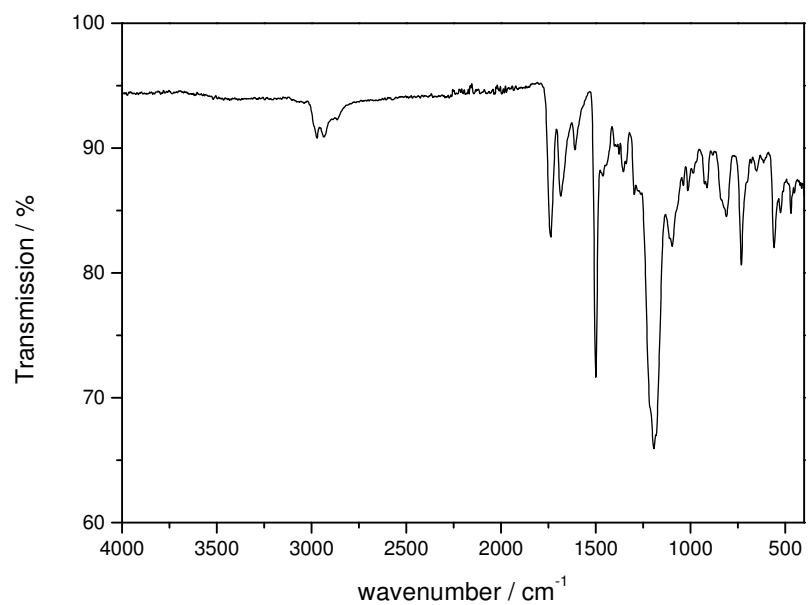
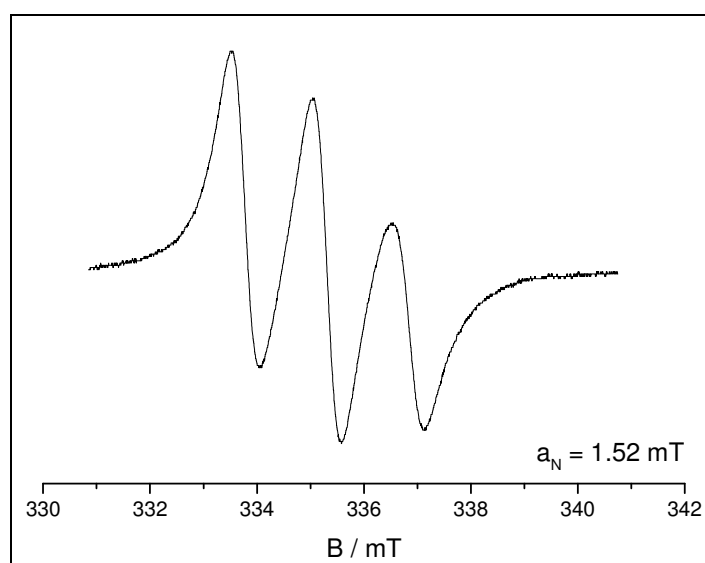


Figure 73: EPR-spectrum of monomer **13**

Polyester with TSPD- and TEMPO-units (14)**Figure 74:** IR-spectrum of polymer **14****Figure 75:** EPR-spectrum of polymer **14**

7.3 List of chemicals

Chemical	Distributor	Prod. no.	Purity	CAS
(4-Bromophenoxy)- tert- butyldimethylsilane	Sigma-Aldrich	444774	97 %	67963-68-2
1,3,5- Benzenetricarbonyl trichloride	Sigma-Aldrich	147532	98 %	4422-95-1
1,4-Diaminobenzene	Sigma-Aldrich	78429	≥ 99.0 % (GC/NT)	106-50-3
1,4-Dibromobenzene	Sigma-Aldrich	D39029	-	106-37-6
1,4-Dioxan, anhydrous	Sigma-Aldrich	296309	99.8 %	123-91-1
1-Fluoro-4- nitrobenzene	Sigma-Aldrich	F11204	99 %	350-46-9
1-Methyl-2- pyrrolidinone, anhydrous	Sigma-Aldrich	328634	99.5 %	872-50-4
2,2,6,6-Tetramethyl-4- piperidone	Sigma-Aldrich	459119	95 %	826-36-8
2,2'-Azobis(2- methylpropionitrile)	Sigma-Aldrich	441090	98 %	78-67-1
2-picoline borane complex	Sigma-Aldrich	654213	95 %	3999-38-0
3-Chloroperbenzoic acid	Sigma-Aldrich	273031	≤ 77 %	937-14-4
4-Bromo-N,N- dimethylaniline	Sigma-Aldrich	242950	97 %	586-77-6
Acetic acid	Sigma-Aldrich	320099	≥ 99.7 %	64-19-7
Acetonitrile, ACS reagent	Sigma-Aldrich	360457	≥ 99.5 %	75-05-8
Acryloyl chloride	Alfa Aesar	L10363	96 %	814-68-6
Ammonium chloride, ACS reagent	Sigma-Aldrich	213330	≥ 99.5 %	12125-02-9
Bromobenzene	Fluka	244220	> 99.5 %	108-86-1
Chloroform, A.C.S. spectrophotometric grade, stabilized with 0.5-1.0 % ethanol	Sigma-Aldrich	366919	≥ 99.8 %	67-66-3
Chloroform-[D1] (99,8% D)	VWR	87153.0100	≥ 99.9 %	865-49-6
Cyclohexane, AnalaR, Normapur	VWR	23224.362	≥ 99.5 %	110-82-7

Chemical	Distributor	Prod. no.	Purity	CAS
Dichloromethane, analytical reagent grade	Fisher Chemical	D/1852/21	99.99 %	75-09-2
Dimethyl sulfoxide, anhydrous	Sigma-Aldrich	276855	≥ 99.9 %	67-68-5
Dimethyl sulfoxide-[D6] (99,8% D)	VWR	87154.0025	≥ 99.9 %	2206-27-1
Ethanol, denatured, GPR, rectapur	VWR	84835.460	99 %	64-17-5
Ethyl acetate, AnalaR, Normapur	VWR	23882.321	99.9 %	141-78-6
Hydrazine monohydrate (N ₂ H ₄ 64-65 %)	Sigma-Aldrich	207942	98 %	7803-57-8
Hydrochloric acid solution, 6 M	Fluka	31087	-	7647-01-0
Isophthaloyl dichloride	Sigma-Aldrich	119403	≥ 99.9 %	99-63-8
Kynar® 761 (polyvinylidene fluoride)	Arkema			24937-79-9
Methanol, AnalaR, normapur	VWR	20847.360	≥ 99.8 %	67-56-1
Methanol-[D4] (99,8% D) MagniSolv®	VWR	1.06028.0025	≥ 99.9 %	811-98-3
N,N'-Diphenyl-p-phenylenediamine	Sigma-Aldrich	292265	98 %	74-31-7
N,N-Dimethylformamide, anhydrous	Sigma-Aldrich	227056	99.8 %	68-12-2
Palladium on carbon, extent of labeling: 10 wt% loading, matrix activated carbon	Sigma-Aldrich	205699	-	-
Palladium(II) acetate	Sigma-Aldrich	520764	99.9+ %, trace metals basis	3375-31-3
Piperazine	Sigma-Aldrich	P45907	99 %	110-85-0
Piperazine	Sigma-Aldrich	P45907	99 %	110-85-0
Potassium <i>tert</i> -butoxide	Sigma-Aldrich	156671	95 %	865-47-4
Sodium chloride, reagent grade	Sigma-Aldrich	310166	≥ 98 %	7647-14-5

Chemical	Distributor	Prod. no.	Purity	CAS
Sodium hydrogen carbonate, GPR, rectapur	VWR	27776.296	≥ 99 %	144-55-8
Sodium hydroxide, pellets, AnalaR, normapur	VWR	28244.295	-	1310-73-2
Sodium sulphate, anhydrous, AnalaR, normapur	VWR	28114.296	99.9 %	7757-82-6
Sodium <i>tert</i> -butoxide	Sigma-Aldrich	359270	97 %	865-48-5
Super P®	Timcal			
Tetrabutylammonium fluoride solution (1.0 M in THF)	Sigma-Aldrich	216143		429-41-4
Tetrabutylammonium perchlorate, for electrochemical analysis	Fluka	86893	≥ 99 %	1923-70-2
Tetrahydrofuran GPR rectapur	VWR	28552.461	≥ 99 %	109-99-9
Toluene GPR rectapur	VWR	28675.465	≥ 99 %	108-88-3
Triethylamine	Sigma-Aldrich	471283	≥ 99.5 %	121-44-8
Tri- <i>tert</i> -butylphosphine solution (1.0 M in toluene)	Sigma-Aldrich	G55325		13716-12-6

7.4 List of Figures

Figure 1: Working principle of an all-organic radical battery	11
Figure 2: IR spectra of polymer 1 and piperazine.....	35
Figure 3: Cyclic voltammogram of a composite cathode containing polymer 1 as active material (scan rate $v = 0.1$ mV/s).....	36
Figure 4: Cyclic voltammogram of polymer 4 in solution ($v = 50$ mV/s, 1 mM in CHCl_3 containing 0.1 M TBAP).....	38
Figure 5: Cyclic voltammograms of polymer 4 (a) in solution ($v = 20$ mV/s, 1 mM in CHCl_3 containing 0.1 M TBAP) and (b) on ITO ($v = 50$ mV/s, electrolyte: 0.1 M TBAP in acetonitrile).....	39
Figure 6: Cyclic voltammogram of polyamide 7 on ITO ($v = 50$ mV/s, 0.1 M TBAP in acetonitrile).....	41
Figure 7: SEM images of (a-c) composite cathode A and (d) Super P®	43
Figure 8: Cyclic voltammogram of composite cathode A containing polyamide 7 as active material ($v = 0.1$ mV/s)	44
Figure 9: Cyclic voltammograms at different scan rates of composite cathode A containing polyamide 7 as active material	45
Figure 10: Cyclic voltammograms of composite cathodes A with and without a 72 hour resting step ($v = 1.1$ mV/s).....	46
Figure 11: Rate capability test (3.2-4.0 V vs. Li/Li^+) of composite cathode A containing polyamide 7 as active material	47
Figure 12: Charge/discharge curves at different C-rates of composite cathode A containing polyamide 7 as active material	48
Figure 13: Ragone plots for composite cathode A containing polyamide 7 as active material normalized to the weight of (a) the active material and (b) the composite.....	49
Figure 14: Constant current cycling at 1 C of composite cathode A containing polyamide 7 as active material	50
Figure 15: SEM images of composite cathode A (a+b) before and (c+d) after constant current cycling at 1 C for 200 cycles	51

Figure 16: Constant current cycling at 10 C of a composite cathode A containing polyamide 7 as active material. The inset shows the first 25 cycles in more detail	52
Figure 17: Current-voltage characteristic of IU-charging of half-cells with composite cathodes containing (a) PN (1 C, cut-off potential: 4.0 V vs. Li/Li ⁺ , 1h) and (b) polyamide 7 (1 C, cut-off potential: 4.0 V vs. Li/Li ⁺ , 2h) as active material (composition A).....	53
Figure 18: IU-charging (1 h, 4.0 V vs Li/Li ⁺) and discharging at 1 C of a composite cathode containing polynorbornene with TEMPO-units (PN) as active material (PN :Super P®:binder = 10:80:10 wt-%)	54
Figure 19: IU-charging (2 h, 4.0 V vs Li/Li ⁺) and discharging at 1 C of composite cathode A containing polyamide 7 as active material	55
Figure 20: SEM images of composite cathodes with different compositions – active material content of (a+b) 20 wt-% (B), (c+d) 40 wt-% (C) and (e+f) 60 wt-% (D)	56
Figure 21: Cyclic voltammograms of composite cathodes B , C and D with increasing amount of active material (20, 40 and 60 wt-%, respectively) ($v = 0.1$ mV/s).....	57
Figure 22: Rate capability tests (3.0-4.2 V vs. Li/Li ⁺) of composite cathodes with active materials contents of (a) 20 wt-% (B), (b) 40 wt-% (C), (c) 60 wt-% (D) and (d) corresponding charge/ discharge curves at a rate of 1 C.....	59
Figure 23: ΔE_{ave} values at different C-rates for composite cathodes B , C and D of varying active material content (3.0-4.2 V vs Li/Li ⁺).....	60
Figure 24: Ragone plot for composite cathodes B , C and D (3.0-4.2 V vs Li/Li ⁺) normalized to the weight of (a) the composite and (b) the active material	61
Figure 25: Cyclic voltammograms of (a) N,N,N',N'-tetraphenyl-p-phenylenediamine and (b) 4-acetamido-TEMPO in solution ($v = 50$ mV/s, 1mM in chloroform containing 0.1 M TBAP).....	64
Figure 26: Cyclic voltammogram of model compound 10 in solution ($v = 50$ mV/s, 1mM in chloroform containing 0.1 M TBAP)	65
Figure 27: EPR-spectrum of model compound 10	66
Figure 28: EPR-spectra of (a) monomer 13 and (b) polymer 14	68
Figure 29: Cyclic voltammogram of a composite cathode with polymer 14 as active material (3.2-4.2 V vs. Li/Li ⁺ , $v = 0.1$ mV/s)	69

Figure 30: Cyclic voltammogram of a composite cathode with polymer 14 as active material in a smaller potential window (3.2-3.8 V vs. Li/Li ⁺ , $v = 0.1$ mV/s)	69
Figure 31: Constant current cycling at 1 C of a composite cathode with polymer 14 as active material.....	70
Figure 32: IR-spectrum of polymer 1	82
Figure 33: ¹ H NMR spectrum of compound 2	83
Figure 34: ¹³ C NMR (APT) spectrum of compound 2	83
Figure 35: GC/EI-MS spectrum of compound 2	84
Figure 36: ¹ H NMR spectrum of compound 3	84
Figure 37: ¹³ C NMR (APT) spectrum of compound 3	85
Figure 38: EI-MS spectrum of monomer 3	85
Figure 39: IR-spectrum of compound 3	86
Figure 40: ¹ H NMR spectrum of polymer 4	86
Figure 41: ¹³ C NMR (APT) spectrum of polymer 4	87
Figure 42: IR-spectrum of polymer 4	87
Figure 43: ¹ H NMR spectrum of compound 5	88
Figure 44: ¹³ C NMR (APT) spectrum of compound 5	88
Figure 45: EI-MS spectrum of compound 5	89
Figure 46: IR-spectrum of compound 5	89
Figure 47: ¹ H NMR spectrum of monomer 6	90
Figure 48: ¹³ C NMR (APT) spectrum of monomer 6	90
Figure 49: EI-MS spectrum of monomer 6	91
Figure 50: IR-spectrum of monomer 6	91
Figure 51: ¹ H NMR spectrum of polyamide 7	92
Figure 52: ¹³ C NMR (APT) spectrum of polyamide 7	92
Figure 53: IR-spectrum of polyamide 7	93
Figure 54: ¹ H NMR spectrum of compound 8	93
Figure 55: ¹³ C NMR (APT) spectrum of compound 8	94
Figure 56: EI-MS spectrum of compound 8	94
Figure 57: IR-spectrum of compound 8	95

Figure 58: ^1H NMR spectrum of compound 9	95
Figure 59: ^{13}C NMR (APT) spectrum of compound 9	96
Figure 60: EI-MS spectrum of compound 9	96
Figure 61: IR-spectrum of compound 9	97
Figure 62: EI-MS spectrum of model compound 10	97
Figure 63: IR-spectrum of model compound 10	98
Figure 64: EPR-spectrum of model compound 10	98
Figure 65: ^1H NMR spectrum of compound 11	99
Figure 66: ^{13}C NMR (APT) spectrum of compound 11	100
Figure 67: MALDI-MS spectrum of compound 11	100
Figure 68: IR-spectrum of compound 11	101
Figure 69: MALDI-MS spectrum of monomer precursor 12	101
Figure 70: IR-spectrum of monomer precursor 12	102
Figure 71: MALDI-MS spectrum of monomer 13	102
Figure 72: IR-spectrum of monomer 13	103
Figure 73: EPR-spectrum of monomer 13	103
Figure 74: IR-spectrum of polymer 14	104
Figure 75: EPR-spectrum of polymer 14	104

7.5 List of Schemes

Scheme 1: Examples of conducting polymers in their undoped state: polyacetylene ^{10,11} (I), polyaniline ^{12,13} (II), polypyrrole ¹⁴ (III) and polythiophene ¹⁵ (IV)	4
Scheme 2: Redox couple organic disulfide/thiolate.....	5
Scheme 3: Examples of organic disulfides and their theoretical capacities: tetraethylthiuram disulfide ¹⁷ (V), poly(2,5-dimercapto-1,3,4-thiadiazole ²⁰ (VI) and poly(5,8-dihydro- 1H,4H-2,3,6,7-tetrathiaanthracene ²¹ (VII).....	5
Scheme 4: Examples of carbonyl compounds and their theoretical capacities: dichloroisocyanuric acid ⁷ (VIII), chloranil ²⁶ (IX) and polyquinone ²⁹ (X)	6
Scheme 5: Redox reaction of benzoquinone.....	7

Scheme 6: Examples of polymers based on carbonyl groups and their theoretical capacities: poly(5-amino-p-naphthoquinone) ³⁰ (XI), poly(anthraquinonyl sulfide) ³³ (XII) and polyimide ³⁴ (XIII)	8
Scheme 7: Other organic electrode materials and their theoretical capacities	8
Scheme 8: Structure of 2,2,6,6-tetramethylpiperidine-1-oxyl (TEMPO).....	9
Scheme 9: Redox couples of nitroxyl radicals	10
Scheme 10: Examples of polyradicals used for ORBs and their theoretical capacities.....	10
Scheme 11: Redox couples of N,N,N',N'-tetramethyl-p-phenylenediamine (TMPD)	13
Scheme 12: Example of an electrochromic polymer based on TPPD-units ⁸⁹	13
Scheme 13: Monomer of PEDOT with TAPD-units	14
Scheme 14: Schematic of the 3-electrode Swagelok®-setup	18
Scheme 15: Synthetic route and redox couples for polymer 1 – (a) Pd(OAc) ₂ , P(t-Bu) ₃ , NaO-t-Bu, Toluene, 110 °C.....	34
Scheme 16: Synthetic route for polymer 4 – (a) Pd(OAc) ₂ , P(t-Bu) ₃ , NaO-t-Bu, Toluene, 110 °C, (b) Acryloyl chloride, Et ₃ N, CH ₂ Cl ₂ , 0 °C, and (c) AIBN, Dioxan, 80 °C	37
Scheme 17: Redox couples of polymer 4	38
Scheme 18: Synthetic route for monomer 6 and polyamide 7 – (a) KO-t-Bu, DMSO, 90 °C, (b) H ₂ NNH ₂ *H ₂ O, Pd/C, EtOH, 80 °C, (c) isophthaloyl dichloride, NMP, 0 °C - RT	40
Scheme 19: Redox couples of polyamide 7 (A ⁻ ...electrolyte salt anion).....	422
Scheme 20: Synthetic route for model compound 10 and monomer precursor 12 – (a) picoline-borane, MeOH/AcOH (10:1), RT, (b) Pd(OAc) ₂ , P(t-Bu) ₃ , NaO-t-Bu, Toluene, 110 °C, (c) mCPBA, THF, 0 °C.....	63
Scheme 21: Proposed redox reactions for model compound 10	65
Scheme 22: Synthetic route for monomer 13 and polymer 14 – (a) TBAF, THF, 0 °C, (b) benzene-1,3,5-tricarbonyl trichloride, NMP, 0 °C	67
Scheme 23: Structures and theoretical capacities of polymer 1 and 3	71
Scheme 24: Structures and theoretical capacities of polymer 7 , model compound 10 and polymer 14	72
Scheme 25: Potential polymer structures with higher theoretical capacities	74

7.6 List of Tables

Table 1: Cathode compositions	42
Table 2: Peak-potential separation ΔE_p at different scan rates	45
Table 3: Discharge capacities at different C-rates.....	47
Table 4: Separation between the average charge and discharge potentials (ΔE_{ave})	49
Table 5: Peak-potential separations ΔE_p of composite cathodes with increasing active material content	58
Table 6: Specific discharge capacities (10 th cycle) of half-cells with composite cathodes B , C and D (3.0-4.2 V vs Li/Li ⁺)	60